TESIS DE LA UNIVERSIDAD DE ZARAGOZA

2020 101

Rebeca Monteagudo Oliván

Síntesis de materiales metal-orgánicos y encapsulación de moléculas bioactivas

Departamento

Ingeniería Química y Tecnologías del Medio Ambiente

Director/es

Coronas Ceresuela, Joaquín

ISSN 2254-7606

Prensas de la Universidad Universidad Zaragoza

ISSN 2254-7606

Universidad Zaragoza
1542

Tesis Doctoral

SÍNTESIS DE MATERIALES METAL-ORGÁNICOS Y ENCAPSULACIÓN DE MOLÉCULAS BIOACTIVAS

Autor

Rebeca Monteagudo Oliván

Director/es

Coronas Ceresuela, Joaquín

UNIVERSIDAD DE ZARAGOZA

Ingeniería Química y Tecnologías del Medio Ambiente

2019

UNIVERSIDAD DE ZARAGOZA

Universidad Zaragoza

ÁREA DE INGENIERÍA QUÍMICA, DEPARTAMENTO DE INGENIERÍA QUÍMICA Y TECNOLOGÍAS DEL MEDIO AMBIENTE

"SÍNTESIS DE MATERIALES METAL-ORGÁNICOS Y ENCAPSULACIÓN DE MOLÉCULAS BIOACTIVAS"

Memoria para optar al grado de Doctor por la Universidad de Zaragoza presentada por:

D. Rebeca Monteagudo Oliván

Febrero de 2019

Universidad Zaragoza

D. Joaquín Coronas Ceresuela, Catedrático de Universidad del Departamento de Ingeniería Química y Tecnologías del Medio Ambiente de la Universidad de Zaragoza,

CERTIFICA

Que la presente memoria titulada:

“Síntesis de materiales metal-orgánicos y encapsulación de moléculas bioactivas”

se ha realizado bajo su dirección por D. Rebeca Monteagudo Oliván, autorizando su presentación.

Y para que así conste, firmo el presente certificado en Zaragoza a 27 de febrero de 2019.

Fdo.: Dr. Joaquín Coronas Ceresuela

Table of contents

Preface/Prefacio

Esta tesis doctoral titulada “Síntesis de materiales metal-orgánicos y encapsulación de moléculas bioactivas” se ha realizado en el Departamento de Ingeniería Química y Tecnologías del Medio Ambiente (IQTMA) y en el Instituto de Nanociencia de Aragón (INA) e Instituto de Ciencia de Materiales de Aragón (ICMA), de la Universidad de Zaragoza. Se ha llevado a cabo en el Grupo de Catálisis, Separaciones Moleculares e Ingeniería de Reactores (CREG), dentro del subgrupo dedicado al desarrollo y modificación de materiales nanoestructurados y membranas.

Entre otras líneas, el grupo CREG trabaja desde 1991 en la síntesis de materiales nanoestructurados porosos y su aplicación en membranas inorgánicas y en reactores catalíticos de membrana. En el año 2005 fue reconocido por el Gobierno de Aragón como grupo de investigación de excelencia y comenzando por entonces la línea de investigación de materiales híbridos orgánicos-inorgánicos y procesos de modificación de materiales laminares porosos donde se enmarca el presente trabajo.

La realización de esta tesis doctoral ha sido posible gracias al apoyo económico de la Diputación General de Aragón (T43-17R), del Ministerio de Economía y Competitividad y del Fondo Social Europeo mediante el proyecto de investigación MAT2016-77290-R.

Durante la realización de esta tesis la autora ha colaborado en diversos temas, sin reflejo en la presente memoria de tesis, con las empresas Industrias Químicas del Ebro (IQE, Zaragoza) y Orache Desinfection (Sabiñánigo). En este último caso la colaboración ha dado lugar a la solicitud de una patente española: “Pastillas desinfectantes bicapa con detergente y repelente de suciedad” (P201830195).

Dicho lo anterior, el objetivo de la tesis se centra en el estudio de la síntesis de materiales metalorgánicos porosos (MOFs) usando nuevas rutas, que permitan un mayor control de sus propiedades (capítulos 2 y 3), así como la aplicación de los MOFs a la encapsulación de moléculas bioactivas (cafeína, ácido kójico y carvacrol). En este último caso, además, se han usado metodologías inéditas hasta el momento, como son la encapsulación a alta presión en ausencia de disolvente (capítulo 4) y la encapsulación asistida mediante dióxido de carbono supercrítico (capítulo 5).

Resumen

Se presenta aquí la tesis doctoral con título “Síntesis de materiales metal-orgánicos y encapsulación de moléculas bioactivas” (Synthesis of metal-organic materials and encapsulation of bioactive molecules).

En el capítulo 1 se expone una breve introducción a los materiales metal-orgánico (MOF) en la que se explican los fundamentos de estos materiales y sus aplicaciones.

En los capítulos 2-6 se exponen los resultados de esta tesis que ha estado basada en dos líneas de investigación principales: (i) el diseño de nuevas estrategias de síntesis de MOF (capítulos 2 y 3), y (ii) nuevos métodos de encapsulación de moléculas bioactivas con MOF potencialmente biocompatibles (capítulos 4 y 5).

En lo referente al campo de la síntesis, dos nuevas estrategias se han estudiado en las cuales se ha utilizado la reactividad de los metales en disolución y de la química de la coordinación para favorecer la síntesis de MOF. En primer lugar, el uso de atmósferas gaseosas reactivas a alta presión (6 bar) se estudió en la síntesis de fumaratos de aluminio y hierro(III). Se estudió el efecto de CO y O_2 sobre la formación de MOF y los diferentes productos finales se caracterizaron y compararon entre sí y con otros materiales de la literatura científica. En segundo lugar, se utilizó peróxido de hidrógeno (H_2O_2) para sintetizar tereftalatos de aluminio y hierro(III). Por medio de varias técnicas, este efecto se estudió y compraró con muestras de referencia preparadas sin peróxido para proponer un mecanismo que explique el efecto favorable del H_2O_2.

En lo referente al campo de la encapsulación, se han propuesto dos nuevos métodos, en los cuales se usó alta presión por medio de diferentes aproximaciones. En primer lugar, se estudió el efecto de aplicar alta presión (0,32 GPa) con una prensa hidráulica sobre mezclas MOF-aditivo con cuatro tipos de MOF basados en ligandos carboxilato (MIL-53(Al), Mg-MOF-74, UiO-66 y MIL-101(Cr)) y dos aditivos (cafeína y ácido kójico). Por medio de diferentes técnicas, se demostró el alcance de la encapsulación para los dos aditivos. En segundo lugar, se empleó CO_2 supercrítico (a 40 ºC y 100 bar) para encapsular cafeína y carvacrol en dos MOF potencialmente biocompatibles, MIL-53(Al) y Mg-MOF-74. La cantidad de carga de aditivo se estudió a distintos tiempos y se caracterizaron las interacciones MOF-aditivo.

Finalmente, los resultados más remarcables conseguidos a lo largo de esta tesis se han resumido brevemente en el capítulo 6 (conclusiones).

Summary

The PhD dissertation with the title “Síntesis de materiales metal-orgánicos y encapsulación de moléculas bioactivas” (Synthesis of metal-organic materials and encapsulation of bioactive molecules) is presented here.

In Chapter 1, a brief introduction to metal-organic frameworks (MOFs) is presented, in which a general overview is displayed about of the fundamentals and applications of these materials.

In chapters 2-6, the two main research lines and results of this thesis are presented, (i) new strategies of MOF synthesis (Ch. 3 and 4) and (ii) encapsulation of bioactive molecules in potentially biocompatible MOFs (Ch. 5 and 6)

In the synthesis field, two different approaches were studied, and in both of them the metal reactivity and coordination chemistry were used to promote the MOF synthesis. Firstly, reactive gas atmospheres at high pressure (6 bar) were used in the synthesis of M^{3+}-fumarates of aluminium and iron. The effect of CO and O_2 over the MOF formation was studied, and the resulting final materials were characterized and compared. The results were discussed and published. Secondly, the oxidant hydrogen peroxide (H_2O_2) was used to synthesize M^{3+}-terephthalates of aluminium and iron. Through different techniques, the effect was compared and discussed with reference samples obtained without H_2O_2 to propose a plausible mechanism to explain the favorable effect on MOF synthesis.

In the encapsulation field, two new routes were proposed and in both of them high pressure was used through different ways. First, four carboxylate based MOFs (MIL-53(Al), Mg-MOF-74, UiO-66 and MIL-101(Cr)) and two additives (caffeine and kojic acid) were studied when high pressure (0.32 GPa) was applied with a hydraulic press. By different techniques, the extent of the encapsulation of both additives was demonstrated. Second, supercritical-CO_2 (at 40 ºC and 100 bar) was used to encapsulate two soluble molecules, caffeine and carvacrol, into two potentially biocompatible MOFs, MIL-53(Al) and Mg-MOF-74. The additive loadings were studied through time, and host-guest interactions were characterized.

Finally, the most remarkable goals achieved during this doctoral thesis are briefly summarized in chapter 7 (conclusions).

Having said this, the PhD dissertation with the title “Síntesis de materiales metal-orgánicos y encapsulación de moléculas bioactivas” (Synthesis of metal-organic materials and encapsulation of bioactive molecules) is presented as follows.

Chapter 1

Introduction

1.1.- General considerations of metal-organic frameworks (MOFs)

MOFs (Metal-Organic Frameworks) can be described as extended crystalline networks in 2D or 3D, which show permanent porosity and high specific surface area.[1,2] As any network, MOFs are constituted by knots and connecting units forming channels (1D), sheets (2D) or 3D networks.[2] The composition consists of clusters of metal cations connected through linkers, known as struts, typically bi- or tridentate. As other porous materials, MOFs find general applications in gas adsorption, separation and catalysis, and others more specific.

The inorganic part: metal ion coordination

The metal ions are located in the knots, coordinated to connector groups of the ligand and in some cases among them. These knots are described as secondary building units (SBU).[2,3] This coordination is conditioned by the synthesis conditions and starting reactants, (metal salt and ligand, typically in the acid form). The SBU determines the final structure and the stoichiometry of the porous material.[2] Several examples are, tetramers of tetrahedral Zn^{2+} of MOF-5 [$Zn_4(O)O_{12}C_6$], chains of octahedral Al^{3+}, Cr^{3+}, Fe^{3+}, Ga^{3+}, In^{3+}, Sc^{3+} or V^{3+} of MIL-53,[4–10] hexamers of (octahedral) Zr^{4+} of UiO-66,[11] or monomers of tetrahedral Zn^{2+} or Co^{2+} of ZIFs, among others.[12] The topology of MOFs is assorted: they show different structures, e.g. cubic cages of MOF-5,[13] mono-dimensional channels of MIL-53 series, [4–7] 3D nets of octahedral and tetrahedral pores with triangular windows of UiO-66,[11] and zeolite-like structure of ZIFs (zeolitic imidazolate frameworks).[12]

The organic part: ligands

Regarding the ligand that links the SBUs, a great number of bi- and tridentate ligands have been used to build MOFs.[12,14] The ligands are sometimes named struts as they act likewise connecting the knots of metal centers. Most common binding functionality is carboxylate group, e.g. coming from terephthalic acid or benzene-1,4-dicarboxylic acid (H_2BDC), trimesic acid or benzene-1,3,5-tricarboxylic acid (H_3BTC), and imidazolates (ZIFs). It is important to remark that the starting reactant is normally the ligand in the acid form but in the MOF structure is deprotonated, e.g. departing from terephthalic acid, the struts are formed by terephthalates (BDC) and from trimesic acid, trimesates (BTC). Typically, the ligand is an aromatic ring or a combination of them, which provides higher structural stability. Although, other less rigid ligands are also used, e.g. fumarate,[15] adipate[16] or malate.[17] One of the distinctive MOFs characteristic is the organic part, which can be functionalized in such a way that pore cavities modifies the MOF surface and therefore the properties of the material can be changed, e.g. the interaction with a guest or in molecular separations. Several reports can be found, where the authors compare the properties of the original material with those of the functionalized MOF. [18–20] For example, Devic *et al* 2012 studied the CO_2 adsorption of functionalized MIL-53(Fe)-X, that is, the material was prepared with usual ligand, terephthalate or benzene 1,4-dicarboxilate, and with a group ring X= Cl, Br, CH_3, NH_2, $(COOH)_2$–2,4-substitution), in 2-position of the aromatic.[18] Yang et al 2016 improved the CO_2 adsorption of MIL-53(Al) by introducing -OH groups.[19] They observed that the introduction of two -OH groups per ligand improved CO_2 uptake. The authors justified this fact by the high quadrupolar moment of CO_2 that allowed the interaction with -OH groups. Otherwise the presence of four -OH groups per ligand produced lower CO_2 uptake, in this case the excess of functional groups diminished the pore volume and then the adsorption capacity of the MOF.

The ligand primarily determines the size of the cavities. It is representative the work carried out by Eddaoudi *et al.* 2002 in Yaghi's group.[21] They synthesized a series of MOFs with the same structure of MOF-5, $Zn_4O(BDC)_3$,[13] in which IRMOFs (isoreticular MOFs) whose pore size increases as ligand length is longer. Another similar case was reported in 2012 by the same group, in which a series of

isoreticular MOF-74 (IRMOF-74), a honeycomb structure, were synthesized.[22] The handicap of IRMOFs is that as the larger is the ligand length, the most probable it is the interpenetration of nets or concatenation,[23] apart from the fact that the price of the ligand increases, which may limit the applicability of the MOF.

The importance of tunability can be understood if MOFs are compared with the crystalline inorganic equivalent: the zeolites (see section 6 for further comparison with other porous materials). Zeolites are limited by the base composition of aluminosilicates and structural tetrahedral oxides; some variability might be achieved just by cation exchange. Meanwhile, MOFs can be modified, for example, accordingly the gas to be adsobed.[24]

The intrinsic properties of the ligands can provide distinctive applications to the MOFs, e.g. chirality or fluorescence. Chiral ligands can be used to build MOFs for applications in catalysis, enantioselectivity separations or non-linear optics, e.g. L- or D-POST-1 (made of Zn and L- or D-tartrate, respectively), POST stands for Pohang University of Science and Technology,[25] or those made from chiral amino acids. Otherwise, MOF prepared from fluorescent struts show applications in chemical sensing and biosensing.[26]

A bit of nomenclature

The expression of metal-organic framework was used firstly in 1995 by Omar Yaghi and Hailian Li, from the Arizona University back then.[27] However, MOFs or crystalline hybrid structures date before that year, but they were not named in that way. For example, Konoshita *et al.* reported in 1959 the crystal structure of the 3D network of bis(adiponitrilo)-copper(I) nitrate.[28] The reporting of their special properties started in 1997, when Kondo *et al*, in the group of Kitagawa at Tokyo Metropolitan University, described the CH_4, N_2 and O_2 adsorption behavior of a MOF based on the ligand 4,4´-bypiridine and a divalent metal cation (Co, Ni or Zn).[29] Moreover, especially significant was the first paper on MOF-5 by Li *et al* 1999, composed by Zn^{2+} and 1,4-benzenedicarboxylate, and its exceptionally high BET surface area of 2320 m^2/g, superior to those reported for other porous materials like zeolites and activated carbon.[13] Since then and to say so, three main research sides have stood up in this field, the north American side with the groups of O. Yaghi (Berkeley University), J.Y. Hupp (Northwestern University) and O. Farha (Northwestern University before, King Abdulaziz University nowadays), the side in France of the group of C. Serre and G. Férey (died in 2017) of Lavoisier Versailles Institute (Paris), and the side in Japan of the group of S. Kitagawa (Kyoto University). Nevertheless,, several other groups are important in this field and have developed many interesting advances in hybrid porous materials.

The metal-organic materials are known also as porous coordination polymers (PCP) although in general they are named MOFs.[30,31] Firstly, they were compared to organic polymers because the network can be considered chains expanded in 2 or 3D of the ligand (monomer) connected through the coordination to the metal. However, similarities between MOFs and polymers are scarce in terms of physical and chemical properties. The generic name normally consists of the acronym MOF followed by a hyphen and a number. The metal element that forms the net can be included before the name separated by a hyphen or after it in brackets, e.g. Mg-MOF-74 or MIL-53(Al). In some cases, MOF are denominated with an acronym related to the place of discover, such as the MIL named so for the Materials Institute of Lavoisier of Paris, the series UiO from Oslo University (Universitetet i Oslo),[11] HKUST (Hong Kong University of Science and Technology)[32] or CAU (Christian Albrechts Universität).[33] The nomenclature can be ambiguous in some cases since a material can be referred with different names. For example, among the MOFs used in through this thesis, the Mg-MOF-74[34] is also known as CPO-27,[35] or IRMOF-1. Another example, MIL-53(Al)-FA, named so for being

isostructural with MIL-53(Al) but with the ligand fumarate,[15] is also known as MIL-88A(Al), as basolite A520 in a patent by BASF,[15,36] simply aluminum-fumarate[15] or μp-AF.[37] That makes five different names to refer the same material.

Porosity, structure and flexibility

Several features make MOFs of great interest. Firstly, the permanent porosity, as mentioned before, MOFs are crystalline networks that display typically porosity in the nanoscale. Although some of them have mesoporous, e.g. MOF-100 and 101 with pores of a few nanometers.[38,39] The importance of permanent porosity related to their reusability: crystal structure must be preserved after the removal of adsorbed gas for adsorption-desorption cycles. Their intrinsic crystallinity results in characteristic diffraction patterns that can be compared with references or simulated patterns which are deposited in the crystallographic data center (CCDC) for identification.[40]

One of the most remarkable property of MOFs is the high specific surface area, these materials show the highest values ever reported up to date (~7000 m^2/g).[41] Typically, the Brunauer-Emmett-Teller (BET) method is used to calculate the specific area from adsorption isotherms data and this value allows to to compare among materials. It is remarkable that even among synthesis routes and activation processes, different values are displayed for a given material. The applicability of BET theory for MOFs has been discussed,[42,43] and sometimes is also reported the Langmuir surface area value (BET theory assumes multilayer adsorption and Langmuir theory considers a single monolayer). Nevertheless, Langmuir areas tend to overestimate the apparent surface areas and BET area is considered the most appropriate way to calculate specific surface areas of MOFs.[42] The specific surface area is considered crucial for applications, especially for those related with gas adsorption and separation. It is worthy to mention that high crystallinity is not always required for some applications as long as the adsorption capacity is preserved.

A characteristic feature of some MOFs is their flexibility, in terms of the so-called breathing, the structure is modified due to an external stimulus or a guest present into the pores. Depending on the magnitude of this modification, it is distinguished between flexibility, if the variation is minor, or breathing, if a change in special group is produced.[2] The MIL-88A is an example of flexibility and so MIL-53 of breathing.[2,3] Breathing and flexibility should be distinguished from the rigidity or flexibility of the ligand composing the struts, as they are not related properties, i.e. a rigid ligand can give rise to a flexible structure.

The wide range of possibilities of combination of metal cations and ligands generate a great number of MOFs. In opposition, the number of zeolite types structures is limited.[44] Additionally, MOFs struts can be post-synthetically modified, for example by exchanging a functional group or using a different substituent, and in turn this allows the adjustment of the properties of the material.[45] Consequently, the research in MOFs is a challenging field considering that the study of potential applications is broad. The great versatility of MOFs distinguishes them from other porous materials such as inorganic zeolitic materials and activated carbons.

The MOF functionality for each application depends greatly on the interactions between the MOF pores surface and the guest, either a gas or a liquid. Two different sites have to be considered, the knots and the struts, that is, the environment around the secondary building units or SBUs and the organic linkers.[46,47] *A priori*, the SBUs could form polar interactions with guest, meanwhile the binding with the organic linker would be led mainly by non-polar or less polarized interactions and, in some cases, by π-π stacking. Although, the functionalization of the ligand would also determine these interactions. Hydrogen bonds, either with the ligand or the coordination positions, can be

found.[48] The accessibility of the binding active sites is important for the good performance of MOFs, therefore the activation step is decisive in this point.[49]

Regarding the SBUs and its environment around, the availability of unsaturated metal centers (UMC)[50] or open metal sites can play an important role in some applications, especially in those of gas separations[34,50–54] and others like catalysis.[55,56] The specificity for a gas molecule is improved due to the preferential interaction with UMC. For example, it has been studied for H_2 storage,[51–54] CO_2 capture[34] and NO storage.[57] See section 3.1 in which some representative examples are described.

Strengths and weakness

The major handicaps of MOFs are thermal resistance and low stability in water. The thermal stability limits the application in industry for high temperature processes, in this point MOFs cannot compete with zeolites or other inorganic porous materials. As MOFs are formed by organic components, thermal stability is limited in any event. Most MOFs are no stable above 450 ºC, with some important exceptions like MIL-53(Al) and the series of UiO. The metal can also have influence on the thermal resistance, e.g. for the MIL-53 series, the MOF of Al is the most stable (ca. 500-550 ºC), meanwhile that of Fe is only stable up to 350-400 ºC. In the UiO series, UiO-66 is stable up to 540 ºC. In this MOF, the SBU is extraordinarily strong, formed by a Zr_6-octahedron, and its strength is so high that during the thermal decomposition the carboxylate of the terephthalate is kept with the cluster, separately from the aromatic ring.

Regarding stability in water, the weakest structural point is normally the coordination bond between the ligand and the metal center. In fact, hydrolysis is produced due to the favored solvation of the metal cation by water molecules over the ligand coordination at high temperatures or even at room temperature, solvation might be favored by the anions in solution like phosphates. MOF decomposition leads usually to the metal cation and ligand separation. The water and humidity effects in MOFs have been broadly studied. For example, Mg-MOF-74 is a promising material for CO_2 capture,[34] although the water and humidity instability can limit the actual industrial use.[58] Water stable MOFs can be applied in more potential applications than those that are not.[59]

1.2.- Synthesis, post treatments and post synthetic modifications

1.2.1- Synthesis overview

MOFs are synthetic materials. The synthesis of MOFs is normally carried out in solvothermal or hydrothermal conditions, i.e. in a sealed reactor at high temperature in an organic solvent or in water. Summarizing, the basic synthesis of MOFs consists in placing the ligand and the metal salt together in the solvent (distilled water, an organic solvent or a mixture of both) in a tightly closed inert reactor, or an autoclave at high temperature, or in baker at room temperature. Working temperatures are in the range from room temperature to 250 ºC at maximum, and normally below this temperature. It is worthy to remark the importance of synthesis reactants, especially the metal salt, and pH.

The optimization of syntheses is a challenging issue and stands out because the applicability depends on obtaining an affordable and viable route. In many cases, the reported syntheses require a toxic solvent, typically dimethylformamide (DMF), that implies a more complicated processing, higher expenditure in waste, washing steps of the material or even the final impurity of the obtained products because DMF tends to be strongly occluded in the MOF pores.

Consequently, one of the first aims in the synthesis research is the substitution of DMF by other less toxic solvent. For example, the synthesis of UiO-66, one of the MOFs that shows highest thermal

resistance, was tested in different solvents with a moderate success, only DMF produced pure crystalline UiO-66.[60]

Another challenge is to obtain milder conditions of synthesis. High temperature and relatively long reaction times are usually reported, which also implies the need of a reactor formed by an inert Teflon and a stain less steel jacket able to resist high pressures. For example, the synthesis of MIL-53(Al), also highly stable up to 500 ºC, is carried out in the described setup at 220 ºC for 3 days,[4] which requires a reaction system able to stand high pressure and temperature. In order to achieve milder conditions and reduced energetic expense, the synthesis of MIL-53(Al) has been reported at room temperature departing from sodium terephthalate instead of terephthalic acid.[61] However, this method generates a solid less crystalline and with poorer properties, as they depend strongly on the crystallinity. Hence this must be a key element: a novel synthesis method must arise with a solid of good crystallinity degree or, at least, good enough for each desired application.

The molar ratio metal:ligand is also a key point in MOFs synthesis, the actual obtention of the MOF phase depends a great deal on it. In some cases, an excess of ligand is required, which is the most expensive reactant. For example, ZIF-8, a Zn imidazolate isostructural with the Co imidazolate ZIF-67, can be synthesized in MeOH or mixtures of MeOH/H_2O at room temperature with a high excess of ligand, 1M:8L.[62]

The yield is also a key factor to take into account, not always included in the reported syntheses. Some described syntheses report high quality MOFs although with low yield, limiting the real applicability. Alternative or improved syntheses are needed in those cases. In some reports in which scaling up syntheses are described, the value of space-time yield (STY) is used. STY is defined as the mass of a product formed per volume of the reactor and time (e.g. $kg \cdot m^{-3} \cdot h^{-1}$ or $g \cdot L^{-1} \cdot h^{-1}$).[63]

The importance of the reactants and synthesis conditions

The salt selection can be decisive in the final product, or even in the righteous obtaining of the MOF. As a representative example, Janiak and co-workers carried out a study to obtain MIL-100(Fe) in a solvent media of DMSO/H_2O. They tested different iron (III) salts, that is of nitrate ($Fe(NO_3)_3 \cdot 9$), chlorine ($FeCl_3 \cdot 6H_2O$), mesylate ($Fe(MeSO_3)_3$), hydrogensulfate ($Fe(HSO_4)_3$) and sulfate ($Fe_2(SO_4)_3$). Interestingly, they only obtained the phase MIL-100(Fe) with the nitrate salt for the same conditions of solvent, temperature, reaction time and pH.[64] It is also interesting the replacement of less desirable metal nitrates and chlorines by alternative and in in some cases greener and cheaper salts as those based on acetylacetonates.[65]

Some ligand-metal ion combinations can give rise to different structures depending on the conditions and is not always known the reason why one structure is formed instead the others. For example, departing from terephthalic acid and an iron (III) chlorine four different structures can be obtained, MIL-53(Fe),[6] MIL-68(Fe),[66] MIL-88B(Fe),[67] and MIL-101(Fe),[68] even a fifth structure, MIL-85, can be constructed when ion acetate is incorporated into the structure too.[69]

The ligand can be purchased as protonated or the corresponding salt, although the most used is the protonated ligand.[61] The low pH corresponding to solutions of transition metals may protonate the ligand in any event.

External assistance: beyond solvothermal method

Even though, solvo- and hydrothermal syntheses are the most used, other processes have been developed successfully for some MOFs.[70] Most relevant methods are described below as follows:

-Microwave synthesis. Microwave irradiation (MW) is used to heat the system. The electromagnetic field interacts the mobile charges of the media (ions or polar molecules), which align with the electromagnetic field. The field is oscillating, and, therefore, molecules are constantly changing the orientations.[71] Additionally, the system can spin, meanwhile pressure and temperature are controlled at the same time. Reaction times are considerably lower, from hours or days in the common solvothermal approach to minutes.[70] The first MOF synthesized with this method was that MIL-100(Cr), a reduction of time was produced from 4 days to 4 h.[72]

Several MOFs haven reported to synthesized by microwaves, some of them with better results than the usual method, such as MIL-101(Cr), HKUST-1, MOF-5, Co-MOF-74, MIL-53 of Al, Fe or Cr, ZIF-8.[63] The major handicap can be the scale-up of the process.

-Sonochemical synthesis. The system is perturbed by an ultrasound (US) vibration of a frequency in the range of 20 kHz- 10 MHz. The vibration affects the solvent, and the wavelength is higher than the molecular dimensions, therefore reactants are not directly affected. The US produces cyclic high-low pressure regions (compression and rarefaction). When the low pressure area is below vapor pressure, bubbles are formed. The cavitation, i.e. formation, growth and collapse of bubbles, shows huge energy in the boundaries, temperature and pressure can achieve local values of ca. 5000 K and 1000 bar, while heating and cooling rates are extraordinarily high, more than 10^{10} $K \cdot s^{-1}$. These areas are called “hot spots”.[71] All this promotes the facilitated nucleation of MOF particles, a complex physical chemistry is around the effect on the nucleation.

The first reports of US assisted synthesis of MOFs date from 2008 of ZIF-8 and amino MIL-53, -88 and 101 of iron. Other MOFs synthesized with this methodology are MIL-121, CAU-1, HKUST-1, MOF-14, MOF-5, and other ZIFs (ZIF-7, ZIF-11 and ZIF-20),[73] among others. In general, more crystalline particles are obtained and higher yields. Nevertheless, the industrial application must overcome different challenges, such as applying at large reactors and achieving homogenous bubbles.

-Mechanochemical synthesis. A mechanical force produces the breakage of chemical bonds and the induction of chemical transformations.[71] The MOF is obtained by milling or grinding the starting reactants, sometimes small amounts of solvents can be used assisting the process.[74] Temperature can be also a parameter to play with. The synthesis system can be a simple mortar with a pestle or automated ball mills. In any event, this method of synthesis is not lacking solvent absolutely, because the purification steps may require them due to not complete reaction of precursors. Mechanosyntheses are classified as solvent-free grinding (SFG), liquid-assisted grinding (LAG) and ion-and-liquid assisted grinding (ILAG). LAG uses a minimum amount of liquid and is more effective than SFG. In ILAG, another salt is added to the initial mixture.[63]

The first SFG of MOFs was reported by *Pichon et al* in 2006, the authors described the synthesis of copper(II) isonicotinc, departing from copper acetate and isonicotinic acid (Hina). Other MOFs synthesized by SFG are ZIF-8, HKUST-1, or MIL-101(Cr). First report of LAG date from 2006 by Braga *et al.*, $CuCl_2$(dace) (dace=diaminocyclohexane) with DMSO. Other MOFs synthesized by LAG are Zn-fumarate (2006), HKUST-1 (2010), MOF-14 (2010), IRMOF (2015), UiO-66 (2016) or NH_2-UiO-66 (2016). The ILAG approach shows less examples, e.g. pillared MOF of Zn^{2+} and terephthalate and dabco (1,4-diazabicylooctane), using alkali metal or ammonium nitrate, and ZIF-8, using ammonium salts.[63]

-Electrochemical synthesis. There are two approaches for using electricity to synthesize MOFs, the anodic dissolution and the cathodic deposition.[63,71]

In the anodic dissolution, the source of MOF metal is not a salt in solution but the anode, which is oxidized. The ions pass to the solution and react with the ligand present in the electrolyte solution. By this method, MOF films can be obtained. The anodic dissolution was firstly patented by BASF in 2005, when they described the synthesis of CuBTC (HKUST-1) by this method. Other MOFs have been synthesized by anodic dissolution, such as ZIF-8, MIL-53(Al) and MIL-100(Al) (2012), MIL-100(Fe) (2014), several ZIF (2016), rare earth MOFs TbBTC and GdBTC (2014), and MOF-5.[63,70]

In the cathodic deposition, apart from usual metal salt and ligand in solution, a so-called probe is needed. It consists of a species that is reduced in the cathode, e.g. nitrate to nitrite, which generates a pH increase and in turn promotes the MOF synthesis. First report of the cathodic deposition date of 2011 by Dincă *et al.* in which the authors described the synthesis of MOF-5.[75]

-Flow chemistry synthesis. The MOF synthesis is carried out in a tube instead of a bath reactor under continuous flowing stream, often in microfluidic conditions.[76] Some of the most interesting advantages of this method is the high area to volume ratio or the reactor, which improves the heat and mass transfer and, as a consequence, faster synthesis, and the high control of reaction parameter. Additionally, flow reactors are scalable nowadays. Three types of reactors are used microreactor (MR), plug flow reactors (PFR) and stirred bank reactors (CSTR).[63]

In 2011, *Ameloot et al* reported the first synthesis of a MOF with a flow reactor.[77] Authors described the synthesis of HKUST-1 microcapsules, templated with droplets formed due to the immiscibility of water and oil. Other MOFs synthesized with flow chemistry are HKUST-1, IRMOF-3, MOF-5, UiO-66, MIL-88B(Fe), CeBDC, Ni-CPO-27 (Ni-MOF-74), MIL-53(Al), and CAU-13, among others. [63]

-Spray-drying synthesis. The spray drying process consists in the formation of droplets of liquid or slurry and the immediate evaporation of the solvent with a hot gas. The MOF precursors or reactants are dissolved, and this solution is atomized into microdroplets that are dried to form the MOF.[63] In 2013, Carné-Sanchez, Maspoch and co-workers reported firstly the synthesis of MOF by spray-drying, in the same report the authors described the synthesis of 13, such as HKUST-1, NOT-100, ZIF-8 and MOF-5, which were obtained with high BET values, good yields and even in aqueous conditions.[78] Other MOFs synthesized with spray drying are UiO-66 series and FeBTC (MIL-101(Fe)).[79]

In situ modifications: chemical point of view

It is well-known that solids and molecules can modify particle crystallization, interacting with nuclei and their growth.[80] Alternatively to physical variations described above for which a different reaction system is need, *in situ* chemical variations have been successfully described for MOFs, specifically the coordination modulation method,[81,82] and the use of some additives[83–85].

In the modulated synthesis, a monodentate ligand is added to the liquid media, such as a monocarboxylate or an amine ligand, and typically improves the crystallinity of the MOF and can modify size and shape.[81,82,86,87] Tsuruoka *et al.* described in 2009 the synthesis of $[Cu_2(ndc)_2(dabco)_n]$ (ndc=1,4-naphthalene dicarboxylate, dabco=1,4-diazabicyclo [2.2.2] octane) with acetic acid, which promotes anisotropic growth of crystals by favoring [001] direction to form nanorods instead of cubes.[81] Then, Kitakawa and co-workers reported the synthesis of CuBTC with dodecanoic acid to narrow particle size distribution (2010)[82] and to modulate crystal shape (2011).[88] Other representative examples are those of Schaate *et al.* reporting in 2011 the synthesis of several MOFs of the UiO series with benzoic and acetic acids to increase crystallinity,[88] and of Wiβmann *et al.* in 2011, which achieved the synthesis of Zr-fumarate only in presence of formic acid as modulator.[89]

Other chemicals modify size, shape or surface of MOF particles, such as surfactants or blocking agents, e.g. dimethylammonium halides or sodium dodecyl sulfate.[83–85]

Finally, it is worthy to mention that all the described methods of synthesis, except mechanosynthesis, high pressure and anodic deposition, depart from the raw metal salt and ligand in solutions and the product is the powder MOF. Although other strategies and products have been applied to MOFs synthesis, such as reverse microemulsions,[83] ionothermal process,[83,90] sol-gel method,[91] etc.

1.2.2.- Post treatments

Activation

After the synthesis of a given MOF its pores are normally loaded with an excess of ligand o solvent which have to be removed to activate the MOF porosity. First step is washing with a more volatile and in general less toxic organic solvent, like ethanol or methanol. After drying, pores might be still occluded. The process of pores emptying is known as activation and is a critical step on MOF processing. Typically, it is carried out by thermal treatment, exchange with another solvent, drying in vacuum or supercritical CO_2 drying.[92] Sometimes several of these processes are combined to produce a more efficient MOF activation.

The thermal treatment way is the most frequent method. The dried MOF in powder is placed in an oven and a heating program is optimized for each material, with a maximum temperature below the material degradation which is determined normally by TGA. The activation through calcination can induce the partial o punctual collapse of the structure, damaging its crystallinity.

In solvent exchange, the powder MOF is immersed while optionally heating in a solvent with low boiling point under stirring from hours to days at room or high temperature. High boiling solvent and ligand are substituted by the solvent molecules. Thus, pores are occupied by the exchange solvent molecules that can be removed easily by drying.

By heating under vacuum, a better drying can be carried out without increasing excessively the temperature and then preventing the structure damage.

Finally, the use of supercritical CO_2 allows the use of mild temperature conditions for activation due to its relatively low critical point at 301 K and 74 bar (NIST Database). An effective removal of occluding molecules is achieved, increasing free surface area. In fact, the largest BET specific surface area was obtained with this activation, i.e. 7000 m^2/g for Nu-110E.[41]

Post-synthetic modification

This step is optional, in fact it is not carried out in most reported synthetic procedures. In different reports the pore surface modification has been studied to obtain different properties of separation, catalysis, gas storage, etc. It is necessary to differentiate between MOF functionalization, departing from a modified ligand, and the post-synthetic, in which the MOF is *a posteriori* chemically modified. Post-synthetic modifications (PSM) were firstly tested in Kim´s group[93] and different strategies can be used, e.g. using a reductant, attaching organic groups to the ligand or doping with a metal.[94]

Composite and conjugate materials

For the actual application, MOFs have been prepared in combination with other materials, such as silica,[95] polymers to improve performance with thin films in gas separation,[96] metal surface like gold,[97] biopolymers to increase biocompatibility in drug delivery,[57] with graphene oxide (GO),[98] with biomolecules to target delivery of drugs,[57] etc. The range possibilities is extremely broad, out of the scope of the introduction to MOF of this chapter.

1.3.- Applications

In the finals of the 90´s and the 2000 decade, there was an exponential rise in MOFs studies. MOFs chemistry was deeply studied, and several applications were discovered. Main applications of MOFs are gas storage (H_2 and CO_2),[24,49] gas separation,[24] catalysis[99] and drug delivery,[100] and other more advanced applications are proton conductivity,[101] sensing,[102] magnetic resonance imaging,[26] nonlinear optics effects,[103] supercapacitors,[104] semiconducting,[105] proton conductivity,[101,106] scaffolds for pyrotechnic materials,[107] water capture,[108] and water or solvent adsorption for heat transfer,[37] among others. Nowadays, the research in MOFs is a more mature field and greater effort is put to scale-up their production for industrial applications.[109]

The origin of MOFs applicability arises from their adsorption capacity and the way they interact with the guest molecules. The potential interactions host-guest are stablished through the unsaturated metal centers, hydrogen bonding, acid-base interactions, π-π stacking, the breathing of the net, and electrostatic interactions.[110,111] A brief summary is provided here for the most remarkable applications.

1.3.1.- Gas adsorption and separation. First applications of MOFs were found for small gases adsorption and separation.[29] The porosity of MOFs is of regular nature that allows the separation at nanoscale level, like a molecular sieve. Additionally, the chemical surface shows different selectivity for gases and contributes to selective separation. In some MOFs, there are unsaturated metal centers, that is, positions around the metal coordination do not occupy by the ligand and a gas molecule can interact with it strongly. Permanent porosity is a must for gas application, since some MOFs collapse when the pores are totally evacuated.[24] Most important examples are H_2 storage, CO2 capture and gas mixture separations, such as CO_2/N_2, CO_2/CH_4, H_2/CO_2 and H_2/CH_4.

H_2 storage. [46] The use of green transportation is a current research field, both in academic and industry. There is an increase necessity to substitute the fossil fuels for those that leave no waste and could be obtained through renewable sources. Regarding this, H_2 has been proposed as an excellent alternative for fuel cell vehicles. Its reaction with O_2 (air as natural source) produces only water and the energy is recovered through a fuel membrane -also a trending research topic, even MOFs have been studied for this aim (see section 3.6). However, raw H_2 cannot be storage safely, a material able to storage the H_2 is required for a correct use. Different materials have been tested with this purpose such as zeolites, activated carbon, metal hydrides, single-walled carbon nanotubes and MOFs.[57] The minimum of H_2 uptake has been established in 4.5 wt% hydrogen (1.5 kWh/kg system) by the Office of Energy efficiency & Renewable energy (U.S. Department of Energy).[112]

The porosity and interactions with the pore walls determine the H_2 uptake in MOFs. It has been shown that the bigger pores do not necessarily improve the H_2 uptake.[51,113–115] Otherwise, several articles report a remarkable increase by improving the H_2 binding to the surface, specifically through the unsaturated metal centers.[116] The major challenge in H_2 storage is the increase of the binding energy of the H_2 molecule, so that the required pressure and temperature conditions are viable for commercial use.

Several MOFs have been reported. One of the reported MOFs with highest surface area, NU-100, displays high storages capacities of storage of H_2 and CO_2.[117]

CO_2 capture. CO_2 is a greenhouse gas (GHG), the one produced in greater amount by anthropogenic sources. Even though fossil fuels are being substituted, their use is nowadays the most

extended. In order to mitigate the effect on global warming, CO_2 capture is proposed to decrease its concentration in the atmosphere. One way to reach this is the capture by an adsorbent means. In Wang *et al.* classified solid adsorbents at low (<200 ºC), intermediate (200-400 ºC) and high (>400ºC) temperature of use.[118] MOFs are in those described for low temperature with carbon-based adsorbents, zeolites, alkali carbonates and amine-based solids.[119]

Many works have been reported about this topic with MOFs. Among them, Mg-MOF-74 shows high CO_2 adsorption. With this regard, Yang *et al.* published in 2016 the substitution of terephthalic acid by hydroxylated ligand in the synthesis of MIL-53(Al) to obtain MIL-53(Al)-OH_x. Then, the CO_2 adsorption capacity was improved for the hydroxylated material, due to the better chemical interaction between the OH groups and the CO_2 molecule. Interestingly, an excess of OH groups produced lower uptake due to higher the steric hindrance and lower pore volume.[19]

NO storage. In this case, the purpose is medical application. The NO molecule is an important signaling molecule that shows several important functions in biological signaling.[57] Different MOFs have been tested for the sustained release of NO from MOF for drug delivery, most remarkable are HKUST-1 and MOF-74 of Ni^{2+} and Co^{2+}.[57]

Gas separations of low and high molecular gases. MOFs have been demonstrated to be useful in the efficient separations of small molecules due to selective molecule interactions with the unsaturated metal centers and the pore wall. Remarkable separations are those of carbon dioxide separation and mixtures CO_2/CH_4, and H_2/CH_4.[120] The separations can be carried out using MOFs either as powders in adsorption or as membranes.[119,121] Regarding larger molecules, MOFs show also selective adsorption and separation,[122] to cite some examples they have been reported for chromatography separation of alkanes,[123] and separation also of hydrocarbons.[124]

1.3.2.-Catalysis. One of the first proposed applications of MOFs was catalysis,[125] by analogy to the zeolites, used as catalyst in industry.[126] Moreover catalysis was the first demonstrated use.[127,128] and has been broadly studied.[25,129]

As catalyst, MOFs share with zeolites properties like regular porosity ang high internal area. The major advantage of MOFs is that they contain an organic part which increases the catalytic possibilities. The major handicap, in opposition to zeolites, is the limited water and thermal stability (at the most 500 ºC for some MOFs) which in turn restrict their applicability. Regarding this considerations, MOFs have been proposed as heterogeneous catalyst for high value products and fine chemicals.[128]

MOFs can be classified as catalysts regarding the origin of the catalytic activity in the metal nodes, a homogeneous catalyst used as struts and catalysis due to encapsulated species.[128,130] Finally, MOFs can be used as sacrificing materials to obtain catalytically active metal oxide nanoparticles.[131]

1.3.3. Sensors. MOFs have been described as sensor of small gases and molecules, and biomolecules.

Chemical sensors. Different mechanisms can produce the molecule detection, such as stress detection of flexible MOFs and with luminescent ligands as struts.[102]

First article about the use of the flexibility of some MOFs to induce stress detection was reported by Allendorf *et al.* in 2009. These authors tested HKUST-1, made of Cu^{2+} and BTC, deposited in a piezoresistive cantilever to achieve the detection of different alcohols and CO_2.[132] One interesting examples of MOF as sensors is the explosive detection by luminescence. [133]

Additionally, MOFs can also be used as template for preparing other applicable materials. MOFs can also be calcined to give rise an ordered oxide of the corresponding metal, which show high specific surface are comparing to other oxides. For example, Lü *et al.* reported the synthesis of ZIF-67 and the later calcination to obtain a porous oxide Co_3O_4 of high porosity (121 m^2/g) and similar morphology of the departing cubes of MOFs. The sensing properties of this special structured oxide were tested with different volatile organic compounds, i.e. ethanol, acetone, toluene and benzene.[134] Also, Wang *et al.* calcined MIL-88A(Fe) to obtain an iron oxide Fe3O4, with carbonaceous materials as base on electrochemical sensing.[135]

Biosensors. MOFs have been used for biomolecules detection *in vivo* and *in vitro*. Wang *et al.* classified biosensors accordingly to the sensor mechanism in quenchers for DNA/RNA sensing, fluorescence for small molecule sensing and cell imaging and composites MOF-enzymes. [26]

1.3.4.- Drug delivery and sustained release.

The delivery of drugs to a specific target and their release in a sustained way is a field of extensive research. MOFs are promising carriers that must show several requirements to eventually be used *in vivo*. Those are: (i) size reduced to the nanoscale to avoid precipitation; (ii) surface functionalization to improve biocompatibility and to prevent from particle aggregation; and (iii) biodegradation, in fact selected MOFs are potentially biodegradable because their relatively low hydrostability and the low toxicity of the degradation products (metal ion and ligand).

The use of MOFs for sustained release was also one of the initial studied applications. The competitiveness in this field is huge because of the great interest to improve drug delivery and the broad different types of materials studied for it, such as silicas, polymers, dendrimers, liposomes, cyclodextrins, nanoparticles, etc. The major advantage of MOFs is the long term sustained release, hardly comparable with other systems.

Several articles report the use of MOFs as potential drug carrier, standing out the research developed by Horcajada, Serre and co-workers of the Lavoisier Versailles Institute with MILs. They encapsulated different drugs by liquid phase impregnation, in a highly concentrated solution of the drug in a solvent like ethanol, in which the MOF is suspended under magnetic stirring. In the group CREG, several articles were also published before this thesis, such as the one step encapsulation of caffeine in NH_2-MIL-88(B)[136] and ZIF-8,[137] or that dealing with the use of Hansen solubility parameters to study drug encapsulation in MOFs,[137] among others. Apart from those articles written during this thesis about the encapsulation without solvent by high pressure[138] and the use of supercritical CO_2 as impregnation media.[139]

1.3.5.- Medical imaging and magnetic resonance imaging. Different approaches based on MOFs have been studied for intracellular imaging, MRI (Magnetic Resonance Imaging) and Computed Tomography (CT).[26]

For intracellular imaging, fluorescent probes are needed. Fluorescence can come from the struts composing the net of the MOF, a molecule encapsulated into the porosity or a molecule attached to the MOF surface.[140]

In MRI imaging, magnetic field interact with the hydrogens of water. In order to increase the signal, two types of compounds as contrast agents are used, which increase of the proton relaxation times. These that increase the relaxation time t_1 or r_1, e.g. these made of gadolinium and manganese

ions, Gd^{3+} and Mn^{2+}, respectively, and those that increase the transverse relaxation times t_2 or r_2, e.g. those made of paramagnetic iron, Fe^{3+}.[26,141]

1.3.5.- Other promising applications

Removal of hazardous chemicals and environmental remediation

Two main strategies have been reported for removal of hazardous materials or environmental remediation with MOFs: adsorption and catalytic degradation. [142] One of the most used MOFs are those based on iron, due to their semiconducting properties and redox reactions in Fenton process.[142] In gas phase removal, MOFs have been studied for air purification of toxic gases like warfare agents and simulants, ammonia, carbon monoxide, nitrogen oxides, sulfur-containing compounds, among others.[143] In liquid phase, MOFs have been tested for the removal of heavy metals and its oxoanions,[144] radioactive isotopes,[144] dyes in organic and aqueous phases,[145] etc.

Photodynamic therapy (PDT). PDT is medical treatment that uses a photosensitizer or photosensitizing agent as drug to treat cancer. The photosensitizer, once injected, is exposed to light of an specific wavelength which induces the formation of species oxygen that destroy the cells. The use of nano MOFs has been reported as a way to transport the photosensitizer in struts of the structure. Several MOFs have been described for DPT, which are usually based on porphyrinic and metalloporphyrinic and metals like Zn^{2+}, Hf^{4+} or Zr^{4+}.[146]

Water adsorption for heat transfer. In opposition to air pumps and air conditioners, thermally driven adsorption chillers and adsorption heat pump heat or cool down thank to the energy exchanged during water adsorption and desorption.[37] Among the materials able to adsorbs and desorbs water, some MOFs can potentially fit for that purpose. The inherent drawbacks of MOFs could be limiting this application, i.e. high cost production and hydrothermal stability. The MOF has to be a part of a device, because as raw powder heat-mass transfer would be hindered.[37] Few MOFs have been reported in this field such as ISE-1 (made of Ni, BTC and BTRE, 1,2-bis(1,2,4-triazol-4-yl)ethane, ISE stands for Institut Solare Energiesysteme from Freiburg),[37] or the cost-effective aluminium fumarate (MIL-53(Al)-FA).[37] Other interesting MOF for heat transfer or storage are MIL-101,[147] Al-polycarbonate[148] or HKUST-1.[149]

1.4.- Advances in industrial use

The emerging of industrial applications is conditioned by high synthesis costs, as MOFs compete with other well-stablished porous materials like zeolites or activated carbon. Moreover, they must be processable, e.g. transformable in pellets,[150] and be stable during processing and in the use conditions.[109]

For research purposes, there are some suppliers which offers MOFs such as Sigma Aldrich, Tokyo Chemical Industry (TCI), PlasmaChem, or Stream chemicals. For example, Sigma Aldrich makes available several MOFs, advertised under their own commercial name, such as CuBTC or Basolite® C 300, MIL-53(Al) or Basolite® A100, and ZIF-8 or Basolite® Z1200. The prices of the products are not affordable for industrial use.

Nevertheless, we can find MOFs commercialized through different companies for high scale applications, some relevant are listed and described in the following lines.

-**BASF** is one of the biggest of chemistry companies and one of their research field is the MOFs scale-up production and shaping.

-**MOFapps** is a company based on the production of UiO-66 and other zirconium-based family MOFs, commercialized as the exclusive partner with the University of Oslo. Depending on the application they offer the material in different shaping: disks, pellets, spheres or powder.[151]

-**MOF Technologies** (**MOFT**) commercializes MOFs in powder or shaped in pellets, such as magnesium fumarate and Al(OH)-fumarate, HKUST-1 or CuBTC and FeBTC, ZIF-8 and ZIF-67, MOF-74 of magnesium, cobalt, nickel and copper, among others. They claim the main applications are carbon capture, gas storage, heat transformation, separation and other emerging applications.[152]

-**NuMat Technologies**. The MOFs are not directly sold but they offer solutions for separation and modification or capture and release and advertise ION-X "a next generation electronic gas delivery platform".[153]

-**Promethean particles**. This company offers a diverse range of nanomaterials, including MOFs for gas storage, adsorbents (gas, toxic chemicals, or contaminants), gas separation, drug delivery, water treatment, and catalysis. They offer several MOFs, e.g. HKUST-1 or CuBTC, ZIF-8, MIL-53(Al), and MOF-74.[154]

Other remarkable companies working MOFs are **MOFWORKS** is a start-up within CSIRO (Commonwealth Scientific and Industrial Research Organization),[155]**ACSYNAM** (**A**dvanced **C**hemical **Syn**thesis **a**nd **M**anufacturing)[156] and **NovoMOF**.[157]

It is noticeable that most companies offer the MOFs in different shaping and claim the different applications, but no product was found to include directly the materials (at least a final product and advertised in the webpage). As an exception to this point, NuMat seems to advert direct solutions but no brochure is available.

1.5.- MOF related materials

1.5.1- Covalent Organic Frameworks (COFs). The development of COFs has evolved in parallel with that of MOFs. They are only composed by organic monomers, without metal in the knots, which join by covalent bonding.[158] Most reported COFs are based on boronic acid derivates, whose special chemistry allows the union in 2D layers, e.g. diboronic acid in the synthesis of COF-1-which is formed by sheet stacked together by π-π interactions,[159] and 3D, with a more complex precursors.[160] COFs and MOFs share common properties such as crystalline structure, high porosity and high thermal stability. COFs shows applications in different fields such as gas storage, catalysis or photoelectric applications.[158,161] The major advantages of COFs with respect to MOFs are the higher humidity stability and are not so easily hydrolyzed.[161]

1.5.2.- Metal Organic Gels (MOGs). The synthesis is similar to that of MOFs, but the final product is a gel instead of a powder. Main advantage of MOGs over MOFs is that MOGs can be easily shaped at expense of losing the regular porosity and specific surface area.[162,163] Several examples have been reported, e.g. MOG-1 (Fe^{3+}-BTC)[162] or M(DTA), (M^{2+}=Ni, Cu, Pd and DTA, dithiooxamidate)[164]

1.6.- Recommended bibliography

One of the most challenging issues when a researcher starts working with MOFs is dealing with the extremely wide bibliography. Even now, after almost four years I found this field demanding because more materials, methods, composites and sophisticated applications are constantly reported. Therefore, I would like to finish this introduction with a personal recommendation of those articles that I found more instructive and "easy" reading to whom starts working with MOF or wants to know more about them.

-*The Chemistry and Applications of Metal-Organic Frameworks*. Hiroyasu Furukawa, Kyle E. Cordova, Michael O'Keeffe, Omar M. Yaghi. Science. 2013, 341, 1230444.

It is a general overview of MOFs.

-*A Rationale for the Large Breathing of the Porous Aluminum Terephthalate (MIL-53) Upon Hydration,* Thierry Loiseau, Christian Serre, Clarisse Huguenard, Gerhard Fink, Francis Taulelle, Marc Henry, Thierry Bataille, and Gérard Férey. Chemistry- A European Journal, 2004, 10, 1373-1382

It is described the MOF MIL-53(Al) and its breathing behavior.

-*Best Practices for the Synthesis, Activation, and Characterization of Metal–Organic Frameworks,* Ashlee J. Howarth, Aaron W. Peters, Nicolaas A. Vermeulen, Timothy C. Wang, Joseph T. Hupp, and Omar K. Farha. Chemistry of Materials, 2017, 29, 26−39

The most important techniques of MOFs characterization are described and several factors to consider about them.

-*Synthesis of Metal-Organic Frameworks (MOFs): Routes to Various MOF Topologies, Morphologies, and Composites*, Norbert Stock and Shyam Biswas. Chemical Reviews, 2012, 112, 933–969

It is a general overview of MOFs synthesis.

-*New synthetic routes towards MOF production at scale*, Marta Rubio-Martinez, Ceren Avci-Camur, Aaron W. Thornton, Inhar Imaz, Daniel Maspoch and Matthew R. Hill. Chemical Society Reviews, 2017, 46, 3453.

It is about alternative methods of MOFs syntheses (MW, US, mechanochemical, spray-drying and flow synthesis) with a scale-up view. Also, it is described the MOFs shaping (like pellets, foams or membranes) and some companies working with MOFs.

-*Selective gas adsorption and separation in metal–organic frameworks*, Jian-Rong Li, Ryan J. Kuppler and Hong-Cai Zhou. Chemical Society Reviews, 2009, 38, 1477–1504

It is about the use of MOFs for gas separation and the industrial importance in the context of porous materials.

1.7.- Bibliography

1. Rowsell, J. L. C. & Yaghi, O. M. Metal–organic frameworks: a new class of porous materials. *Microporous Mesoporous Mater.* **73,** 3–14 (2004).
2. Férey, G. Hybrid porous solids: Past, present, future. *Chem. Soc. Rev.* (2008). doi:10.1039/b618320b
3. Férey, G. & Serre, C. Large breathing effects in three-dimensional porous hybrid matter: Facts, analyses, rules and consequences. *Chem. Soc. Rev.* (2009). doi:10.1039/b804302g

4. Loiseau, T., Serre, C., Huguenard, C., Fink, G., Taulelle, F., Henry, M., Bataille, T. & Férey, G. A rationale for the large breathing of the porous aluminum terephthalate (MIL-53) upon hydration. *Chemistry* **10,** 1373–1382 (2004).

5. Serre, C., Millange, F., Thouvenot, C., Noguès, M., Marsolier, G., Louër, D. & Férey, G. Very large breathing effect in the first nanoporous chromium(III)-based solids: MIL-53 or CrIII(OH)·{O2C-C6H4- CO2}·{HO2C-C6H4 - CO2H}x·H2Oy. *J. Am. Chem. Soc.* **124,** 13519–13526 (2002).

6. Whitfield, T. R., Wang, X., Liu, L. & Jacobson, A. J. Metal-organic frameworks based on iron oxide octahedral chains connected by benzenedicarboxylate dianions. *Solid State Sci.* (2005). doi:10.1016/j.solidstatesciences.2005.03.007

7. Vougo-Zanda, M., Huang, J., Anokhina, E., Wang, X. & Jacobson, A. J. Tossing and turning: Guests in the flexible frameworks of metal(III) dicarboxylates. *Inorg. Chem.* (2008). doi:10.1021/ic800008f

8. Anokhina, E. V., Vougo-Zanda, M., Wang, X. & Jacobson, A. J. In(OH)BDC·0.75BDCH2(BDC = benzenedicarboxylate), a hybrid inorganic-organic vernier structure. *J. Am. Chem. Soc.* (2005). doi:10.1021/ja055757a

9. Mowat, J. P. S., Miller, S. R., Griffin, J. M., Seymour, V. R., Ashbrook, S. E., Thompson, S. P., Fairen-Jimenez, D., Banu, A. M., Düren, T. & Wright, P. A. Structural chemistry, monoclinic-to-orthorhombic phase transition, and CO2 adsorption behavior of the small pore scandium terephthalate, Sc2(O2CC6H4CO2) 3, and its nitro-and amino-functionalized derivatives. *Inorg. Chem.* (2011). doi:10.1021/ic201387d

10. Barthelet, K., Marrot, J., Riou, D. & Férey, G. A breathing hybrid organic-inorganic solid with very large pores and high magnetic characteristics. *Angew. Chemie - Int. Ed.* (2002). doi:10.1002/1521-3773(20020118)41:2<281::AID-ANIE281>3.0.CO;2-Y

11. Cavka, J. H., Jakobsen, S., Olsbye, U., Guillou, N., Lamberti, C., Bordiga, S. & Lillerud, K. P. A new zirconium inorganic building brick forming metal organic frameworks with exceptional stability. *J. Am. Chem. Soc.* **130,** 13850–13851 (2008).

12. Banerjee, R., Phan, A., Wang, B., Knobler, C., Furukawa, H., O'Keeffe, M. & Yaghi, O. M. High-throughput synthesis of zeolitic imidazolate frameworks and application to CO2 capture. *Science (80-.).* (2008). doi:10.1126/science.1152516

13. Li, H., Eddaoudi, M., O'Keeffe, M. & Yaghi, O. M. Design and synthesis of an exceptionally stable and highly porous metal-organic framework. *Nature* **402,** 276–279 (1999).

14. Furukawa, H., Cordova, K. E., O'Keeffe, M. & Yaghi, O. M. The chemistry and applications of metal-organic frameworks. *Science (80-.).* (2013). doi:10.1126/science.1230444

15. Alvarez, E., Guillou, N., Martineau, C., Bueken, B., Vandevoorde, B., Leguillouzer, C., Fabry, P., Nouar, F., Taulelle, F., Devos, D., Chang, J. S., Cho, K. H., Ramsahye, N., Devic, T., Daturi, M., Maurin, G. & Serre, C. The structure of the aluminum fumarate metal-organic framework A520. *Angew. Chemie - Int. Ed.* **54,** 3664–3668 (2015).

16. Kim, T. K., Lee, K. J., Choi, M., Park, N., Moon, D. & Moon, H. R. Metal-organic frameworks constructed from flexible ditopic ligands: Conformational diversity of an aliphatic ligand. *New J. Chem.* (2013). doi:10.1039/c3nj00812f

17. Zingiryan, A., Zhang, J. & Bu, X. Cooperative self-assembly of chiral L-malate and achiral succinate in the formation of a three-dimensional homochiral framework. *Inorg. Chem.* (2008). doi:10.1021/ic801404p

18. Devic, T., Salles, F., Bourrelly, S., Moulin, B., Maurin, G., Horcajada, P., Serre, C., Vimont, A., Lavalley, J.-C., Leclerc, H., Clet, G., Daturi, M., Llewellyn, P. L., Filinchuk, Y. & Férey, G. Effect of the organic functionalization of flexible MOFs on the adsorption of CO2. *J. Mater. Chem.* **22,** 10266 (2012).

19. Yang, J., Yan, X., Xue, T. & Liu, Y. Enhanced CO_2 adsorption on Al-MIL-53 by introducing hydroxyl groups into the framework. *RSC Adv.* **6,** 55266–55271 (2016).

20. Rowsell, J. L. C. & Yaghi, O. M. Effects of functionalization, catenation, and variation of the metal oxide and organic linking units on the low-pressure hydrogen adsorption properties of metal-organic frameworks. *J. Am. Chem. Soc.* (2006). doi:10.1021/ja056639q

21. Eddaoudi, M., Kim, J., Rosi, N., Vodak, D., Wachter, J., O'Keeffe, M. & Yaghi, O. M. Systematic design of pore size and functionality in isoreticular MOFs and their application in methane storage. *Science* **295,** 469–472 (2002).

22. Deng, H., Grunder, S., Cordova, K. E., Valente, C., Furukawa, H., Hmadeh, M., Gandara, F., Whalley, A. C., Liu, Z., Asahina, S., Kazumori, H., O'Keeffe, M., Terasaki, O., Stoddart, J. F. & Yaghi, O. M. Large-Pore Apertures in a Series of Metal-Organic Frameworks. *Science (80-.).* **336,** 1018–1023 (2012).

23. Chen, B., Eddaoudi, M., Hyde, S. T., O'Keeffe, M. & Yaghi, O. M. Interwoven metal-organic framework on a

periodic minimal surface with extra-large pores. *Science (80-.).* (2001). doi:10.1126/science.1056598

24. Li, J.-R., Kuppler, R. J. & Zhou, H.-C. Selective gas adsorption and separation in metal-organic frameworks. *Chem. Soc. Rev.* **38,** 1477–1504 (2009).

25. Seo, J. S., Whang, D., Lee, H., Jun, S. I., Oh, J., Jeon, Y. J. & Kim, K. A homochiral metal-organic porous material for enantioselective separation and catalysis. *Nature* (2000). doi:10.1038/35010088

26. Wang, H. S. Metal–organic frameworks for biosensing and bioimaging applications. *Coord. Chem. Rev.* **349,** 139–155 (2017).

27. Yaghi, O. M. & Li, H. Hydrothermal Synthesis of a Metal-Organic Framework Containing Large Rectangular Channels. *J. Am. Chem. Soc.* (1995). doi:10.1021/ja00146a033

28. Kinoshita, Y., Matsubara, I. & Saito, Y. The Crystal Structure of Bis(adiponitrilo)copper(I) Nitrate. *Bull. Chem. Soc. Jpn.* (1959). doi:10.1246/bcsj.32.741

29. Kondo, M., Yoshitomi, T., Seki, K., Matsuzaka, H. & Kitagawa, S. Three-Dimensional Framework with Channeling Cavities for Small Molecules: {[M2(4,4′-bpy)3(NO3)4]·xH2O}n(M = Co, Ni, Zn). *Angew. Chemie (International Ed. English)* (1997). doi:10.1002/anie.199717251

30. Batten, S. R., Champness, N. R., Chen, X.-M., Garcia-Martinez, J., Kitagawa, S., Öhrström, L., O'Keeffe, M., Suh, M. P. & Reedijk, J. Coordination polymers, metal–organic frameworks and the need for terminology guidelines. *CrystEngComm* **14,** 3001 (2012).

31. Batten, S. R., Champness, N. R., Chen, X.-M., Garcia-Martinez, J., Kitagawa, S., Öhrström, L., O'Keeffe, M., Paik Suh, M. & Reedijk, J. Terminology of metal–organic frameworks and coordination polymers (IUPAC Recommendations 2013). *Pure Appl. Chem.* **85,** (2013).

32. Chui, S. S. A Chemically Functionalizable Nanoporous Material [Cu3(TMA)2(H2O)3]n. *Science (80-.).* **283,** 1148–1150 (1999).

33. Modrow, A., Zargarani, D., Herges, R. & Stock, N. The first porous MOF with photoswitchable linker molecules. *Dalt. Trans.* (2011). doi:10.1039/c0dt01629b

34. Caskey, S. R., Wong-Foy, A. G. & Matzger, A. J. Dramatic tuning of carbon dioxide uptake via metal substitution in a coordination polymer with cylindrical pores. *J. Am. Chem. Soc.* **130,** 10870–10871 (2008).

35. Dietzel, P. D. C., Blom, R. & Fjellvåg, H. Base-induced formation of two magnesium metal-organic framework compounds with a bifunctional tetratopic ligand. *Eur. J. Inorg. Chem.* 3624–3632 (2008). doi:10.1002/ejic.200701284

36. Leung, E., Müller, U., Trukhan, N., Mattenheimer, H., Cox, G. & Blei, S. Process for preparing porous metal-organic frameworks based on alumininum fumarate US Patent 2012/0082864 A1. (2012).

37. Jeremias, F., Fröhlich, D., Janiak, C. & Henninger, S. K. Advancement of sorption-based heat transformation by a metal coating of highly-stable, hydrophilic aluminium fumarate MOF. *RSC Adv.* **4,** 24073–24082 (2014).

38. Férey, G., Serre, C., Mellot-Draznieks, C., Millange, F., Surblé, S., Dutour, J. & Margiolaki, I. A hybrid solid with giant pores prepared by a combination of targeted chemistry, simulation, and powder diffraction. *Angew. Chemie - Int. Ed.* (2004). doi:10.1002/anie.200460592

39. Férey, C., Mellot-Draznieks, C., Serre, C., Millange, F., Dutour, J., Surblé, S. & Margiolaki, I. Chemistry: A chromium terephthalate-based solid with unusually large pore volumes and surface area. *Science (80-.).* (2005). doi:10.1126/science.1116275

40. Gándara, F. & Bennett, T. D. Crystallography of metal-organic frameworks. *IUCrJ* **1,** 563–570 (2014).

41. Farha, O. K., Eryazici, I., Jeong, N. C., Hauser, B. G., Wilmer, C. E., Sarjeant, A. A., Snurr, R. Q., Nguyen, S. T., Yazaydin, A. Ö. & Hupp, J. T. Metal-organic framework materials with ultrahigh surface areas: Is the sky the limit? *J. Am. Chem. Soc.* **134,** 15016–15021 (2012).

42. Walton, K. S. & Snurr, R. Q. Applicability of the BET method for determining surface areas of microporous metal-organic frameworks. *J. Am. Chem. Soc.* **129,** 8552–8556 (2007).

43. Gómez-Gualdrón, D. A., Moghadam, P. Z., Hupp, J. T., Farha, O. K. & Snurr, R. Q. Application of Consistency Criteria to Calculate BET Areas of Micro- and Mesoporous Metal-Organic Frameworks. *J. Am. Chem. Soc.* (2016). doi:10.1021/jacs.5b10266

44. Database of zeolites structures, available at: http:/www.iza-structure.org/databases/, accesed: 19th February 2019.

45. Wang, Z. & Cohen, S. M. Postsynthetic modification of metal–organic frameworks. *Chem. Soc. Rev.* (2009).

doi:10.1039/b802258p

46. Rosi, N. L., Eckert, J., Eddaoudi, M., Vodak, D. T., Kim, J., O'Keeffe, M. & Yaghi, O. M. Hydrogen storage in microporous metal-organic frameworks. *Science* (2003). doi:10.1126/science.1083440

47. Rowsell, J. L. C., Eckert, J. & Yaghi, O. M. Characterization of H2 binding sites in prototypical metal-organic frameworks by inelastic neutron scattering. *J. Am. Chem. Soc.* (2005). doi:10.1021/ja0542690

48. Corma, A., García, H. & Llabrés i Xamena, F. X. Engineering Metal Organic Frameworks for Heterogeneous Catalysis. *Chem. Rev.* **110,** 4606–4655 (2010).

49. Férey, G., Serre, C., Devic, T., Maurin, G., Jobic, H., Llewellyn, P. L., De Weireld, G., Vimont, A., Daturi, M. & Chang, K. S. Why hybrid porous solids capture greenhouse gases? *Chem. Soc. Rev.* (2011). doi:10.1039/c0cs00040j

50. Li, H., Davis, C. E., Groy, T. L., Kelley, D. G. & Yaghi, O. M. Coordinatively unsaturated metal centers in the extended porous framework of Zn3(BDC)3·6Ch3OH (BDC = 1,4-benzenedicarboxylate) [8]. *J. Am. Chem. Soc.* (1998). doi:10.1021/ja974172g

51. Sun, D., Ma, S., Ke, Y., Collins, D. J. & Zhou, H. C. An interweaving MOF with high hydrogen uptake. *J. Am. Chem. Soc.* (2006). doi:10.1021/ja058777l

52. Dinča, M., Dailly, A., Liu, Y., Brown, C. M., Neumann, D. A. & Long, J. R. Hydrogen storage in a microporous metal-organic framework with exposed Mn2+coordination sites. *J. Am. Chem. Soc.* (2006). doi:10.1021/ja0656853

53. Vitillo, J. G., Regli, L., Chavan, S., Ricchiardi, G., Spoto, G., Dietzel, P. D. C., Bordiga, S. & Zecchina, A. Role of exposed metal sites in hydrogen storage in MOFs. *J. Am. Chem. Soc.* (2008). doi:10.1021/ja8007159

54. Liu, Y., Kabbour, H., Brown, C. M., Neumann, D. A. & Ahn, C. C. Increasing the density of adsorbed hydrogen with coordinatively unsaturated metal centers in metal-organic frameworks. *Langmuir* (2008). doi:10.1021/la703864a

55. Hwang, Y. K., Hong, D. Y., Chang, J. S., Jhung, S. H., Seo, Y. K., Kim, J., Vimont, A., Daturi, M., Serre, C. & Férey, G. Amine grafting on coordinatively unsaturated metal centers of MOFs: Consequences for catalysis and metal encapsulation. *Angew. Chemie - Int. Ed.* (2008). doi:10.1002/anie.200705998

56. Neogi, S., Sharma, M. K. & Bharadwaj, P. K. Knoevenagel condensation and cyanosilylation reactions catalyzed by a MOF containing coordinatively unsaturated Zn(II) centers. *J. Mol. Catal. A Chem.* (2009). doi:10.1016/j.molcata.2008.10.008

57. Keskin, S. & Kızılel, S. Biomedical Applications of Metal Organic Frameworks. *Ind. Eng. Chem. Res.* **50,** 1799–1812 (2011).

58. DeCoste, J. B., Peterson, G. W., Schindler, B. J., Killops, K. L., Browe, M. a. & Mahle, J. J. The effect of water adsorption on the structure of the carboxylate containing metal–organic frameworks Cu-BTC, Mg-MOF-74, and UiO-66. *J. Mater. Chem. A* **1,** 11922 (2013).

59. Wang, C., Liu, X., Keser Demir, N., Chen, J. P. & Li, K. Applications of water stable metal-organic frameworks. *Chem. Soc. Rev.* (2016). doi:10.1039/c6cs00362a

60. Zhao, Q., Yuan, W., Liang, J. & Li, J. Synthesis and hydrogen storage studies of metal-organic framework UiO-66. in *Int. J. Hydrogen Energy* (2013). doi:10.1016/j.ijhydene.2013.01.163

61. Sanchez-Sanchez, M., Getachew, N., Diaz, K., Diaz-Garcia, M., Chebude, Y. & Diaz, I. Synthesis of metal-organic frameworks in water at room temperature: salts as linker sources. *Green Chem.* **17,** 1500–1509 (2015).

62. Cravillon, J., Münzer, S., Lohmeier, S. J., Feldhoff, A., Huber, K. & Wiebcke, M. Rapid room-temperature synthesis and characterization of nanocrystals of a prototypical zeolitic imidazolate framework. *Chem. Mater.* **21,** 1410–1412 (2009).

63. Rubio-Martinez, M., Avci-Camur, C., Thornton, A. W., Imaz, I., Maspoch, D. & Hill, M. R. New synthetic routes towards MOF production at scale. *Chem. Soc. Rev.* (2017). doi:10.1039/c7cs00109f

64. Jeremias, F., Henninger, S. K. & Janiak, C. Ambient pressure synthesis of MIL-100(Fe) MOF from homogeneous solution using a redox pathway. *Dalt. Trans.* (2016). doi:10.1039/c6dt01179a

65. Avci-Camur, C., Perez-Carvajal, J., Imaz, I. & Maspoch, D. Metal Acetylacetonates as a Source of Metals for Aqueous Synthesis of Metal–Organic Frameworks. *ACS Sustain. Chem. Eng.* **6,** 14554–14560 (2018).

66. Fateeva, A., Horcajada, P., Devic, T., Serre, C., Marrot, J., Grenèche, J.-M., Morcrette, M., Tarascon, J.-M., Maurin, G. & Férey, G. Synthesis, Structure, Characterization, and Redox Properties of the Porous MIL-68(Fe) Solid. *Eur. J. Inorg. Chem.* **2010,** 3789–3794 (2010).

67. Surblé, S., Serre, C., Mellot-Draznieks, C., Millange, F. & Férey, G. A new isoreticular class of metal-organic-frameworks with the MIL-88 topology. *Chem. Commun.* (2006). doi:10.1039/b512169h

68. Taylor-Pashow, K. M. L., Della Rocca, J., Xie, Z., Tran, S. & Lin, W. Postsynthetic modifications of iron-carboxylate nanoscale metal-organic frameworks for imaging and drug delivery. *J. Am. Chem. Soc.* (2009). doi:10.1021/ja906198y

69. Serre, C., Millange, F., Surblé, S., Grenèche, J.-M. & Férey, G. Synthesis, Characterization, and Properties of an Open-Framework Iron(III) Dicarboxylate: MIL-85 or FeIII2O{O2C–CH3}2{O2C–C6H4–CO2}·2CH3OH. *Chem. Mater.* (2004).

70. Lee, Y. R., Kim, J. & Ahn, W. S. Synthesis of metal-organic frameworks: A mini review. *Korean J. Chem. Eng.* **30,** 1667–1680 (2013).

71. Stock, N. & Biswas, S. Synthesis of metal-organic frameworks (MOFs): Routes to various MOF topologies, morphologies, and composites. *Chem. Rev.* **112,** 933–969 (2012).

72. Sung, H. J., Lee, J. H. & Chang, J. S. Microwave synthesis of a nanoporous hybrid material, chromium trimesate. *Bull. Korean Chem. Soc.* (2005). doi:10.5012/bkcs.2005.26.6.880

73. Seoane, B., Zamaro, J. M., Tellez, C. & Coronas, J. Sonocrystallization of zeolitic imidazolate frameworks (ZIF-7, ZIF-8, ZIF-11 and ZIF-20). *CrystEngComm* (2012). doi:10.1039/c2ce06382d

74. Paseta, L., Potier, G., Sorribas, S. & Coronas, J. Solventless synthesis of MOFs at high pressure. *ACS Sustain. Chem. Eng.* **4,** 3780–3785 (2016).

75. Li, M. & Dincă, M. Reductive electrosynthesis of crystalline metal-organic frameworks. *J. Am. Chem. Soc.* (2011). doi:10.1021/ja2041546

76. Echaide-Górriz, C., Clément, C., Cacho-Bailo, F., Téllez, C. & Coronas, J. New strategies based on microfluidics for the synthesis of metal–organic frameworks and their membranes. *J. Mater. Chem. A* **6,** 5485–5506 (2018).

77. Stassen, I., Styles, M., Van Assche, T., Campagnol, N., Fransaer, J., Denayer, J., Tan, J. C., Falcaro, P., De Vos, D. & Ameloot, R. Electrochemical film deposition of the zirconium metal-organic framework uio-66 and application in a miniaturized sorbent trap. *Chem. Mater.* (2015). doi:10.1021/cm504806p

78. Avci-Camur, C., Troyano, J., Pérez-Carvajal, J., Legrand, A., Farrusseng, D., Imaz, I. & Maspoch, D. Aqueous production of spherical Zr-MOF beads: Via continuous-flow spray-drying. *Green Chem.* (2018). doi:10.1039/c7gc03132g

79. Carné-Sánchez, A., Imaz, I., Cano-Sarabia, M. & Maspoch, D. A spray-drying strategy for synthesis of nanoscale metal-organic frameworks and their assembly into hollow superstructures. *Nat. Chem.* (2013). doi:10.1038/nchem.1569

80. Cölfen, H. & Mann, S. Higher-order organization by mesoscale self-assembly and transformation of hybrid nanostructures. *Angew. Chemie - Int. Ed.* (2003). doi:10.1002/anie.200200562

81. Tsuruoka, T., Furukawa, S., Takashima, Y., Yoshida, K., Isoda, S. & Kitagawa, S. Nanoporous nanorods fabricated by coordination modulation and oriented attachment growth. *Angew. Chemie - Int. Ed.* **48,** 4739–4743 (2009).

82. Diring, S., Furukawa, S., Takashima, Y., Tsuruoka, T. & Kitagawa, S. Controlled multiscale synthesis of porous coordination polymer in nano/micro regimes. *Chem. Mater.* (2010). doi:10.1021/cm101778g

83. Stock, N. & Biswas, S. Synthesis of metal-organic frameworks (MOFs): Routes to various MOF topologies, morphologies, and composites. *Chem. Rev.* (2012). doi:10.1021/cr200304e

84. Xiong, W. W. & Zhang, Q. Surfactants as Promising Media for the Preparation of Crystalline Inorganic Materials. *Angew. Chemie - Int. Ed.* (2015). doi:10.1002/anie.201502277

85. Seoane, B., Dikhtiarenko, A., Mayoral, A., Tellez, C., Coronas, J., Kapteijn, F. & Gascon, J. Metal organic framework synthesis in the presence of surfactants: Towards hierarchical MOFs? *CrystEngComm* (2015). doi:10.1039/c4ce02324b

86. Umemura, A., Diring, S., Furukawa, S., Uehara, H., Tsuruoka, T. & Kitagawa, S. Morphology design of porous coordination polymer crystals by coordination modulation. *J. Am. Chem. Soc.* (2011). doi:10.1021/ja204233q

87. Pham, M. H., Vuong, G. T., Fontaine, F. G. & Do, T. O. Rational synthesis of metal-organic framework nanocubes and nanosheets using selective modulators and their morphology-dependent gas-sorption properties. *Cryst. Growth Des.* (2012). doi:10.1021/cg300297p

88. Schaate, A., Roy, P., Godt, A., Lippke, J., Waltz, F., Wiebcke, M. & Behrens, P. Modulated synthesis of Zr-based metal-organic frameworks: From nano to single crystals. *Chem. - A Eur. J.* **17,** 6643–6651 (2011).

89. Wißmann, G., Schaate, A., Lilienthal, S., Bremer, I., Schneider, A. M. & Behrens, P. Modulated synthesis of Zr-fumarate MOF. *Microporous Mesoporous Mater.* (2012). doi:10.1016/j.micromeso.2011.12.010

90. Parnham, E. R. & Morris, R. E. Ionothermal synthesis of zeolites, metal-organic frameworks, and inorganic-organic hybrids. *Acc. Chem. Res.* (2007). doi:10.1021/ar700025k

91. Sumida, K., Liang, K., Reboul, J., Ibarra, I. A., Furukawa, S. & Falcaro, P. Sol-Gel Processing of Metal-Organic Frameworks. *Chem. Mater.* (2017). doi:10.1021/acs.chemmater.6b03934

92. Howarth, A. J., Peters, A. W., Vermeulen, N. A., Wang, T. C., Hupp, J. T. & Farha, O. K. Best practices for the synthesis, activation, and characterization of metal–organic frameworks. *Chem. Mater.* (2017). doi:10.1021/acs.chemmater.6b02626

93. Alhamami, M., Doan, H. & Cheng, C. H. A review on breathing behaviors of metal-organic-frameworks (MOFs) for gas adsorption. *Materials (Basel).* **7,** 3198–3250 (2014).

94. Wang, Z. & Cohen, S. M. Postsynthetic modification of metal-organic frameworks. *Chem. Soc. Rev.* (2009). doi:10.1039/b802258p

95. Sorribas, S., Zornoza, B., Téllez, C. & Coronas, J. Ordered mesoporous silica-(ZIF-8) core-shell spheres. *Chem. Commun.* (2012). doi:10.1039/c2cc34893d

96. Seoane, B., Sebastián, V., Téllez, C. & Coronas, J. Crystallization in THF: The possibility of one-pot synthesis of mixed matrix membranes containing MOF MIL-68(Al). *CrystEngComm* (2013). doi:10.1039/c3ce40847g

97. Hermes, S., Schröder, F., Chelmowski, R., Wöll, C. & Fischer, R. A. Selective nucleation and growth of metal-organic open framework thin films on patterned COOH/CF3-terminated self-assembled monolayers on Au(111). *J. Am. Chem. Soc.* (2005). doi:10.1021/ja053523l

98. Petit, C. & Bandosz, T. J. MOF-graphite oxide composites: Combining the uniqueness of graphene layers and metal-organic frameworks. *Adv. Mater.* (2009). doi:10.1002/adma.200901581

99. Lee, J., Farha, O. K., Roberts, J., Scheidt, K. A., Nguyen, S. T. & Hupp, J. T. Metal–organic framework materials as catalysts. *Chem. Soc. Rev.* **38,** 1450 (2009).

100. Cunha, D., Ben Yahia, M., Hall, S., Miller, S. R., Chevreau, H., Elkaïm, E., Maurin, G., Horcajada, P. & Serre, C. Rationale of drug encapsulation and release from biocompatible porous metal-organic frameworks. *Chem. Mater.* **25,** 2767–2776 (2013).

101. Shimizu, G. K. H., Taylor, J. M. & Kim, S. Proton conduction with metal-organic frameworks. *Science (80-.).* (2013). doi:10.1126/science.1239872

102. Kreno, L. E., Leong, K., Farha, O. K., Allendorf, M., Van Duyne, R. P. & Hupp, J. T. Metal-organic framework materials as chemical sensors. *Chem. Rev.* (2012). doi:10.1021/cr200324t

103. Mingabudinova, L. R., Vinogradov, V. V., Milichko, V. A., Hey-Hawkins, E. & Vinogradov, A. V. Metal-organic frameworks as competitive materials for non-linear optics. *Chem. Soc. Rev.* (2016). doi:10.1039/c6cs00395h

104. Sheberla, D., Bachman, J. C., Elias, J. S., Sun, C. J., Shao-Horn, Y. & Dincă, M. Conductive MOF electrodes for stable supercapacitors with high areal capacitance. *Nat. Mater.* (2017). doi:10.1038/nmat4766

105. Silva, C. G., Corma, A. & García, H. Metal-organic frameworks as semiconductors. *J. Mater. Chem.* (2010). doi:10.1039/b924937k

106. Sadakiyo, M., Yamada, T. & Kitagawa, H. Rational designs for highly proton-conductive metal-organic frameworks. *J. Am. Chem. Soc.* (2009). doi:10.1021/ja9040016

107. Blair, L. H., Colakel, A., Vrcelj, R. M., Sinclair, I. & Coles, S. J. Metal-organic fireworks: MOFs as integrated structural scaffolds for pyrotechnic materials. *Chem. Commun.* (2015). doi:10.1039/c5cc04174k

108. Kim, H., Yang, S., Rao, S. R., Narayanan, S., Kapustin, E. A., Furukawa, H., Umans, A. S., Yaghi, O. M. & Wang, E. N. Water harvesting from air with metal-organic frameworks powered by natural sunlight. *Science (80-.).* (2017). doi:10.1126/science.aam8743

109. Slater, A. G. & Cooper, A. I. Function-led design of new porous materials. *Science (80-.).* (2015). doi:10.1126/science.aaa8075

110. Khan, N. A., Hasan, Z. & Jhung, S. H. Adsorptive removal of hazardous materials using metal-organic frameworks (MOFs): A review. *J. Hazard. Mater.* (2013). doi:10.1016/j.jhazmat.2012.11.011

111. Wen, J., Fang, Y. & Zeng, G. Progress and prospect of adsorptive removal of heavy metal ions from aqueous solution using metal–organic frameworks: A review of studies from the last decade. *Chemosphere* (2018). doi:10.1016/j.chemosphere.2018.03.047

112. Office of Energy efficiency & Renewable energy, available at: www.energy.gov/eere/fuelcells/hydrogen-storage, 19 Februar 2019.

113. Pan, L., Sander, M. B., Huang, X., Li, J., Smith, M., Bittner, E., Bockrath, B. & Johnson, J. K. Microporous Metal Organic Materials: Promising Candidates as Sorbents for Hydrogen Storage. *J. Am. Chem. Soc.* (2004). doi:10.1021/ja0392871

114. Chae, H. K., Siberio-Pérez, D. Y., Kim, J., Go, Y., Eddaoudi, M., Matzger, A. J., O'Keeffe, M. & Yaghi, O. M. A route to high surface area, porosity and inclusion of large molecules in crystals. *Nature* (2004). doi:10.1038/nature02311

115. Rowsell, J. L. C., Millward, A. R., Park, K. S. & Yaghi, O. M. Hydrogen Sorption in Functionalized Metal–Organic Frameworks. *J. Am. Chem. Soc.* **126,** 5666–5667 (2004).

116. Chen, B., Ockwig, N. W., Millward, A. R., Contreras, D. S. & Yaghi, O. M. High H2 adsorption in a microporous metal-organic framework with open metal sites. *Angew. Chemie - Int. Ed.* (2005). doi:10.1002/anie.200462787

117. Farha, O. K., Yazaydin, A. Ö., Eryazici, I., Malliakas, C. D., Hauser, B. G., Kanatzidis, M. G., Nguyen, S. T., Snurr, R. Q. & Hupp, J. T. De novo synthesis of a metal-organic framework material featuring ultrahigh surface area and gas storage capacities. *Nat. Chem.* (2010). doi:10.1038/nchem.834

118. Wang, Q., Luo, J., Zhong, Z. & Borgna, A. CO2 capture by solid adsorbents and their applications: Current status and new trends. *Energy Environ. Sci.* (2011). doi:10.1039/c0ee00064g

119. Liu, J., Thallapally, P. K., McGrail, B. P., Brown, D. R. & Liu, J. Progress in adsorption-based CO 2 capture by metal-organic frameworks. *Chem. Soc. Rev.* (2012). doi:10.1039/c1cs15221a

120. Britt, D., Furukawa, H., Wang, B., Glover, T. G. & Yaghi, O. M. Highly efficient separation of carbon dioxide by a metal-organic framework replete with open metal sites. *Proc. Natl. Acad. Sci.* (2009). doi:10.1073/pnas.0909718106

121. Seoane, B., Coronas, J., Gascon, I., Benavides, M. E., Karvan, O., Caro, J., Kapteijn, F. & Gascon, J. Metal-organic framework based mixed matrix membranes: A solution for highly efficient CO2 capture? *Chem. Soc. Rev.* (2015). doi:10.1039/c4cs00437j

122. Yaghi, O. M., Li, G. & Li, H. Selective binding and removal of guests in a microporous metal–organic framework. *Nature* (1995). doi:10.1038/378703a0

123. Chen, B., Liang, C., Yang, J., Contreras, D. S., Clancy, Y. L., Lobkovsky, E. B., Yaghi, O. M. & Dai, S. A microporous metal-organic framework for gas-chromatographic separation of alkanes. *Angew. Chemie - Int. Ed.* (2006). doi:10.1002/anie.200502844

124. Pan, L., Olson, D. H., Ciemnolonski, L. R., Heady, R. & Li, J. Separation of hydrocarbons with a microporous metal-organic framework. *Angew. Chemie - Int. Ed.* (2006). doi:10.1002/anie.200503503

125. Hoskins, B. F. & Robson, R. Design and Construction of a New Class of Scaffolding-like Materials Comprising Infinite Polymeric Frameworks of 3D-Linked Molecular Rods. A Reappraisal of the Zn(CN)2 and Cd(CN)2 Structures and the Synthesis and Structure of the Diamond-Related Framework. *J. Am. Chem. Soc.* (1990). doi:10.1021/ja00160a038

126. Yilmaz, B., Trukhan, N. & Müller, U. Industrial Outlook on Zeolites and Metal Organic Frameworks. *Chinese J. Catal.* (2012). doi:10.1016/S1872-2067(10)60302-6

127. Fujita, M., Washizu, S., Ogura, K. & Kwon, Y. J. Preparation, Clathration Ability, and Catalysis of a Two-Dimensional Square Network Material Composed of Cadmium(II) and 4, 4′-Bipyridine. *J. Am. Chem. Soc.* (1994). doi:10.1021/ja00082a055

128. Lee, J., Farha, O. K., Roberts, J., Scheidt, K. A., Nguyen, S. T. & Hupp, J. T. Metal-organic framework materials as catalysts. *Chem. Soc. Rev.* (2009). doi:10.1039/b807080f

129. Ma, L., Abney, C. & Lin, W. Enantioselective catalysis with homochiral metal-organic frameworks. *Chem. Soc. Rev.* (2009). doi:10.1039/b807083k

130. Wu, C. De & Zhao, M. Incorporation of Molecular Catalysts in Metal–Organic Frameworks for Highly Efficient Heterogeneous Catalysis. *Adv. Mater.* (2017). doi:10.1002/adma.201605446

131. Zamaro, J. M., Pérez, N. C., Miró, E. E., Casado, C., Seoane, B., Téllez, C. & Coronas, J. HKUST-1 MOF: A matrix to synthesize CuO and CuO-CeO 2 nanoparticle catalysts for CO oxidation. *Chem. Eng. J.* (2012). doi:10.1016/j.cej.2012.04.091

132. Allendorf, M. D., Houk, R. J. T., Andruszkiewicz, L., Talin, A. A., Pikarsky, J., Choudhury, A., Gall, K. A. & Hesketh, P. J. Stress-induced chemical detection using flexible metal-organic frameworks. *J. Am. Chem. Soc.* **130,**

14404–14405 (2008).

133. Lan, A., Li, K., Wu, H., Olson, D. H., Emge, T. J., Ki, W., Hong, M. & Li, J. A luminescent microporous metal-organic framework for the fast andreversible detection of high explosives. *Angew. Chemie - Int. Ed.* (2009). doi:10.1002/anie.200804853

134. Lü, Y., Zhan, W., He, Y., Wang, Y., Kong, X., Kuang, Q., Xie, Z. & Zheng, L. MOF-templated synthesis of porous Co3O4concave nanocubes with high specific surface area and their gas sensing properties. *ACS Appl. Mater. Interfaces* (2014). doi:10.1021/am405858v

135. Wang, L., Zhang, Y., Li, X., Xie, Y., He, J., Yu, J. & Song, Y. The MIL-88A-Derived Fe3O4-Carbon Hierarchical Nanocomposites for Electrochemical Sensing. *Sci. Rep.* **5,** 14341 (2015).

136. Liédana, N., Lozano, P., Galve, A., Téllez, C. & Coronas, J. The template role of caffeine in its one-step encapsulation in MOF NH $_2$ -MIL-88B(Fe). *J. Mater. Chem. B* **2,** 1144–1151 (2014).

137. Paseta, L., Potier, G., Abbott, S. & Coronas, J. Using Hansen solubility parameters to study the encapsulation of caffeine in MOFs. *Org. Biomol. Chem.* **13,** 1724–1731 (2015).

138. Monteagudo-Olivan, R., Paseta, L., Potier, G., López-Ram-de-Viu, P. & Coronas, J. Solvent-Free Encapsulation at High Pressure with Carboxylate-Based MOFs. *Eur. J. Inorg. Chem.* (2018). doi:10.1002/ejic.201800985

139. Monteagudo-Olivan, R., Cocero, M. J., Coronas, J. & Rodríguez-Rojo, S. Supercritical CO2 encapsulation of bioactive molecules in carboxylate based MOFs. *J. CO2 Util.* **30,** 38–47 (2019).

140. Keskin, S. & Kizilel, S. Biomedical Applications of Metal Organic Frameworks. *Ind. Eng. Chem. Res.* (2011). doi:10.1021/ie101312k

141. Della Rocca, J., Liu, D. & Lin, W. Nanoscale Metal–Organic Frameworks for Biomedical Imaging and Drug Delivery. *Acc. Chem. Res.* **44,** 957–968 (2011).

142. Kharisov, B. I., Rasika Dias, H. V., Kharissova, O. V., Manuel Jiménez-Pérez, V., Olvera Pérez, B. & Muñoz Flores, B. Iron-containing nanomaterials: Synthesis, properties, and environmental applications. *RSC Adv.* (2012). doi:10.1039/c2ra20812a

143. Decoste, J. B. & Peterson, G. W. Metal-organic frameworks for air purification of toxic chemicals. *Chem. Rev.* (2014). doi:10.1021/cr4006473

144. Li, J., Wang, X., Zhao, G., Chen, C., Chai, Z., Alsaedi, A., Hayat, T. & Wang, X. Metal–organic framework-based materials: superior adsorbents for the capture of toxic and radioactive metal ions. *Chem. Soc. Rev.* (2018). doi:10.1039/C7CS00543A

145. Hasan, Z. & Jhung, S. H. Removal of hazardous organics from water using metal-organic frameworks (MOFs): Plausible mechanisms for selective adsorptions. *J. Hazard. Mater.* (2015). doi:10.1016/j.jhazmat.2014.09.046

146. Lismont, M., Dreesen, L. & Wuttke, S. Metal-Organic Framework Nanoparticles in Photodynamic Therapy: Current Status and Perspectives. *Adv. Funct. Mater.* (2017). doi:10.1002/adfm.201606314

147. Ehrenmann, J., Henninger, S. K. & Janiak, C. Water adsorption characteristics of MIL-101 for heat-transformation applications of MOFs. *Eur. J. Inorg. Chem.* (2011). doi:10.1002/ejic.201001156

148. Cadiau, A., Lee, J. S., Damasceno Borges, D., Fabry, P., Devic, T., Wharmby, M. T., Martineau, C., Foucher, D., Taulelle, F., Jun, C. H., Hwang, Y. K., Stock, N., De Lange, M. F., Kapteijn, F., Gascon, J., Maurin, G., Chang, J. S. & Serre, C. Design of Hydrophilic Metal Organic Framework Water Adsorbents for Heat Reallocation. *Adv. Mater.* (2015). doi:10.1002/adma.201502418

149. Perea-Cachero, A., Dechnik, J., Lahoz, R., Janiak, C., Téllez, C. & Coronas, J. HKUST-1 coatings on laser-microperforated brass supports for water adsorption. *CrystEngComm* (2017). doi:10.1039/c6ce02490d

150. Dhainaut, J., Avci-Camur, C., Troyano, J., Legrand, A., Canivet, J., Imaz, I., Maspoch, D., Reinsch, H. & Farrusseng, D. Systematic study of the impact of MOF densification into tablets on textural and mechanical properties. *CrystEngComm* (2017). doi:10.1039/c7ce00338b

151. MOFapps, available at: www.mofapps.com, accesed:19th February 2019.

152. MOF Technologies, available at: www.moftechnologies.com, accesed 19th February 2019.

153. NuMat Technologies, available at: www.numat-tech.com, accesed 19th February 2019.

154. Promethean particles, available at: www.prometheanparticles.co.uk/mofs-metal-organic-frameworks/, accesed:19th February 2019.

155. MOFWORKS, available at: www.mofworx.com, accesed: 19th February 2019.

156. ACSYNAM, available at: www.acsynam.com, accesed: 19th Februay 2019.

157. NovoMOF, available at: www. novomof.com, accesed: 19th February 2019.

158. Feng, X., Ding, X. & Jiang, D. Covalent organic frameworks. *Chem. Soc. Rev.* (2012). doi:10.1039/c2cs35157a

159. Côté, A. P., Benin, A. I., Ockwig, N. W., O'Keeffe, M., Matzger, A. J. & Yaghi, O. M. Chemistry: Porous, crystalline, covalent organic frameworks. *Science (80-.).* (2005). doi:10.1126/science.1120411

160. El-Kaderi, H. M., Hunt, J. R., Mendoza-Cortés, J. L., Côté, A. P., Taylor, R. E., O'Keeffe, M. & Yaghi, O. M. Designed synthesis of 3D covalent organic frameworks. *Science (80-.).* (2007). doi:10.1126/science.1139915

161. Ding, S. Y. & Wang, W. Covalent organic frameworks (COFs): From design to applications. *Chem. Soc. Rev.* (2013). doi:10.1039/c2cs35072f

162. Nune, S. K., Thallapally, P. K. & McGrail, B. P. Metal organic gels (MOGs): A new class of sorbents for CO2 separation applications. *J. Mater. Chem.* (2010). doi:10.1039/c0jm01907k

163. Chen, Y., Huang, X., Zhang, S., Li, S., Cao, S., Pei, X., Zhou, J., Feng, X. & Wang, B. Shaping of Metal-Organic Frameworks: From Fluid to Shaped Bodies and Robust Foams. *J. Am. Chem. Soc.* (2016). doi:10.1021/jacs.6b06959

164. Vallejo-Sánchez, D., Amo-Ochoa, P., Beobide, G., Castillo, O., Fröba, M., Hoffmann, F., Luque, A., Ocón, P. & Pérez-Yáñez, S. Chemically Resistant, Shapeable, and Conducting Metal-Organic Gels and Aerogels Built from Dithiooxamidato Ligand. *Adv. Funct. Mater.* (2017). doi:10.1002/adfm.201605448

Chapter 2:

Reactive gas atmospheres as a tool for the synthesis of MOFs: the creation of a metal hybrid fumarate with a controlled Fe/Al composition profile

State of the article:

Published in Journal of Materials Chemistry A, 2018, 6, 14352-14358. DOI:10.1039/C8TA03557A and reproduced by permission of The Royal Society of Chemistry

Rebeca Monteagudo-Olivan,[a] Manuel Arruebo,[a,b] Pilar López-Ram-de-Viu,[c] Victor Sebastian*[a,b] and Joaquín Coronas*[a]

[a] Chemical and Environmental Engineering Department and Instituto de Nanociencia de Aragón (INA), Universidad de Zaragoza, 50018 Zaragoza, Spain.

[b] Networking Research Center on Bioengineering, Biomaterials and Nanomedicine, CIBER-BBN, 28029 Madrid, Spain.

[c] Departamento de Química Orgánica, Universidad de Zaragoza, and Instituto Universitario de Catálisis Homogénea (Universidad de Zaragoza-CSIC), 50009 Zaragoza, Spain

Journal metrics:

Impact factor 9.931 (year 2019) and Q1 (Chemistry, miscellaneous)

2.1. Summary and graphical abstract

The use of gas reacting atmospheres is proposed here as a new tool to control the synthesis of MOFs. With the addition of Al to an Fe-fumarate synthesis medium (which produces the typical structure of MOF MIL-88A(Fe)), a hybrid Fe/Al-fumarate that exhibits the structure of MOF MIL-53(Al)-FA was obtained even though both metals could be identified in the resulting material by STEM-HAADF. The use of CO and O_2 atmospheres (6 bar) in the synthesis of both MIL-88A(Fe) and MIL-53(Fe/Al)-FA might accelerate their synthesis and gave rise to a highly crystalline solid and to core-shell nanoparticles (190±42 nm) with an Fe-rich core surrounded by an Al-rich shell, i.e., with a controlled Fe/Al atomic distribution. After pyrolysis the MIL-53(Fe/Al)-FA particles exhibited superparamagnetism while keeping some texture (244 m^2/g vs. 862 m^2/g of the as made material).

2.2. Reactive gas atmospheres as a tool for the synthesis of MOFs: the creation of a metal hybrid fumarate with a controlled Fe/Al composition profile

INTRODUCTION

The effect of using different gas environments during the growth of nanoparticles (NPs) is considered of paramount importance because the crystallization kinetics can be in this manner modified to control their size and shape.[1] For instance, the influence of a variety of reactive gas atmospheres has been studied to produce faceted Pd NPs: 1) O_2 promoted the formation of rod shaped NPs, 2) CO directed the synthesis towards 1.5 nm thick-nanosheets and unique surface plasmon resonance characteristics, and 3) N_2 rendered randomly shaped NPs. Additionally, a variety of iron oxide-based magnetic NPs with different crystalline phases and shapes can be obtained just by selecting different gas atmospheres.[2]

Reactive gas synthesis conditions can also modify the structure of preformed NPs. The CO and NO adsorption energies on certain facets of Pt and Pd can be large enough to cause the surface energies to be negative, and promote the breakup of metal surfaces and the dispersion of metal NPs.[3] H_2 and CO gas environments were also selected to tune the atomic distribution and the catalytic performance of Pt-Cu NPs by a post-synthesis reaction.[4] Other structural phenomena in reactive gas conditions are: reconstruction,[5] reshaping,[6] resegregation[7] and phase transition.[8]

The growth of metal-organic frameworks (MOFs) under reactive gas synthesis conditions is unexplored. Just CO environments were considered in a variety of post-synthesis treatments on MOFs: 1) to study the binding of carbonyl species to MOFs composed of Fe^{2+} or Co^{2+},[9] 2) to modify amino-MOFs (NH_2-MIL-53(Al)) to their isocyanate analogues using CO,[10] 3) to load CO in a metal-CO complex to control its release in therapeutic applications,[11] and 4) CO removal.[12] MOF Fe-BTTri exhibited an unprecedented spin state change mechanism for the highly selective reversible adsorption of CO over H_2, N_2, CO_2 and various hydrocarbons.[13] The effects caused by the presence of gases can be concomitant with those caused by high temperatures, giving rise to the segregation of 5-15 nm CuO NPs in case of HKUST-1.[14]

In liquid phase it is also known the effect of some small molecules on the shape and crystallinity of MOF particles. In the coordination modulation approach[15] a monocaboxylate ligand is added to the reaction media although it is not part of the final structure and does not aim to accelerate the synthesis. For example, acetic acid improved the crystallinity of $[\{Cu_2(ndc)_2(dabco)\}_n]$[15] and UiO-66,[16] and sodium formate that of

ZIF-8.[17] Not only carboxylates but other different species can be used with the purpose of controlling the MOF synthesis. For instance, caffeine was used in the synthesis of amino-MIL-88B(Fe),[18] and different radicals produced new isostructural MOFs incorporating them as pendant or guest species.[19]

We propose here the application of air, O_2 and CO atmospheres to modify the synthesis of MOFs: i) accelerating and improving their crystallization kinetics, and ii) making possible the production of hybrid core-shell structures, i.e., fumarate- containing MOFs[20–22] with a controlled Fe/Al atomic distribution. Gases, generally with limited solubility in the liquid reaction medium, have the advantage of leaving the reaction once the pressure is decreased, while the other above-mentioned species may remain in the liquid phase polluting the mother liquor and products.

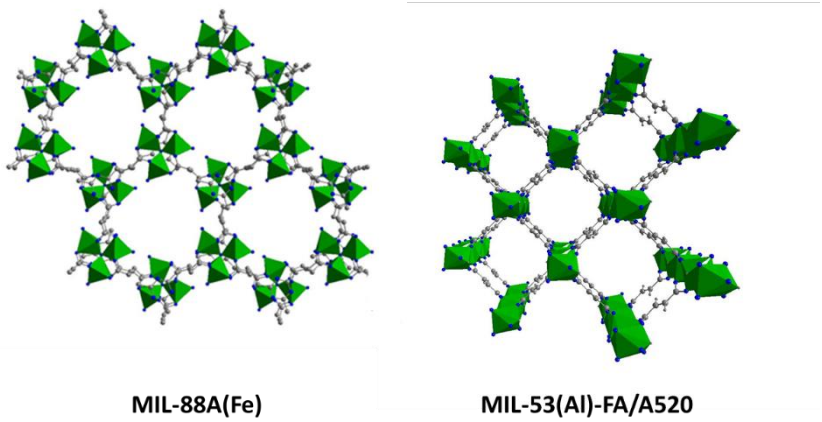

Figure 1. MOFs addressed in this work. Color code: coordination polyhedral of the metal centers (green), oxygen atoms (blue) and carbon atoms (grey). The structures were represented by using Diamond 3.2. with the crystallographic information files in CCDC.[21,22]

Hybrid MOF-based materials can be of two different types. MOF-MOF type, e.g., by seeding the IRMOF-3 synthesis medium with IRMOF-1 particles.[23] The other type corresponds to either mixed-metal MOFs, e.g., MOF-74 with different combinations of divalent metals,[24] or mixed-ligand MOFs, as in the case of ZIF-300, -301 and 302 synthesized by incorporating two distinct imidazolates.[25] Hybrid MOFs may find application as efficient catalysts, adsorbents[25] and membrane fillers,[26] among others. In addition, hybrid MOFs can be considered as functionalized MOFs, and these can help the rational design and synthesis of adsorbents and separation materials.[27]

We have attempted the production of MOFs using either single or sequential reactive gas environments. Fe-fumarate (MIL-88A(Fe)), Al-fumarate (MIL-53(Al)-FA) (Figure 1) and Fe/Al-fumarate hybrids have been synthesized under different reactive gas

atmospheres. This has given rise to new MOF type nanomaterials with a controlled distribution of Fe and Al atoms and with the structure of the recently solved Al-fumarate MIL-53(Al)-FA (an analogue of the MIL-53(Al)-BDC, previously known as MOF A520).[22,28] Finally, one of the new MOFs was pyrolyzed to obtain particles with magnetic properties. The carbonization of MOFs, using them as sacrificial templates, has been carried out as a way of obtaining catalytic nanoparticles,[14] nanoporous carbons,[29] metal/carbon composites,[30] magnetic nanoparticles,[31] Zn-air battery components[32] and hybrid supercapacitors,[33] among others.

EXPERIMENTAL SECTION

Chemicals and methods

The experimental setup for the synthesis of the nanoparticulated MOFs consisted in a high-pressure Teflon-lined stainless-steel autoclave with a capacity of 40 mL and a connection for feeding gases. The autoclave was immersed in a water bath at 90 °C with magnetic stirring. Three types of reactive atmospheres were used: the self-generated or autogenous in air, and with CO or O_2 at 6 bar. The preparation of reagents was carried out under air atmosphere and the resulting reaction mixture was introduced in the autoclave and was flushed under CO or O_2 flow. The autoclave atmosphere was swept several times to achieve a pure gas atmosphere of CO or O_2 and remove any trace of air. The required chemicals were dimethylformamide (DMF, Scharlau, 99.5%) as solvent, fumaric acid (FA, Acros Organics, ≥99%), iron (III) chloride hexahydrate ($FeCl_3 \cdot 6H_2O$, Sigma Aldrich, ≥98%) and aluminum nitrate nonahydrate ($Al(NO_3)_3 \cdot 9H_2O$, Sigma Aldrich, ≥98%). These chemicals were used as received.

Table 1 summarizes the three reactive atmospheres (self-generated or autogenous in air, CO or O_2 at 6 bar) and gas exposure times used during the growth of MOFs at 90°C. In the syntheses corresponding to the Fe-fumarate (MIL-88A(Fe), series 1 of experiments in Table 1), fumaric acid (232 mg, 2 mmol) was dissolved in 5 mL of DMF and separately $FeCl_3 \cdot 6H_2O$ (540 mg, 2 mmol) in 5 mL of DMF. Final concentrations for each reactant were 200 mM. The same procedure was used for Al-fumarates (MIL-53(Al)-FA, series 2 of experiments) but with an $Al(NO_3)_3 \cdot 9H_2O$ solution (750 mg, 2 mmol) instead of that of iron. To synthesize Fe/Al-fumarate hybrids (series 3 of experiments), fumaric acid (FA, 232 mg, 2 mmol) was dissolved in 5 mL of DMF and separately $Al(NO_3)_3 \cdot 9H_2O$ (375 mg, 1 mmol) with $FeCl_3 \cdot 6H_2O$ (270 mg, 1 mmol) in 5 mL of DMF. The molar ratio was 1Fe:1Al:2FA. Both solutions were mixed in each experiment just before to be added to the reactor.

Table 1 Reaction conditions at 90 °C with CO and O_2 at 6 bar each and their corresponding dwelling times. Phase numeration refers to MIL-88A(Fe) [1], yellowish solution-black colloid [2], MIL-53(Al)-FA [3], core-shell MIL-53(Fe/Al)-FA [4], MIL-53(Fe/Al)-FA [5], no solid obtained [6] and insufficient amount for XRD characterization [7].

Run	Molar ratio	CO	O_2	Autogenous	Phase
1.1	2Fe.2FA.129DMF			6 h	[1]
1.2		6 h			[2]
1.3				1.25 h	[1]
1.4			1.25 h		[1]
1.5		1 h	15 min		[1]
2.1	2Al:2FA:129DMF			6 h	[3]
2.2		6 h			[3]
2.3				1.25 h	[6]
2.4			1.25 h		[6]
3.1	1Fe:1Al.2FA.129DMF	1 h	5 min		[7]
3.2		1 h	10 min		[4]
3.3		1 h	15 min		[4]
3.4		1 h	1 h		[5]
3.5		3 h	3 h		[5]
3.6				1.25 h	[6]
3.7				6 h	[5]

Characterization techniques

The characterization of the powdered samples was carried by X-ray diffraction (XRD, Siemens D-500 diffractometer) with a copper anode and a graphite monochromator (Cu-$K_{\alpha 1}$ radiation, λ= 1.540 Å) in the 4-40° 2θ range with a scanning rate of 0.01°/s. The UV-Vis spectra were recorded with a V-670 Jasco spectrophotometer. Thermogravimetric analysis (TGA, Mettler Toledo TGA/STDA 851e) was measured from 30 to 700 °C in air with a heating ramp of 10°C/min. The N_2 isotherms were obtained with a Micrometrics TriStar 3000 and specific surface areas were calculated by the BET method. A transmission electron microscope (TEM, Tecnai FEI T20) operating at an acceleration voltage 200 kV with a LaB6 electron source fitted with a "SuperTwin®" objective lens allowing a point-to-point resolution of 2.4 Å was selected to study the nanocrystal morphology. Tecnai F30 transmission electron microscopy fitted with a SuperTwin® lens allowing a point resolution of 1.9 Å was also selected. High-Angle Annular Dark Field (HAADF) and EDS detectors were used to determine the location of Al and Fe by Z-contrast imaging.

The magnetic behavior of the iron-containing oxidized MOFs was measured at 37 °C in a superconducting quantum interference device (SQUID MPMS-5S, Quantum Design Inc.) from 0 to 4 Tesla. The powdered samples were measured in a gelatin capsule and a diamagnetic correction for the sample holder was performed.

RESULTS AND DISCUSSION

Synthesis of MIL-88A(Fe) in different atmospheres

Figure 2-a,b shows that the transparent orange MIL-88A(Fe) precursors rendered a dark orange colloid after 6 h of reaction under autogenous pressure (run **1.1** in Table 1). Elongated square bipyramid microcrystals (ca. 1x2 μm) with a monodisperse size and regular morphology were obtained under these conditions. A green-yellowish solution when the MIL-88A(Fe) precursors were exposed to a 6 bar CO atmosphere for 6 h was obtained (run **1.2**). This solution was not stable and after 10 min a black suspension was obtained (Figure 2-c). The hue exhibited a color transition from the air-liquid interphase to the bottom (Figure 2-c). This fact would imply that the observed transition was sensitive to the presence of O_2. After centrifugation, a black slurry was recovered which became an orange solid once dried. TEM images revealed 80-90 nm nanocrystals (Figure 2-c). The black color of the suspension was preserved if the CO treated solution was kept under an inert atmosphere. Similar results were obtained when the solution was treated with CO for 1 h, but no color change was observed in the precursor or in the product if the reagents were treated with CO for 5 min.

Considering that the resulting CO treated solution was sensitive to oxygen, it was subsequently exposed to an O_2 atmosphere (run **1.5**). This promoted the formation of an orange colloid instead of the above-mentioned black colored slurry (Figure 2- c). Even if the final product was also orange, it showed a narrower value of FWHM (full width at half maximum) for the most intense XRD peak at 10.1° than the previous two materials obtained under autogenous pressure (run **1.3**) and 6 bar O_2 (run **1.4**), 3.8 and 1.6 times lower, respectively (see Figure 3-B). Regarding the TEM morphology, more heterogeneous and aggregated particles are observed in the case of using an O_2-based synthesis only (Figure 3C). In addition, the modification of the reaction environment produced an increase in the MOF weight yield (based on the ligand FA calculated by TGA): 1% in autogenous atmosphere (run **1.3**), 2% under O_2 (run **1.4**) and 17% with the combination of CO and O_2 (run **1.5**).

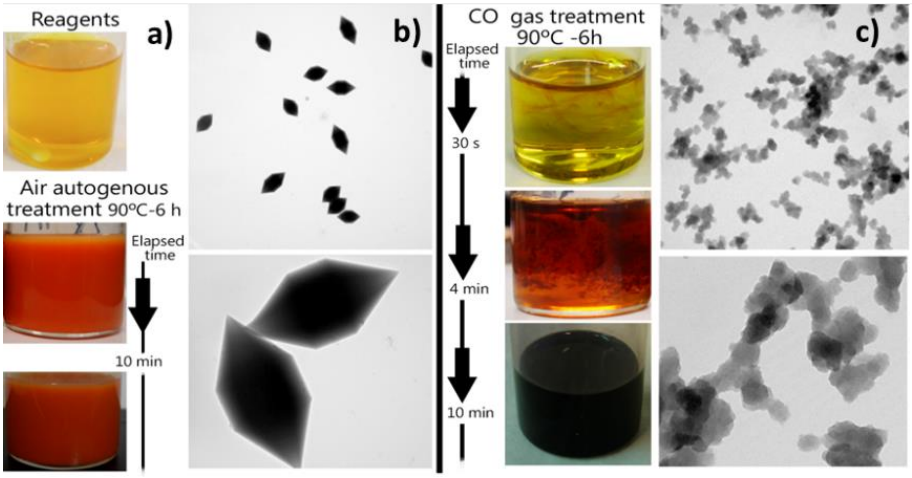

Figure 2. Synthesis of MIL-88A(Fe) crystals at 6 h and 90 °C with autogenous (run **1.1**) and CO atmosphere (run **1.2**). Optical and TEM images of: (a) MIL-88A(Fe) precursors. (b) MIL-88A(Fe) colloid and crystals produced with autogenous pressure (run **1.1**). (c) MIL-88A(Fe) colloid and crystals produced under 6 bar CO atmosphere (run **1.2**) where the color transition was completed in 10 min.

To explain the favorable effect of the CO atmosphere on the crystallization of MIL-88A(Fe) we focused on the solution chemistry of the MOF precursors. Fe^{3+} coupled with carboxylate ligands produces two main secondary building blocks: a) a chain of corner sharing octahedra with iron atoms linked through a μ_2-oxo bridge; and b) μ_3-oxo centered trimers of iron octahedra. The coupling of these clusters with linear dicarboxylate ligands gives rise to solids such as MIL-53, MIL-68 (both from chains Fe O-Fe), MIL-88 and MIL-101 (from trimeric Fe_3O units).[34] As shown in Figure 2, the syntheses produced suspensions with visible properties. This suggested the use of UV-Vis spectroscopy to gain insight into the influence of the CO atmosphere on the MOF synthesis. In fact, this spectroscopy has recently been used to monitor the synthesis of bimetallic MOF hybrid structures.[35] The UV-Vis spectrum of the MIL-88A(Fe) precursors solution (Figure 3A-b) shows two intense bands at 318 and 360 nm, characteristic of ligand-to-metal charge transfer (LMCT) transitions from the μ_2-oxo ligand to iron in diferric Fe-O-Fe complexes. [34]

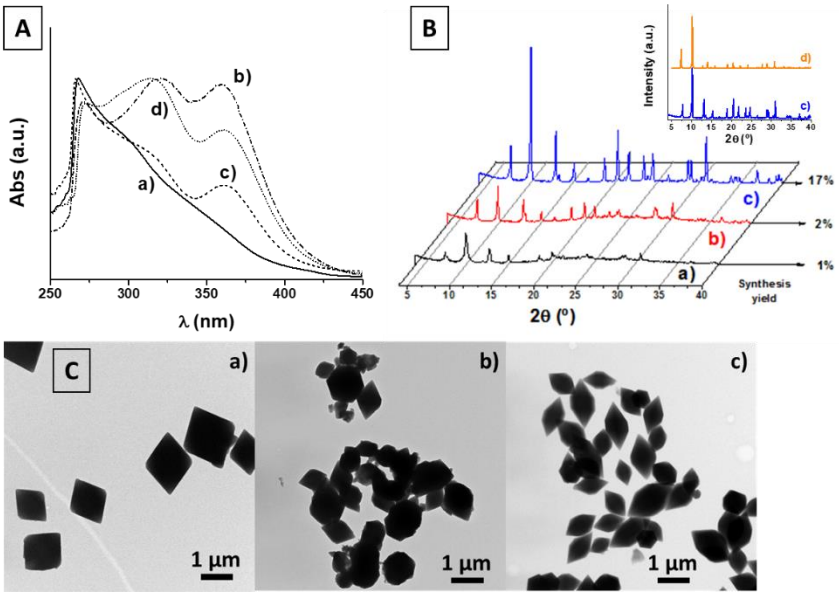

Figure 3. A) UV-Vis spectra of: (a) Fe^{2+} + FA, (b) Fe^{3+} + FA, (c) Fe^{3+} + FA + 1 h CO and (d) Fe^{3+} + FA + 1 h CO + 15 min O_2. B) Diffraction patterns of the resulting products of the syntheses for 1.25 h at 90 °C with different gases from bottom to top: (a) autogenous atmosphere (run **1.3**), (b) O_2 at 6 bar (run **1.4**), (c) 1 h CO at 6 bar + 15 min O_2 at 6 bar (run **1.5**), and (d) simulated pattern of MIL-88A(Fe).[21] C) TEM images of syntheses for 1.25 h at 90 °C in: (a) autogenous atmosphere (run **1.3**), (b) O_2 at 6 bar (run **1.4**), (c) 1 h CO at 6 bar + 15 min O_2 at 6 bar (run **1.5**).

Accordingly, we hypothesize that dimers $[Fe(\mu_2\text{-}O)(\mu_2\text{-}OOC\text{-}R)_2FeL_2]^{2+}$ (L= solvent molecule) or related polynuclear chains are firstly formed in solution and a solid from these octahedral units is obtained (Figure 4-a). For further MIL-88A(Fe) nucleation, intermediate solid would redissolve to release dimeric Fe-O-Fe units that would equilibrate with trimers Fe_3O for crystallization of MIL-88A(Fe). In fact, the formation and dissolution of different clusters in MOF crystallization has been previously described.[36] Since the MOF crystallinity increases with time, it is probable that the dimers-trimers equilibrium is slow.

The UV-Vis spectrum of the green-yellowish solution obtained when MIL-88A(Fe) precursors are in contact with CO atmosphere (Figure 3A-c) shows a decrease in the LMCT transitions assigned to μ_2-oxo-Fe being similar to that of Fe^{2+}/FA in DMF (Figure 3A-a). Then, a reduction of diferric to diferrous Fe-O-Fe complexes due to the reductive CO atmosphere is plausible. (Figure 4-b). Stable structures of oxo bridged diferrous complexes with carboxylate ligands appear to require a μ_2-hydroxo bridge.[33,34,36–38] Diferrous Fe-(OH)-Fe complexes have been described to give greenish-yellow solutions that change to reddish-brown by oxidation to diferric Fe-O-Fe species in presence of air.[34–39] From these observations, we postulate the formation of a diferrous $[Fe^{II}(\mu_2\text{-}OH)(\mu_2\text{-}OOC\text{-}R)_2Fe^{II}L_2]^{+}$ complex in the green-yellowish solution exposed to the CO atmosphere. This soluble complex would be partially oxidized by air leading to mixed

valence iron Fe^{2+}/Fe^{3+} polynuclear species that aggregate to render the unstable black solid, which can be further over-oxidized to the orange solid derived from ferric trimers Fe_3O (Figure 4-b). However, the complete oxidation of green diferrous Fe-(OH)-Fe complex by treatment with O_2 leads directly to the orange solid MIL-88A(Fe) with high crystallinity (run **1.5**). The UV-Vis spectrum of the resulting solution (Figure 3A-d) shows LMCT-transitions at 314 nm and 360 nm that are assigned to trimers $[Fe_3(\mu_3\text{-}O)(\mu_2\text{-}OOC\text{-}R)_6L_3]^+$ and aggregate to form MIL-88A(Fe). The fast formation of trimers Fe_3O by oxidation from diferrous Fe-(OH)-Fe complexes can be explained by the occurrence of intermediate dimeric mixed species Fe^{2+}-O-Fe^{3+} in equilibrium with trimeric mixed species $Fe^{2+}{}_2Fe^{3+}O$, well known in organometallic chemistry.[40,41]

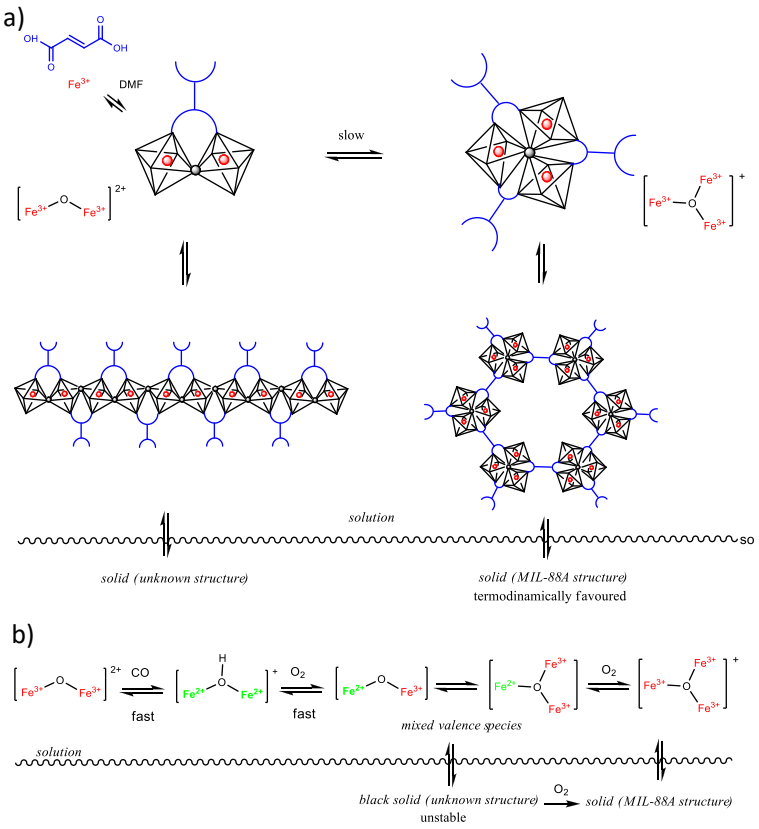

Figure 4. a) Hypothetical scheme of synthesis of MIL-88(Fe) in autogenous atmosphere. Iron (III) atoms are represented by red balls; each corner of octahedra is occupied by oxygen atoms but only shared oxygens are represented by grey balls; for simplicity, bidentate fumaric ligands are represented by blue connectors and only one of each pair of ligands is depicted. b) Scheme of the synthesis of MIL-88(Fe) in CO and O_2 atmospheres.

Synthesis of hybrids of Fe and Al with the MIL-53(Al)-FA structure

The CO atmosphere had no influence on the synthesis of Al-fumarate with MIL-53(Al)-FA structure at 90 °C for 6 h, probably due to lack of Al redox activity in the

working conditions. The syntheses for 6 h in autogenous (run 2.1) and CO (run 2.2) atmospheres generated white products with identical diffraction patterns (Figure 5A) and similar particle morphologies (Figure 5C). When the reaction time was reduced to 1.25 h (run 2.3) no solid product was obtained, even in O_2 atmosphere (run 2.4).

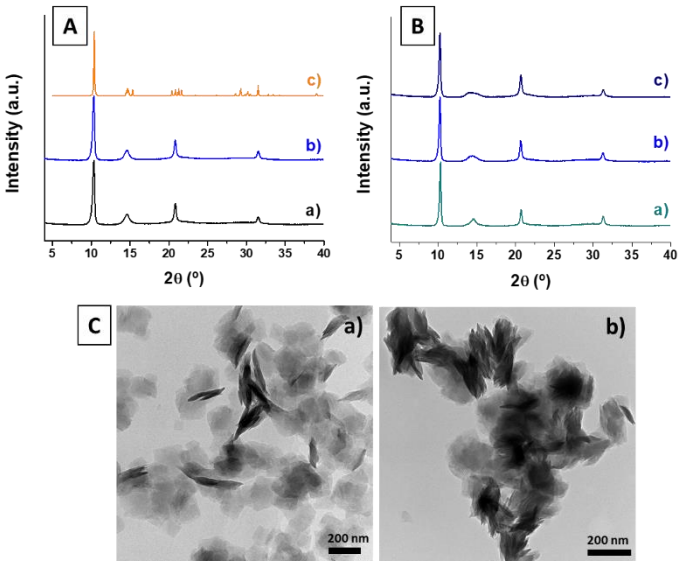

Figure 5. A) XRD results of synthesis of Al-fumarate at 90°C for 6 h under: (a) autogenous atmosphere (run **2.1**), (b) CO at 6 bar (run **2.2**), and (c) simulated pattern.[22] B) Synthesis of Fe/Al-fumarate at 90°C for 1.25 h (a) 1 h CO + 10 min O_2 (**3.2**), (b) 1 h CO + 15 min O_2 (run **3.3**) and (c) 1 h CO + 1 h O_2 (run **3.4**). C) TEM images of Al-fumarate corresponding to: (a) autogenous atmosphere (run **2.1**), and (b) CO at 6 bar (run **2.2**).

A series of experiments (Figure 6-a) were performed with the molar ratio of 1Fe:1Al:2FA, a previous treatment for 1 h in CO at 6 bar and a final exposure to O_2 at 6 bar for 5 min (run **3.1**), 10 min (run **3.2**), 15 min (run **3.3**) and 60 min (run **3.4**). The obtained products showed the MIL-53(Al)-FA structure, as verified by XRD (Figure 5B), except for the sample exposed during 5 min which yielded an insufficient amount of powder for its XRD characterization. EDS analysis revealed that particles produced after 5 min of O_2 treatment were composed practically of iron (Figure 6-b). This is consistent with a faster nucleation for the Fe based phase than that based on Al. Core-shell nanoparticles were synthesized if the O_2 treatment duration was between 5 and 15 min (Figure 6-c). These nanoparticles consist of a core rich in Fe (high brightness by Z contrast) surrounded by a shell where Al predominates (Figure 6-h). No core-shell structure was observed by Z contrast if the O_2 treatment were maintained for 1 h or more (Figure 6-d), but EDS analysis depicted a constant Fe/Al profile across the metal fumarate particles and confirmed the non- segregated location of Fe and Al (Figure 6-h). These results indicate that the obtained particles were Fe/Al-MOF hybrid entities. The mechanism for the transformation of the Fe-rich core would involve the diffusion of the

ligand fumarate from the reaction media to the inner of the nanoparticle or probably by the exchange of Fe by Al (favored by the existence of a common MIL-53-FA structure). It is worth mentioning that until now the reported pure Fe-fumarates have the MIL-88A(Fe) structure,[21] meanwhile Al-fumarates that of MIL-53(Al)-FA (Figure 5).[22] However, the hybrid Fe/Al–fumarate obtained here exhibits only the XRD intensities corresponding to the MIL-53(Al)-FA structure with no other crystalline phases present. This agrees with a material having such crystalline structure in both core and shell. This argument based on the powder XRD is reinforced by the high BET specific surface area of 862 m^2/g currently measured for the hybrid Fe/Al–fumarate, not far from that of MIL-53(Al)-FA (939 m^2/g).[42] Nevertheless, the presence of some of an amorphous Fe based compound in the core may not be totally discarded.

The duration of the O_2 treatment had a strong influence on the atomic distribution of both Fe and Al. A constant Fe/Al ratio across the MOF was obtained with autogenous atmosphere conditions (run **3.7**). A short O_2 treatment (6 bar, 15 min) (run **3.3**) after 6 bar CO favored the crystallization of 190±42 nm particles with a core rich in Fe (Figure 6-e,f), i.e., relatively high Fe/Al, surrounded by a shell with a low Fe/Al atomic ratio. Figure S1 illustrates the STEM–HAADF image corresponding to a MIL-53(Fe/Al)-FA nanoparticle after tilting it from +33° to -35°, inferring with this insight that a core-shell structure was obtained in agreement with the EDS analysis profile depicted in Figure 6-h.

The organic component of the core-shell particles (run **3.3**) was reduced by treating them at 400 °C for 1h. At this temperature, the organic part of the material was totally degraded, as shown in the corresponding thermogravimetric curve (Figure S2), resulting in a dark brown powder with amorphous structure (Figure S3). Nanoporous carbon materials have been already reported by direct carbonization of Zn- and Co-MOFs,[31,43] even giving rise to magnetic Co nanoparticles with a magnetization up to 59 emu/g.[31] However, to the best of our knowledge, no single report can be related to such type of particles from MIL-53 structures. STEM-HAADF images confirmed that the core-shell structure was maintained after calcination (Figure 6-i,j). EDS profile also confirmed the location of the Fe-rich core (Figure 6-k). Interestingly, calcined NPs showed magnetic behavior as they were attracted to a permanent magnet. The magnetic properties were studied by SQUID showing superparamagnetic behavior with no coercivity or remanent magnetization up to 4 Tesla (Figure S4). Their magnetic moment at 4 Tesla and 37°C was 1.4 emu/g.

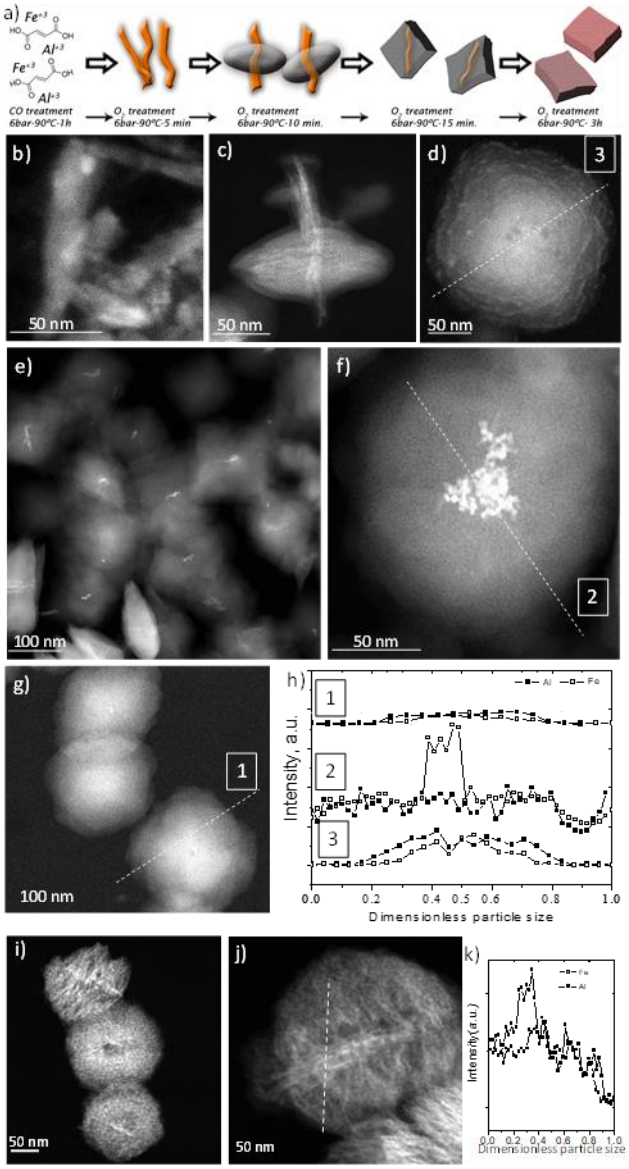

Figure 6. STEM-HAADF images of Al-Fe MOF nanoparticles produced at different conditions (90°C and with the gases at 6 bar). (a) Scheme of the formation mechanism. (b) 1 h CO + 5 min O_2 (run **3.1**), (c) 1 h CO + 10 min O_2 (run **3.2**), (d) 3 h CO + 3h O_2 (run **3.5**). (e-f) 1 h CO + 15 min O_2 (run **3.3** (g) 6 h autogenous atmosphere (run **3.7**). (h) EDS analysis profiles from NPs produced at different conditions: 1) 6 h autogenous atmosphere (run **3.7**), 2) 1 h CO + 15 min O_2 (run **3.3**), 3) 3 h CO + 3 h O_2 run (**3.5**). (i-j) sample (run **3.3**) calcined at 400 °C for 1h; (k) EDS analysis profile from the white marked line in (j).

Additionally, the BET specific surface area and pore volume were calculated from N_2 adsorption data before (862 m^2/g and 0.763 cm^3/g at P/P_0 0.989) and after (244 m^2/g and 0.591 cm^3/g at P/P_0 0.987) calcination. Even if the adsorption capacity (Figure S4) and specific surface area decreased upon the partial calcination of the material, the remaining values are relatively high, highlighting the potential use of the resulting material in typical MOF applications such as catalysis,[44] drug delivery[45] and electronics,[43] among others.

Conclusions

In summary, we carried out the synthesis of MOFs MIL-88A(Fe) and MIL-53(Fe/Al)-FA in CO and O_2 gas reacting atmospheres for the first time in the field of MOF materials. Furthermore, these conditions made possible the creation of a metal hybrid fumarate with a controlled Fe/Al profile: core-shell particles with a Fe-rich core surrounded by an Al-rich shell.

The crystallinity, particle size in the nanometer range, superparamagnetism and textural properties exhibited by some of the particles obtained here allows one to highlight their potential use in several fields related to catalysis, medicine and electronics.

References

1. Sebastian, V., Smith, C. D. & Jensen, K. F. Shape-controlled continuous synthesis of metal nanostructures. *Nanoscale* **8,** 7534–7543 (2016).
2. Larrea, A., Sebastian, V., Ibarra, A., Arruebo, M. & Santamaria, J. Gas Slug Microfluidics: A Unique Tool for Ultrafast, Highly Controlled Growth of Iron Oxide Nanostructures. *Chem. Mater.* **27,** 4254–4260 (2015).
3. Zhu, B., Meng, J. & Gao, Y. Equilibrium Shape of Metal Nanoparticles under Reactive Gas Conditions. *J. Phys. Chem. C* **121,** 5629–5634 (2017).
4. Shan, J. *et al.* Tuning Catalytic Performance through a Single or Sequential Post-Synthesis Reaction(s) in a Gas Phase. *ACS Catal.* **7,** 191–204 (2017).
5. Tao, F. *et al.* Restructuring of hex-Pt(100) under CO gas environments: Formation of 2-D nanoclusters. *Nano Lett.* **9,** 2167–2171 (2009).
6. Vendelbo, S. B. *et al.* Visualization of oscillatory behaviour of Pt nanoparticles catalysing CO oxidation. *Nat. Mater.* **13,** 884–890 (2014).
7. Tao, F. *et al.* Reaction-driven restructuring of Rh-Pd and Pt-Pd core-shell nanoparticles. *Science (80-.).* **322,** 932–934 (2008).
8. Baldi, A., Narayan, T. C., Koh, A. L. & Dionne, J. a. In situ detection of hydrogen-induced phase transitions in individual palladium nanocrystals. *Nat. Mater.* **13,** 1143–1148 (2014).
9. Gallagher, A. T., Malliakas, C. D. & Harris, T. D. CO Binding at a Four-Coordinate Cobaltous Porphyrin Site in a Metal-Organic Framework: Structural, EPR, and Gas Adsorption Analysis. *Inorg. Chem.* **56,** 4654–4661 (2017).

10. Lescouet, T., Vitillo, J. G., Bordiga, S., Canivet, J. & Farrusseng, D. An alternative pathway for the synthesis of isocyanato- and urea-functionalised metal-organic frameworks. *Dalton Trans.* **42,** 8249–58 (2013).

11. Diring, S. *et al.* Light responsive metal–organic frameworks as controllable CO-releasing cell culture substrates. *Chem. Sci.* **8,** 2381–2386 (2017).

12. Zhang, X., Zhan, Z., Li, Z. & Di, L. Thermal Activation of CuBTC MOF for CO Oxidation: The Effect of Activation Atmosphere. *Catalysts* **7,** 106 (2017).

13. Reed, D. A. *et al.* Reversible CO scavenging via adsorbate-dependent spin state transitions in an iron(II)-triazolate metal-organic framework. *J. Am. Chem. Soc.* **138,** 5594–5602 (2016).

14. Zamaro, J. M. *et al.* HKUST-1 MOF: A matrix to synthesize CuO and CuO-CeO 2 nanoparticle catalysts for CO oxidation. *Chem. Eng. J.* **195–196,** 180–187 (2012).

15. Tsuruoka, T. *et al.* Nanoporous nanorods fabricated by coordination modulation and oriented attachment growth. *Angew. Chemie - Int. Ed.* **48,** 4739–4743 (2009).

16. Schaate, A. *et al.* Modulated synthesis of Zr-based metal-organic frameworks: From nano to single crystals. *Chem. - A Eur. J.* **17,** 6643–6651 (2011).

17. Cravillon, J. *et al.* Controlling zeolitic imidazolate framework nano- and microcrystal formation: Insight into crystal growth by time-resolved in situ static light scattering. *Chem. Mater.* **23,** 2130–2141 (2011).

18. Liedana, N., Lozano, P., Galve, A., Tellez, C. & Coronas, J. The template role of caffeine in its one-step encapsulation in MOF NH2-MIL-88B(Fe). *J. Mater. Chem. B* **2,** 1144–1151 (2014).

19. Faust, T. B. & D'Alessandro, D. M. Radicals in metal-organic frameworks. *RSC Adv.* **4,** 17498–17512 (2014).

20. Serre, C., Millange, F., Surblé, S. & Férey, G. A Route to the Synthesis of Trivalent Transition-Metal Porous Carboxylates with Trimeric Secondary Building Units. *Angew. Chemie Int. Ed.* **43,** 6285–6289 (2004).

21. Serre, C. *et al.* Role of Solvent-Host Interactions That Lead to Very Large Swelling of Hybrid Frameworks. *Science (80-.).* **315,** 1828–1831 (2007).

22. Alvarez, E. *et al.* The structure of the aluminum fumarate metal-organic framework A520. *Angew. Chemie - Int. Ed.* **54,** 3664–3668 (2015).

23. Yoo, Y. & Jeong, H. K. Heteroepitaxial growth of isoreticular metal-organic frameworks and their hybrid films. *Cryst. Growth Des.* **10,** 1283–1288 (2010).

24. Wang, L. J. *et al.* Synthesis and characterization of metal-organic framework-74 containing 2, 4, 6, 8, and 10 different metals. *Inorg. Chem.* **53,** 5881–5883 (2014).

25. Nguyen, N. T. T. *et al.* Selective capture of carbon dioxide under humid conditions by hydrophobic chabazite-type zeolitic imidazolate frameworks. *Angew. Chemie - Int. Ed.* **53,** 10645–10648 (2014).

26. Sánchez-Laínez, J. *et al.* Tuning the Separation Properties of Zeolitic Imidazolate Framework

Core-Shell Structures via Post-Synthetic Modification. *J. Mater. Chem. A* **5,** 25601–25608 (2017).

27. Han, Y. *et al.* In-situ ligand formation-driven preparation of a heterometallic metal-organic framework for highly selective separation of light hydrocarbons and efficient mercury adsorption. *ACS Appl. Mater. Interfaces* **8,** 23331–23337 (2016).

28. Yot, P. G. *et al.* Mechanical energy storage performance of an aluminum fumarate metal-organic framework. *Chem. Sci.* **7,** 446–450 (2016).

29. Chaikittisilp, W., Ariga, K. & Yamauchi, Y. A new family of carbon materials: synthesis of MOF-derived nanoporous carbons and their promising applications. *J. Mater. Chem. A* **1,** 14–19 (2013).

30. Raoof, J. B., Hosseini, S. R., Ojani, R. & Mandegarzad, S. MOF-derived Cu/nanoporous carbon composite and its application for electro-catalysis of hydrogen evolution reaction. *Energy* **90,** 1075–1081 (2015).

31. Torad, N. L. *et al.* Direct synthesis of MOF-derived nanoporous carbon with magnetic Co nanoparticles toward efficient water treatment. *Small* **10,** 2096–2107 (2014).

32. Guo, Z. *et al.* In Situ Encapsulation of Core–Shell–Structured Co@Co3O4 into Nitrogen-Doped Carbon Polyhedra as a Bifunctional Catalyst for Rechargeable Zn–Air Batteries. *J. Mater. Chem. A* **6,** 1443 (2017).

33. Kim, J. *et al.* Nanoarchitecture of MOF-derived nanoporous functional composites for hybrid supercapacitors. *J. Mater. Chem. A* **5,** 15065–15072 (2017).

34. Solomon, E. I., Tuczek, F., Root, D. E. & Brown, C. A. Spectroscopy of Binuclear Dioxygen Complexes. *Chem. Rev.* **94,** 827–856 (1994).

35. Guo, W. *et al.* Kinetic-Controlled Formation of Bimetallic Metal–Organic Framework Hybrid Structures. *Small* (2017). doi:10.1002/smll.201702049

36. Millange, F. *et al.* Time-resolved in situ diffraction study of the solvothermal crystallization of some prototypical metal-organic frameworks. *Angew. Chemie - Int. Ed.* **49,** 763–766 (2010).

37. Chaudhury, P., Wieghardt, K., Nuber, B. & Weiss, J. [L2Fe 2II(μ-OH)(μ-CH3CO2)2](ClO4)·H2O, a Model Compound for the Diiron Centers in Deoxyhemerythrin. *Angew. Chemie Int. Ed. English* **24,** 778–779 (1985).

38. Hartman, J. R. *et al.* Synthesis and Characterization of (μ-Hydroxo)bis(μ-acetato)diiron(II) and (μ-Oxo)bis(;u-acetato)diiron(III) 1,4,7-Trimethyl-1,4,7-triazacyclononane Complexes as Models for Binuclear Iron Centers in Biology; properties of the Mixed Valence Diiron(II,III) S. *J. Am. Chem. Soc.* **109,** 7387–7396 (1987).

39. Do, L. H. & Lippard, S. J. Evolution of strategies to prepare synthetic mimics of carboxylate-bridged diiron protein active sites. *J. Inorg. Biochem.* **105,** 1774–1785 (2011).

40. M. Bond, A. *et al.* Synthesis, characterisation and electrochemical reductions of oxo-centred, carboxylate-bridged triiron complexes, [Fe3(μ3-O)-(μ-O2CR)6L3]X (R = Me, But, Ph, CH2Cl, CCl3, CH2CN or 4-NO2C6H4; L = py, 3-H2Npy, 4-H2Npy, 3-NCpy, 4-NCpy or 4-CH2CHpy; X = ClO4- . *J. Chem. Soc., Dalt. Trans.* 1845–1852 (1998). doi:10.1039/A708880I

41. Lawrence, M. A. W., Thomas, S. E., Maragh, P. T. & Dasgupta, T. P. Mechanistic studies on the

intramolecular electron transfer in an adduct species of the oxo-centred trinuclear iron(III) cation and l-ascorbic acid in aqueous solution. *Transit. Met. Chem.* **36,** 553–563 (2011).

42. Paseta, L., Simón-Gaudó, E., Gracia-Gorría, F. & Coronas, J. Encapsulation of essential oils in porous silica and MOFs for trichloroisocyanuric acid tablets used for water treatment in swimming pools. *Chem. Eng. J.* **292,** 28–34 (2016).

43. Salunkhe, R. R. *et al.* Fabrication of symmetric supercapacitors based on MOF-derived nanoporous carbons. *J. Mater. Chem. A* **2,** 19848–19854 (2014).

44. Ai, L., Li, L., Zhang, C., Fu, J. & Jiang, J. MIL-53(Fe): A metal-organic framework with intrinsic peroxidase-like catalytic activity for colorimetric biosensing. *Chem. - A Eur. J.* **19,** 15105–15108 (2013).

45. Ke, F., Qiu, L. G., Yuan, Y. P., Jiang, X. & Zhu, J. F. Fe 3O 4@MOF core-shell magnetic microspheres with a designable metal-organic framework shell. *J. Mater. Chem.* (2012). doi:10.1039/c2jm31167d

2.3. Supporting Information

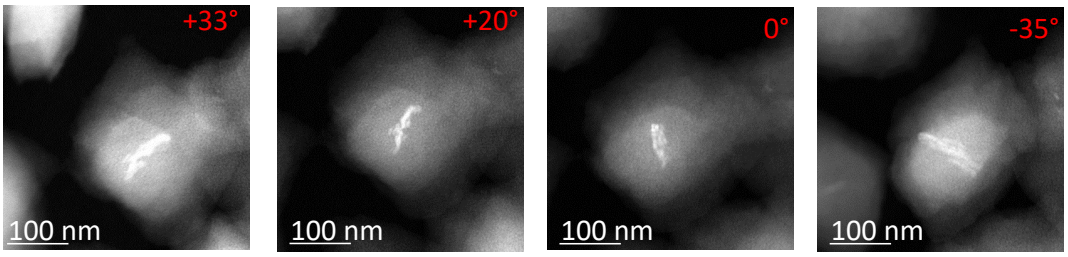

Figure S1. STEM-HAADF images of Al-Fe MOF NPs taken on the same particle after tilting the STEM holder from -35° to 35° (run **3.3**).

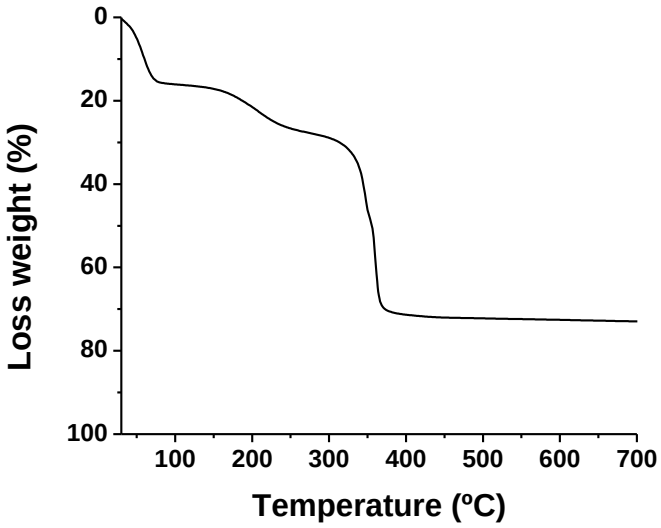

Figure S2. TGA (in air) curve of the as-made core-shell particles (run **3.3**)

.

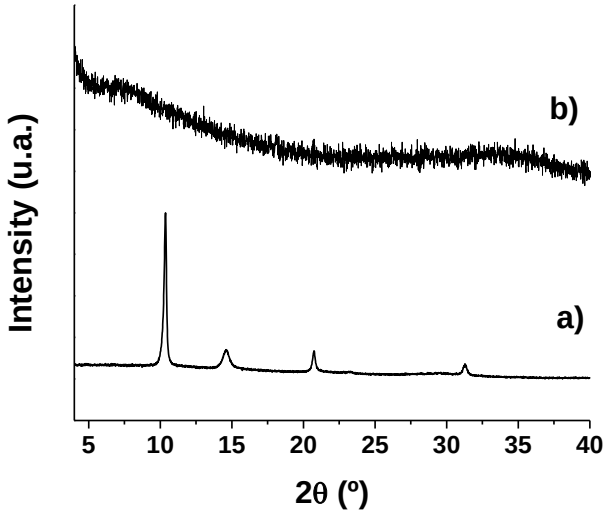

Figure S3. Compared diffraction patterns of the sample (**3.3**) before (a) and after (b) calcination at 400°C for 1 h.

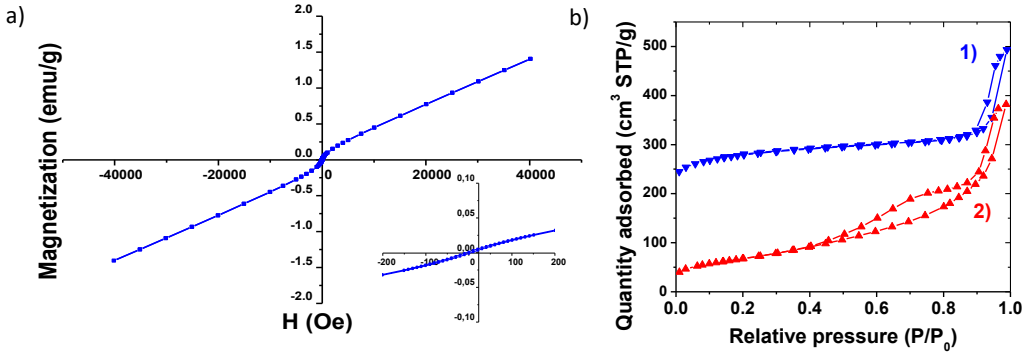

Figure S4. (a) Magnetization curve with the inset showing the region close to the origin with no remanence or coercive field; (b) N_2 adsorption isotherms at 77 K for: 1) the as-made core-shell particles (run **3.3**), and 2) the corresponding calcined product.

Chapter 3:

Hydrogen peroxide effect on the synthesis of terephthalate-based MOF

State of the article:

Under review

Rebeca Monteagudo-Olivan,[a] Isabel Jiménez-Fernández,[a] Pilar López-Ram-de-Viu,[c] Victor Sebastian*[a,b] and Joaquín Coronas*[a]

[a] Chemical and Environmental Engineering Department and Instituto de Nanociencia de Aragón (INA), Universidad de Zaragoza, 50018 Zaragoza, Spain.

[b] Networking Research Center on Bioengineering, Biomaterials and Nanomedicine, CIBER-BBN, 28029 Madrid, Spain.

[c] Departamento de Química Orgánica, Universidad de Zaragoza, and Instituto Universitario de Catálisis Homogénea (Universidad de Zaragoza-CSIC), 50009 Zaragoza, Spain

3.1. Summary

Hydrogen peroxide (H_2O_2) is used to promoter the synthesis of terephthalate-based MOFs, specifically those made from Fe^{3+} and Al^{3+} and mixtures of both. Kinetics and reaction yield were significantly improved, while crystallinity and N_2 adsorption properties were mostly maintained. A reaction mechanism was envisaged from the mass spectroscopy analysis of the solutions involved in the terephthalate synthesis suggesting a μ-hydroxo bridge promoter role for H_2O_2.

3.2. Hydrogen peroxide effect on the synthesis of terephthalate-based MOF

INTRODUCTION

The efficient MOF (metal-organic framework) synthesis is a decisive point for the industrial use of these materials, which are effective in several key applications related to gas separations and storage,[1] selective membranes,[2] catalysis,[3] encapsulation[4,5] and medicine,[6] among others. The commonest synthesis method is the solvothermal or hydrothermal, in which the precursors, i.e. a metal salt and an organic ligand, are dispersed in an organic solvent or water.[7,8] The mixture can be heated up at high temperature (working under autogenous pressure) for relatively long reaction times.

Several methodologies are reported as assisted or alternative to the solvothermal synthesis. The most studied are the microwave[9] and the sonochemical[10] assisted syntheses, which require a more complicated setup. These methods increase nucleation through the perturbances they create in the media. Consequently, they affect crystallization and growth, differently to the basic solvothermal method.[8] Other remarkable methods, the mechanosynthesis and high pressure driven synthesis, i.e. in absence of solvents, have been proved useful, but also only with some MOFs.[8,11]

Alternatively to external physical modifications, *in situ* chemical variations have been successfully described, such as the coordination modulation approach,[12,13] and the use of some additives[14–16] and reactive gas atmospheres.[17] In liquid phase, for modulating the synthesis, a monodentante ligand is added to the liquid media, such as monocarboxylate or amine ligand, and typically improves the crystallinity of the MOF and can modify its shape.[12,13,18] Other chemicals modify size, shape or surface of MOF particles, such as surfactants[14,15] or blocking agents.[16] In the modification of the atmospheres, CO or O_2 at high pressure have been used to improve the crystallinity and to accelerate the synthesis, allowing the creation of particles with different profiles of metal composition.[17]

Hydrogen peroxide (H_2O_2) is a common reductant and strong oxidant used for several applications such as water treatment, pulp and textile bleaching, and chemical synthesis, among others.[19] In water and soil treatment, it is well-known the Fenton reactions of H_2O_2 with iron ions[20,21] to remove persistent organic pollutants, promoting their oxidation.[19] Representative Fenton reactions are as follows:

$$H_2O_2 + Fe^{2+} \rightarrow {\cdot}OH + Fe^{3+} + OH^- \quad (1)$$

$$H_2O_2 + Fe^{3+} \rightarrow HO_2{\cdot} + Fe^{2+} + H^+ \quad (2)$$

with respective k values of 51 $M^{-1}s^{-1}$ and 0.01 $M^{-1}s^{-1}$, in aqueous media at room temperature.[22] Equation (2) is disfavored compared to (1), although (2) is favored in high concentrated solutions of Fe^{3+}.[23] In bleaching, hydrogen peroxide removes the organic components. In chemical synthesis, H_2O_2 role can turn complex. For example, it can promote the hydroxylation in presence of Fe^{2+} of tartaric acid[20] and terephthalic acid,[24] or epoxidation of alkenes.[25,26]

Herein, we observed the promoter or enhancer effect of H_2O_2 on the synthesis of terephthalate-based MOFs with trivalent metals (Fe^{3+} and Al^{3+}), which has not been previously described in the synthesis of hybrid materials, to the best of our knowledge. Firstly, we performed reference experiments to observe the effect of stablished conditions on the final obtained phase, considering that the basis conditions used here are not as those reported. Then, the same experiments were carried out with the addition of different quantities of H_2O_2 to the synthesis media, as promoter of the MOF formation. In all the products, the crystallinity, morphology and N_2 adsorption were compared with the reference synthesis without the promoter to observe changes in the obtained solids. Finally, the MOF synthesis was monitored through different techniques to elucidate the mechanism for H_2O_2 promoter effect.

EXPERIMENTAL SECTION

Chemicals and methods

The experimental setup comprised a Teflon-lined stainless-steel autoclave of 40 mL immersed in a water bath heated at 90 ºC with magnetic stirring. Two types of media were studied: (i) reference experiments with the corresponding metal salts and the ligand using DMF as solvent (set 1), and (ii) departing from these conditions the addition of hydrogen peroxide to the media (sets 2 and 3). The required reagents were terephthalic acid (H_2BDC, Sigma Aldrich, 99%, 2 mmol, 332 mg), iron (III) chloride hexahydrate ($FeCl_3{\cdot}6H_2O$, Sigma Aldrich, ≥98%, 2 mmol, 540 mg or 1 mmol, 270 mg for hybrids), aluminum nitrate nonahydrate ($Al(NO_3)_3{\cdot}9H_2O$, Sigma Aldrich, ≥98%, 2 mmol, 750 mg or 1 mmol, 375 mg for hybrids) and peroxide solution 30% (H_2O_2 (aq), Sigma Aldrich, 204 µL (x1) or 408 µL (x2)). Dimethylformamide (DMF, Scharlau, 99.5%, 10 mL) was used as solvent. Hybrids correspond to the simultaneous use of Fe and Al metals. Solid products were recovered by centrifugation, washed with 5 mL of DMF, dried at room temperature and finally heated at 100 ºC for 24 h to eliminate the encapsulated DMF. Samples with sole aluminum were calcinated at 270 ºC for 3 h with a heating ramp of 3 h.

Table 1. Reaction conditions for the three sets of experiments at 90 ºC. Molar ratio of metal ions, terephthalic acid and solvent for all runs were 2M^{3+} (Al^{3+}, Fe^{3+} or Al^{3+}/ Fe^{3+}, same mol):2H_2BDC:129DMF

Metal(s)	Molar ratio	Run	H_2O_2	Run	H_2O_2	Run	H_2O_2	Time	Phase
Al	2Al:2H_2BDC	1.1		2.1		3.1		1.25 h	MIL-53(Al)
		1.2		2.2		3.2		2.25 h	*as*
Fe	2Fe:2H_2BDC	1.3		2.3		3.3		1.25 h	MIL-68(Fe)
		1.4	---	2.4	x1	3.4	x2	2.25 h	
Al/Fe	1Al:1Fe:2H_2BDC	1.5		2.5		3.5		1.25 h	MIL-68(Al/Fe)
		1.6		2.6		3.6		2.25 h	

Characterization

The crystallinity of powder samples was characterized by X-ray diffraction (XRD, Siemens D-500 diffractometer) in the range of 4-40º 2θ at a scan rate of 0.01º s^{-1} with a copper anode and a graphite monochromator (Cu-$K_{\alpha 1}$ radiation, λ=1.540 Å). Thermogravimetric analysis (TGA, Mettler Toledo TGS/STDA 851e) was carried out under air atmosphere from 30 ºC to 700 ºC with a heating rate of 10 ºC min^{-1}. N_2 adsorption was measured with a Micrometrics TriStar 3000 and specific surface areas were calculated by BET method. Samples were outgassed prior to the analysis under vacuum for 8 h at 200 ºC. Spectroscopic characterization with Raman (WITec alpha 300) was carried out with the 783 nm laser and working at 17 mW (integration time 1.5 s, 25 accumulations and a resolution of 2 cm^{-1}). Particle imaging and morphology were characterized with a scanning electron microscope (SEM, FEI Inspect F50), with a previous Pt coating. Intermediate particle morphology was observed with a transmission electron microscope (TEM, Tecnai F30), operating at an acceleration voltage of 300 kV with a LaB_6 electron source fitted with a "SuperTwin®" objective lens with a point-to-point resolution of 2.4 Å. High-angle annular dark field (HAADF) and EDS (energy dispersive X-ray spectroscopy) detectors were used to determine which chemical elements were present in the produced materials. ^{1}H and ^{13}C NMR spectra in solution were acquired on a Bruker AV-400 spectrometer, the chemical shifts (□) are reported in parts per million from tetramethylsilane with the solvent resonance as the internal standard. The ^{13}C NMR spectra of condensed phases were measured with cross-polarized magic angle spinning solid nuclear magnetic resonance (CP MAS-NMR) in a Bruker Avance III WB 400. High resolution mass spectra (HRMS) were recorded using a Bruker Daltonics MicroToF-Q instrument from methanolic solutions using the positive electrospray ionization mode (ESI+), where cationic fragments were registered at their m/z values.

RESULTS AND DISCUSSION

Influence of metal cations on the final phase

At the same synthesis conditions, different cations in solution (Al^{3+}, Fe^{3+} or the equimolecular mixture of both) gave rise to different phases (Fig. 1). The resulting diffraction patterns were compared with the simulated ones: synthesis based on $Al(NO_3)_3$ was compared with MIL-53(Al) *as* or *ht* (*as*-made and activated at high temperature *ht*),[27] on $FeCl_3$ with MIL-68(Fe)[28] and on both salts with MIL-68(Al/Fe), in which the final product showed the characteristic pattern of MIL-68(Al) (equivalent pattern to that of MIL-68(V))[29,30] with Fe^{3+} partially substituting Al^{3+} in the SBUs. MIL-53(Al) structure consists of 1D rhombohedral channels defined by chains of octahedral coordinated Al^{3+}, connected through μ-OH and μ-terephthalate bridges.[27] Instead, MIL-68 is constructed also by these chains although forming trigonal and hexagonal channels in the final structure.[28] It is not well known the reason why one structure is formed over the other in some conditions.[31]

The colors of the powders were in concordance with their compositions, MIL-53(Al) white, MIL-68(Fe) orange and MIL-68(Al/Fe) pale orange, almost white. Figure 1 shows small undefined rod-like particles of ca. 10-20 nm for MIL-53(Al), rhombohedral particles of ca. 1 μm for MIL-65(Al) and globular particles of 50-150 nm in case of MIL-68(Al/Fe). The small size of MIL-53(Al) particles, in the nanoscale range, was experimentally noticeable by the more difficult separation by centrifugation of the MOF from the solvent. It is also remarkable that in the combined synthesis with both metals, Al^{3+} and Fe^{3+}, there was a higher content of aluminum in the resulting solid as it is inferred by the white pale color of the solid instead of orange color of the iron phase, but iron seemed to direct the final phase to MIL-68 instead of MIL-53, that showed for sole aluminium. The hybrid shows the pattern of MIL-68(Al) instead that of MIL-53(Al) or MIL-68(Fe) (of the MOF synthesized separately). The iron-terephthalate might be nucleating faster, although aluminium is incorporated to the net afterwards. This might be related to ionic radius,[32] MIL-68 of Al and V show the same diffraction pattern[30] and ionic radius for Fe^{3+} and V^{3+},[32,33] are similar.

The most stable phase under heating was MIL-53(Al), which losses the structure integrity at ca. 500 ºC, and the most sensitive to temperature that of MIL-68(Fe), with a degradation step ca. 350 ºC (TGA curves for the three phases after activation are in Fig. S1).

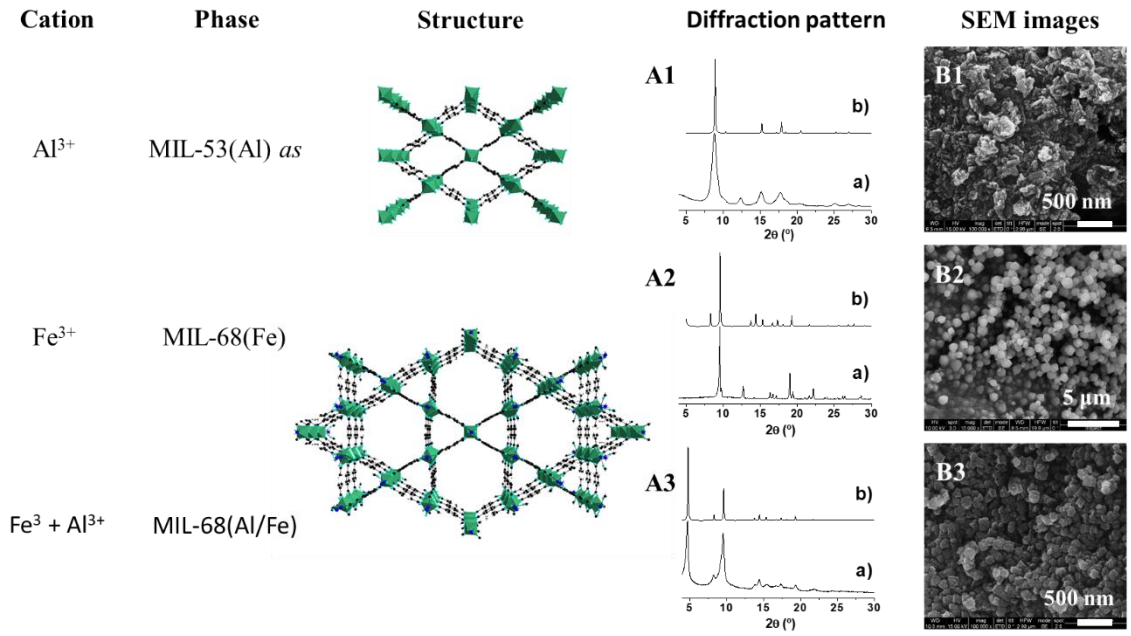

Figure 1. Final phases obtained with Fe^{3+}, Al^{3+} or an equimolar blend of both for 1.25 h, their respective diffraction patterns (A1a, A2a and A3a) compared with the simulated (A1b, A2b and A3b, CIFs 220475, 778931 and 222072), [27–30] and the SEM images of each phase (B1-B3).

After synthesis, encapsulated DMF impurified the MIL-53(Al) *as* phase (see TGA in Fig. S2), which was experimentally noticeable by the harsher activation conditions needed as compared to the MIL-68 phases of Fe^{3+} and Al^{3+}/Fe^{3+}. The actual encapsulation was observed by the thermal stabilization, boiling point temperature for DMF is 152 ºC, although the evaporation step is observed at 250 ºC. In this manner, encapsulated DMF was removed by calcination at 270 ºC for 3 h. However, this activation temperature and time were lower than those reported elsewhere for MIL-53(Al) activation (330 ºC for 72 h, or 380 ºC for 24 h).[5,27] In the reported synthesis in water, some ligand H_2BDC remains encapsulated into the pores and requires high temperature to be degraded above 350 ºC. H_2BDC is poorly soluble in most solvents. In water, encapsulation of H_2BDC might be favored by the better interaction with the pore walls rather than water molecules. Although, the solubility in DMF can be enough to remain in the organic liquid phase instead of into the pores.

Finally, Table S1 shows that the three MOFs were obtained here in milder conditions than those previously reported. It might be explained by the system itself, where a water bath is used to achieve a faster heat transfer than the conventional air convention oven. In addition, a fast heat transfer promotes the nucleation a growth processes that accelerate the MOF production.[34] We also used magnetic stirring, in opposition to the steady reactor, favoring the reaction.

Effect of hydrogen peroxide on the synthesis of MIL-53(Al) *as*

Considering previous results reported by our group where the crystallization of MOFs was accelerated in oxidant atmospheres, it was considered to use H_2O_2 as MOF crystallization promoter.[17] The addition of H_2O_2 (x1 and x2 equivalents or molar proportion with respect to the reactants) to the synthesis media of MIL-53(Al) produced an increment of the reaction yield (Table 2), more remarkable for 1.25 h, when increased from 5% to 49% (runs **1.1**, **2.1** and **3.1**). The highest yield of 74% was obtained for 2.25 h and H_2O_2 with a molar ratio x2 (run **3.2**). The peaks in the diffraction patterns appeared wider in the runs with H_2O_2, suggesting a loss of crystallinity or the reduction of particle size (Fig. S4). However, BET areas remained similar for all experiments, and close to the reported values for MIL-53(Al) (1140 m^2/g).[27]

Regarding the MIL-53(Al) XRD patterns, Figure S3 shows that the main peak at 8.7º shows a shoulder at 9.3º, and a peak at 12.5º also appeared with low intensity for some samples (runs **1.1**, **3.1**, **3.2**). This is in agreement with the presence of a part of the material in the hydrated form, as it can be inferred by the comparison with the simulated pattern of the hydrated or *lt* form, in which water molecules are bound by hydrogen bonds to adjacent carboxylates of terephthalate that narrows the pores and gives rise to different diffraction patterns.[27] Raman spectroscopy highlights these different configurations (Fig. S5 and Table S2). Significant shifts of the carboxylate bands were observed, as hydrogen bonding are lacking, compared to the Raman spectrum of MIL-53 *lt*, while the vibrations corresponding to aromatic stretching and deformations are mainly kept. The band at 179 cm^{-1} of MIL-53(Al) synthesized here is also a remarkable difference, the network in the open pore form shows a lattice vibration (contraction and expansion) of the network (as it is displayed for carbon nanotubes in the radial breathing mode).[35] Solid ^{13}C-NMR (Fig. S6) allowed to gain insight into potential structural differences and chemical environments of MIL-53(Al) synthesized samples with H_2O_2 here and MIL-53(Al) synthesized in water, clear spectra were obtained in both cases, with three peaks corresponding to the three different types of C atoms present in the terephthalate of MOF structure. Since the spectra were almost identical, the chemical environment of the carbon atoms showed no differences, even though the pore configuration was different for each sample.

Table 2. Yield and BET area values for synthesis of MIL-53(Al), MIL-68(Fe) and MIL-68(Al/Fe) in different conditions.

		Blanks			x1 H_2O_2			x2 H_2O_2		
Phase	**Time (h)**	**Run**	**Yield (%)**	**BET area (m^2/g)**	**Run**	**Yield (%)**	**BET area (m^2/g)**	**Run**	**Yield (%)**	**BET area (m^2/g)**
MIL-53 (Al)	1.25	1.1	5.0	-	2.1	27	824	3.1	49	1072
	2.25	1.2	39	1145	2.2	40	1245	3.2	74	1025
MIL-68 (Fe)	1.25	1.3	4.1	-	2.3	0.5	-	3.3	18	-
	2.25	1.4	6.2	186	2.4	4.7	-	3.4	36	53
MIL-68 (Al/Fe)	1.25	1.5	18	1189	2.5	31	1077	3.5	39	396
	2.25	1.6	30	1235	2.6	48	1139	3.6	56	947

All in all, for MIL-53 syntheses a clear increase in yield was observed, preservation of textural properties and generation of smaller particles (SEM images Fig. S4) with broadening diffraction peaks. H_2O_2 displayed a clear promoter effect on the synthesis, affecting the reactants and/or the solvent. Firstly, the chemical modification of the ligand by hydroxylation (given the oxidant function of H_2O_2) of the aromatic ring of the terephthalic acid to form 2-hydroxyterephthalic acid was discarded from the Raman spectra. The shifts for the final phase of MIL-53(Al) treated with H_2O_2 showed the same band pattern of para-substituted aromatic ring, as the reference MIL-53(Al) (see Raman spectra in Fig. S5 and Table S2).

Additionally, the reaction was studied by ^{1}H- and 13C-NMR and high resolution mass spectroscopy (HRMS), with and without H_2O_2, in order to understand why MOF formation evolves differently in presence of hydrogen peroxide. For these studies, an aliquot was taken after 45 min of reaction in both cases. For ^{1}H-NMR analysis, 0.5 mL of the studied solution was mixed with some drops of $CDCl_3$. Even if DMF (reaction solvent) and partially deuterated DMF (formed in analysis mixture) signals were large they allowed to observe potential modifications in the linker terephthalic signals from the aromatic area. However, in agreement with above mentioned Raman study, (Fig.S5) the observed NMR peaks in the reactions with and without H_2O_2 were the same and they correspond to the reference terephthalic acid (Fig. S7).

The reactions were also analyzed by HRMS with and without H_2O_2 (Fig. S8) to study the effect of it on chain precursor formation of MIL-53(Al) (Fig. 2a). Some microliters of samples, taken also at 45, min were diluted in methanol and ionized using the positive electrospray ionization mode (ESI+). Without H_2O_2, several peaks at different m/z ratios were observed. The resolved peaks correspond to positive molecular ions in which Al^{3+} cations are linked by terephthalate bridges, and some molecules of the ionized solvent complete the coordination sphere of metal atoms (m/z 433 and 611). A

single unit is also observed, with one terephthalate ligand linked to the Al^{3+} nucleus (m/z 296) (Fig. 2b). In the sample with H_2O_2, the only observed peak corresponds to a single cation with two terephthalate ligands linked to one Al^{3+} nucleus (m/z 430) (Fig. 2c). In this sample, molecular ions with chains Al-μ-terephthalate-Al of Figure 2b were not observed. Taking into account that 1D structure is known to be present as a ribbon of aluminium linked through μ-OH and μ-terephthalate bridges,[27] it is plausible to suppose that μ -OH bridges were unstable to ionization conditions and they cannot be detected even they were present in the studied solutions.

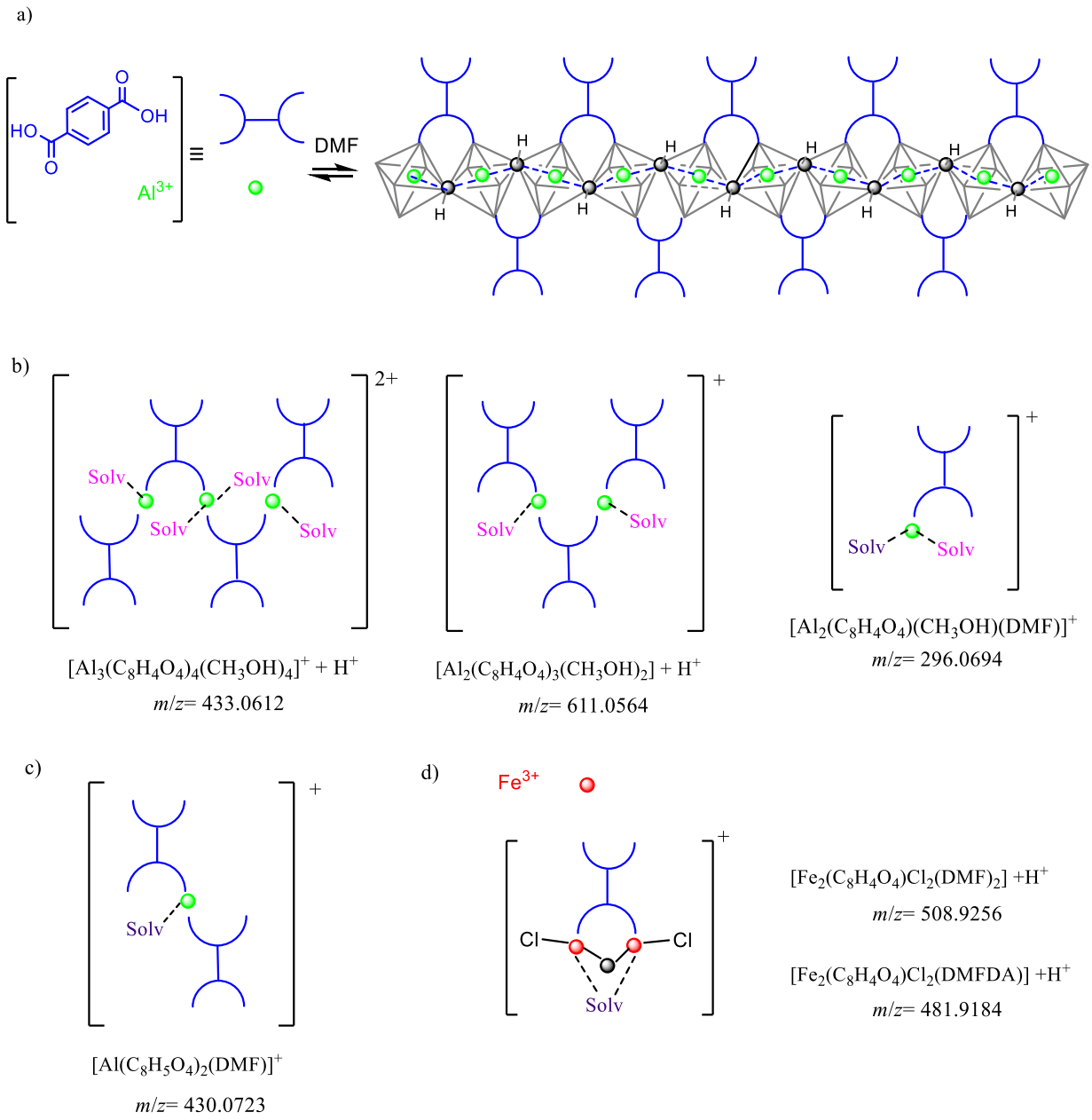

Figure 2. Chain precursor formation of μ-hydroxo and μ-terephthalate bridges to form MIL-53(Al) (a). MS fragments without H_2O_2 (b) and with H_2O_2 (c) from MIL-53(Al) precursor synthesis. MS fragments from MIL-68(Fe) precursor synthesis (d). Color code: Al (green), Fe (red), bridge O (grey).

Differences between the observed species in HRMS with and without H_2O_2 could be due to a different mechanism operating in the MOF nucleation. Without H_2O_2, chains of terephthalate bridges would form first, and be observable in HRMS. From these chains, μ-hydroxo bridges would generate slowly to finally yield the MOF. In presence of H_2O_2, μ-hydroxo bridges would form directly at first. Then, terephthalate would link aluminium nucleus (this molecular entity was observed through MS, obviously without OH bridges) (Fig. 2c), and finally μ-carboxylate bridges would form easily between aluminium atoms that were already close. This difference in the mechanism of formation of μ-hydroxo bridges is consistent with a faster nucleation and growth and a higher reaction yield in presence of H_2O_2.

The role of DMF is not totally clear in the mechanism. In general, the use of DMF has been discussed not only as common solvent but sometimes as an *a priori* irreplaceable solvent in the MOF synthesis. Here, it completes coordination around metal ions. The combination of polar properties of DMF to dissolve the metal-ligand complexes and the acid pH, which allows to have the free cations in solutions, promotes the precursor formation instead of inorganic polymerization or oxides formation.[32]

Effect of hydrogen peroxide on the synthesis of MIL-68(Al/Fe) and MIL-68(Fe)

To validate the use of H_2O_2 in the synthesis of carboxylate type MOFs, the approach followed with MIL-53(Al) was extended to Fe and Al/Fe terephthalates. First, a solution of both metal salts in DMF (without H_2BDC) was treated in the same set-up system at the same reaction conditions (90 ºC and 1.25 h) without and with H_2O_2. An orange solution was obtained without H_2O_2 (Fig. 3Aa). In presence of H_2O_2, the solution change in color (Fig. 3Ab, x1), with an increase of redness (Fig. 3Ab, x2), suggesting the formation of nanoparticles. The particles of the salt solution treated with x2 H_2O_2 (Fig. 3Ac) were recovered by centrifugation for 30 min and analyzed by TEM and STEM, observing sharpened needle-shape nanoparticles (3-45 nm wide and 100-550 nm length, depending on agglomeration) (Figs. 3B and 3C). The EDS analysis showed that the composition was based on iron (Fig. 3D), and no aluminum was detected. The formation of these particles could be explained from a redox process. As mentioned in the introduction, the combination of Fe^{3+} and H_2O_2 is well-known for producing Fenton reactions. The formation of $HO_2^{\cdot}$ species and Fe^{2+} is possible due to great excess of Fe^{3+}, and maybe favored by the use of DMF as solvent and the relatively high temperatures. This could lead to the formation of particles of mixed valence iron complexes.

Nevertheless, Fenton reaction produces hydroxyl radicals ·OH that must lead to the quick transformation of terephthalic acid into 2-hydroxyterephthalic acid, and this fact was discarded from Raman spectra (Fig. S5 and Table S2) as discussed above. Moreover, neither the solution reactions (Fig. 3A) nor the obtained MOFs with Fe^{3+} (with or without H_2O_2) showed fluorescence with a UV lamp at 254 or 365 nm corresponding to 2-hydroxyterephthalic acid.[24] Otherwise, and from an oxidation point of view, H_2O_2 could have promoted the formation of iron oxides that condense at the working conditions, being these species responsible of color change observed in the reactions with hydrogen peroxide. This oxide was expected to be formed in higher extension for sole iron synthesis, and Raman bands at 332 and 44 cm^{-1} attributed to Fe-O bonds vibrations of oxides and hydroxides seem to corroborate it, as they are not observed in the other phases.

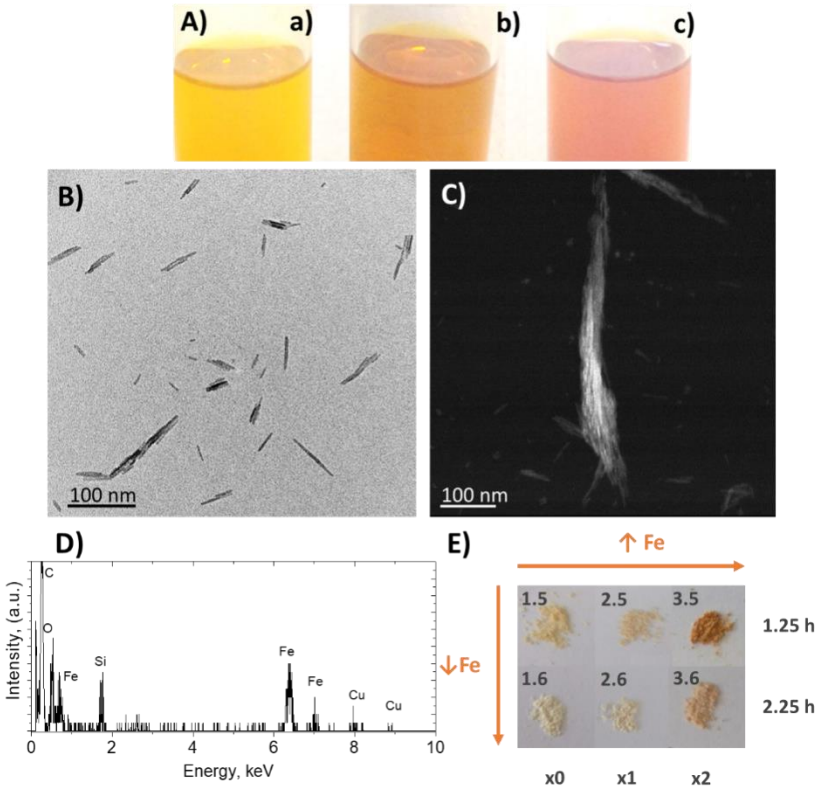

Figure 3. Photos corresponding to the solutions of metal salts (A) of blank (a), x1 H_2O_2 (b) and x2 H_2O_2 (c); TEM (B) and STEM-HAADF (C) images of the particles recovered from A(c); and EDS analysis profile (D) of C). Photos of the obtained solids in the Al^{3+}/Fe^{3+}-terephthalate experiments (E).

A yield increase was observed for both synthesis, MIL-68(Fe) and MIL-68(Al/Fe) (Table 2). However, the yield only raised its value by using the double proportion of H_2O_2 in case of MIL-68(Fe) (**3.3** and **3.4**). In fact, it decreased significantly for 1.25 h and x1 H_2O_2 (**2.3**). The formation of the described sharp particles with H_2O_2, just the metals and the solvent, could hinder the MOF growth in first place.

Hence, the effect of hydrogen peroxide is not clear in the formation of iron phases. Studies by RMN in solution could not be properly carried out due to paramagnetic effect of Fe^{3+}. The study by HRMS of the reaction with H_2O_2 revealed the existence of iron dimers with both μ-oxo and μ-terephthalic bridges between both iron nuclei. One chloride atom (coming from the ferric chloride used as reactive) linked to each metal atom and with some small molecules (DMF or N,N-dimethylformamide dimethylacetal, DMFDA, formed by reaction of DMF with methanol upon ionization) complete the coordination sphere of metal atoms (Figs. S9 and 2d). Hydrogen peroxide could increase the formation of oxygen bridges between Fe^{3+}, as described above for aluminium, or increase the formation of ferric oxides.

Regarding the textural properties, the BET areas were low for all MIL-68(Fe) samples (see Table 2) and some experiments did not yield enough amount of powder for the measurements. Moreover, the reported experimental value for MIL-68(Fe) is relatively low, 355 m^2/g, with a previous degasification at 250 ºC.[28] A temperature of 200 ºC was used here, which may justify the lower values obtained. The BET areas in the mixed phase MIL-68(Al/Fe) were slightly reduced, particularly with x2 H_2O_2. This can be explained by the increase of the iron content when more H_2O_2 was added, comparing the respective values in the pure phases (low for Fe-based and high for Al-based) and the color change observed for the final phases (Fig. 3E). For example, in the experiments for 2.25 h, the BET areas values were with x2 H_2O_2 1025 m^2/g for MIL-53(Al) (**3.2**), 53 m^2/g for MIL-68(Fe) (**3.4**) and 947 m^2/g for mixed MIL-68(Al/Fe) (**3.6**, orange color), meanwhile for those without H_2O_2, 1145 m^2/g for MIL-53(Al) (**1.2**), 186 m^2/g for MIL-68(Fe) (**1.4**) and 1235 m^2/g for mixed MIL-68(Al/Fe) (**1.6**, raw white color). Besides that, a differentiated low value was obtained at 1.25 h and x2 H_2O_2 (**3.3**), 396 m^2/g, in agreement with the lower crystallinity (Fig. S10). MIL-68(Al) can exhibit a BET area as high as ca. 1400 m^2/g,[36] what agrees with the fact that the highest BET area sample (**1.6**) was almost white consistent with a low or null Fe content.

For MIL-68(Al/Fe), no significant changes were observed in crystallinity (Fig. 10) or in morphology in SEM images (Fig. S11) comparing the reference samples with those produced in H_2O_2, except for the diffraction pattern of sample synthesized for 1.25 h with x2 H_2O_2 (**3.5**) in agreement with the low BET area. This diffraction pattern might be compatible with that corresponding with a mixture of MIL-53(Al) and MIL-53(Fe), the latter not presenting appreciable BET area.[37] Additionally, considering the excess of promoter (x2 H_2O_2) and the reduced time, more nuclei were formed and the growth of particles (Fig. 3A) was limited by the shorter time. In case of MIL-68(Fe), the morphology was noticeably modified, the reference rhombohedral particles turned into

polydisperse rods for samples with x2 H_2O_2 (Fig. S12). In fact, it was observed an increased XRD background and peak broadening, therefore some crystallinity was lost (Fig. S13).

Conclusions

MIL-53(Al), MIL-68(Fe) and MIL-68(Al/Fe) were obtained at milder conditions rather than the reported syntheses: lower temperature, shorter times, milder purification procedures and good yields. In MIL-68(Fe) and MIL-53(Al) syntheses, Fe^{3+} allowed the solubilization of terephthalic acid in DMF, and therefore the ligand was absent in the final product, which normally impurifies the MOFs. We observed that H_2O_2 produced an increase of synthesis yield for MIL-53(Al) and MIL-68(Al/Fe), while MIL-68(Fe) seemed to be impurified by some oxide. The crystallinity and the BET were roughly kept for MIL-53(Al) and MIL-68(Al/Fe). For iron-based phases, the formation of needle-like particles of iron oxide was favored with H_2O_2 and mixed MOFs with different iron content were produced by means of controlling the synthesis time and the amount of H_2O_2. While the effect of H_2O_2 was not clear in the formation of MOFs containing only Fe as metal, in case of Al containing MOFs a different mechanism seems to work with or without H_2O_2. The hydrogen peroxide would promote the early formation of μ-hydroxo bridges and then terephthalate species would link aluminium containing species to give rise to the μ -carboxylate bridges between metallic atoms already close, leading to a faster growth of the final MOF. Contrarily, in absence of H_2O_2 chains of terephthalate bridges would form first, delaying the synthesis of the MOF.

References

1. Kuppler, R. J. *et al.* Potential applications of metal-organic frameworks. *Coord. Chem. Rev.* **253,** 3042–3066 (2009).

2. Sorribas, S., Gorgojo, P., Téllez, C., Coronas, J. & Livingston, A. G. High flux thin film nanocomposite membranes based on metal-organic frameworks for organic solvent nanofiltration. *J. Am. Chem. Soc.* **135,** 15201–15208 (2013).

3. Lee, J. *et al.* Metal–organic framework materials as catalysts. *Chem. Soc. Rev.* **38,** 1450 (2009).

4. Paseta, L., Potier, G., Abbott, S. & Coronas, J. Using Hansen solubility parameters to study the encapsulation of caffeine in MOFs. *Org. Biomol. Chem.* **13,** 1724–1731 (2015).

5. Monteagudo-Olivan, R., Paseta, L., Potier, G., López-Ram-de-Viu, P. & Coronas, J. Solvent-Free Encapsulation at High Pressure with Carboxylate-Based MOFs. *Eur. J. Inorg. Chem.* (2018).

doi:10.1002/ejic.201800985

6. Horcajada, P. *et al.* Porous metal-organic-framework nanoscale carriers as a potential platform for drug delivery and imaging. *Nat Mater* **9,** 172–178 (2010).

7. Farha, O. K. & Hupp, J. T. Rational design, synthesis, purification, and activation of metal-organic framework materials. *Acc. Chem. Res.* **43,** 1166–1175 (2010).

8. Stock, N. & Biswas, S. Synthesis of metal-organic frameworks (MOFs): Routes to various MOF topologies, morphologies, and composites. *Chemical Reviews* **112,** 933–969 (2012).

9. Klinowski, J., Paz, F. A. A., Silva, P. & Rocha, J. Microwave-assisted synthesis of metal-organic frameworks. *Dalton Trans.* **40,** 321–330 (2011).

10. Khan, N. A. & Jhung, S. H. Synthesis of metal-organic frameworks (MOFs) with microwave or ultrasound: Rapid reaction, phase-selectivity, and size reduction. *Coordination Chemistry Reviews* (2015). doi:10.1016/j.ccr.2014.10.008

11. Paseta, L., Potier, G., Sorribas, S. & Coronas, J. Solventless synthesis of MOFs at high pressure. *ACS Sustain. Chem. Eng.* **4,** 3780–3785 (2016).

12. Tsuruoka, T. *et al.* Nanoporous nanorods fabricated by coordination modulation and oriented attachment growth. *Angew. Chemie - Int. Ed.* **48,** 4739–4743 (2009).

13. Diring, S., Furukawa, S., Takashima, Y., Tsuruoka, T. & Kitagawa, S. Controlled multiscale synthesis of porous coordination polymer in nano/micro regimes. *Chem. Mater.* (2010). doi:10.1021/cm101778g

14. Xiong, W. W. & Zhang, Q. Surfactants as Promising Media for the Preparation of Crystalline Inorganic Materials. *Angew. Chemie - Int. Ed.* (2015). doi:10.1002/anie.201502277

15. Seoane, B. *et al.* Metal organic framework synthesis in the presence of surfactants: Towards hierarchical MOFs? *CrystEngComm* (2015). doi:10.1039/c4ce02324b

16. Stock, N. & Biswas, S. Synthesis of metal-organic frameworks (MOFs): Routes to various MOF topologies, morphologies, and composites. *Chemical Reviews* (2012). doi:10.1021/cr200304e

17. Monteagudo-Olivan, R., Arruebo, M., López-Ram-De-Viu, P., Sebastian, V. & Coronas, J. Reactive gas atmospheres as a tool for the synthesis of MOFs: The creation of a metal hybrid fumarate with a controlled Fe/Al composition profile. *J. Mater. Chem. A* **6,** (2018).

18. Umemura, A. *et al.* Morphology design of porous coordination polymer crystals by coordination modulation. *J. Am. Chem. Soc.* (2011). doi:10.1021/ja204233q

19. Brillas, E., Sirés, I. & Oturan, M. A. Electro-fenton process and related electrochemical technologies based on fenton's reaction chemistry. *Chem. Rev.* (2009). doi:10.1021/cr900136g

20. Fenton, H. J. H. LXXIII. - Oxidation of tartaric acid in presence of iron. *Journal of the Chemical Society, Transactions* (1894). doi:10.1039/CT8946500899

21. Haber, F. & Weiss, J. The Catalytic Decomposition of Hydrogen Peroxide by Iron Salts. *Proc. R. Soc. A Math. Phys. Eng. Sci.* (1934). doi:10.1098/rspa.1934.0221

22. Petrucci, E., Da Pozzo, A. & Di Palma, L. On the ability to electrogenerate hydrogen peroxide and

to regenerate ferrous ions of three selected carbon-based cathodes for electro-Fenton processes. *Chem. Eng. J.* (2016). doi:10.1016/j.cej.2015.08.030

23. Hayyan, M., Hashim, M. A. & Alnashef, I. M. Superoxide Ion: Generation and Chemical Implications. *Chemical Reviews* (2016). doi:10.1021/acs.chemrev.5b00407

24. Barreto, J. C., Smith, G. S., Strobel, N. H. P., McQuillin, P. A. & Miller, T. A. Terephthalic acid: A dosimeter for the detection of hydroxyl radicals in vitro. *Life Sci.* (1994). doi:10.1016/0024-3205(94)00925-2

25. Lane, B. S. & Burgess, K. Metal-catalyzed epoxidations of alkenes with hydrogen peroxide. *Chemical Reviews* (2003). doi:10.1021/cr020471z

26. Grigoropoulou, G., Clark, J. H. & Elings, J. A. Recent developments on the epoxidation of alkenes using hydrogen peroxide as an oxidant. *Green Chemistry* (2003). doi:10.1039/b208925b

27. Loiseau, T. *et al.* A rationale for the large breathing of the porous aluminum terephthalate (MIL-53) upon hydration. *Chemistry* **10,** 1373–1382 (2004).

28. Fateeva, A. *et al.* Synthesis, Structure, Characterization, and Redox Properties of the Porous MIL-68(Fe) Solid. *Eur. J. Inorg. Chem.* **2010,** 3789–3794 (2010).

29. Seoane, B., Sebastián, V., Téllez, C. & Coronas, J. Crystallization in THF: The possibility of one-pot synthesis of mixed matrix membranes containing MOF MIL-68(Al). *CrystEngComm* (2013). doi:10.1039/c3ce40847g

30. Barthelet, K., Marrot, J., Ferey, G. & Riou, D. VIII(OH)[O2C-C6H4-CO2].(HO2C-C6H4-CO2H)x(DMF)y(H2O)z(or MIL-68), a new vanadocarboxylate with a large pore hybrid topology: reticular synthesis with infinite inorganic building blocks? *Chem. Commun. (Camb).* 520–521 (2004). doi:10.1039/b312589k

31. Loiseau, T., Volkringer, C., Haouas, M., Taulelle, F. & Férey, G. Crystal chemistry of aluminium carboxylates: From molecular species towards porous infinite three-dimensional networks. *Comptes Rendus Chim.* (2015). doi:10.1016/j.crci.2015.08.006

32. Devic, T. & Serre, C. High valence 3p and transition metal based MOFs. *Chemical Society Reviews* (2014). doi:10.1039/c4cs00081a

33. Shannon, R. D. Revised effective ionic radii and systematic studies of interatomic distances in halides and chalcogenides. *Acta Crystallogr. Sect. A* **32,** 751–767 (1976).

34. Paseta, L. *et al.* Accelerating the controlled synthesis of metal-organic frameworks by a microfluidic approach: A nanoliter continuous reactor. *ACS Appl. Mater. Interfaces* **5,** 9405–9410 (2013).

35. Maultzsch, J., Telg, H., Reich, S. & Thomsen, C. Radial breathing mode of single-walled carbon nanotubes: Optical transition energies and chiral-index assignment. *Phys. Rev. B - Condens. Matter Mater. Phys.* **72,** 205438 (2005).

36. Seoane, B., Sebastián, V., Téllez, C. & Coronas, J. Crystallization in THF: The possibility of one-pot synthesis of mixed matrix membranes containing MOF MIL-68(Al). *CrystEngComm* (2013). doi:10.1039/c3ce40847g

37. Denny, M. S. & Cohen, S. M. In Situ Modification of Metal-Organic Frameworks in Mixed-Matrix Membranes. *Angew. Chemie - Int. Ed.* (2015). doi:10.1002/anie.201504077

3.3. Supporting Information

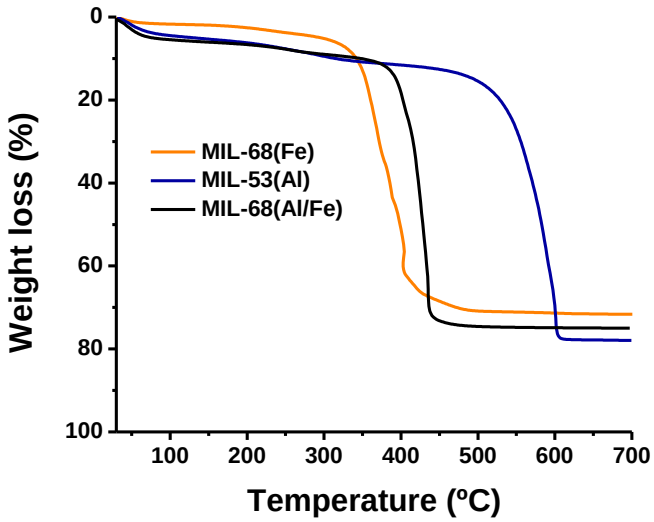

Figure S1. TGA curves of MOFs after drying at 100°C and calcination at 270°C for MIL-53(Al).

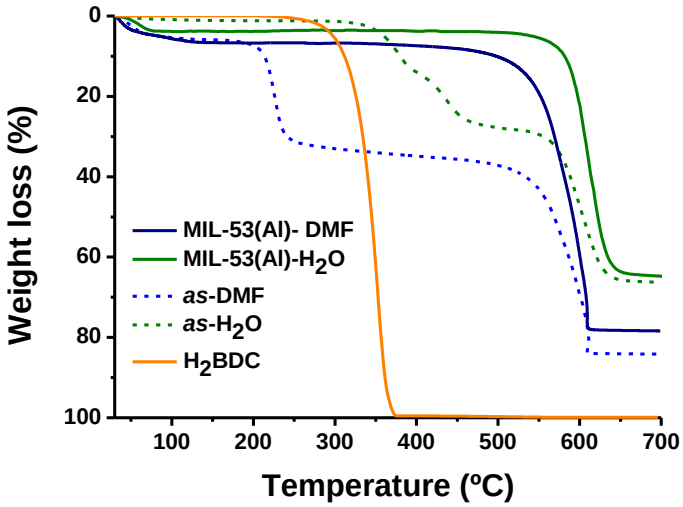

Figure S2. TGA curves of MIL-53(Al) in DMF (blue) and before activation (as, blue dotted), and of MIL-53(Al) in H_2O (green) and before (as, green dotted)

Table S1. Comparison of the published synthesis conditions for MIL53(Al),[1] MIL-68(Fe)[2] and MIL-68(Al)[3,4] with the ones developed in this report.

	Time	**Temp.**	**Solvent**	**Postreatment**
ref. MIL-53(Al)	72 h	220 °C	H_2O	Calcination 330 °C 72 h
obt. MIL-53(Al)	2.25 h	90 °C	DMF	Calcination 270 °C 6 h
ref. MIL-68(Fe)	120 h	100 °C	DMF with HF	Washing in DMF 100 °C 18 h Calcination 300 °C 24 h
obt. MIL-68(Fe)	2.25 h	90 °C	DMF	Drying 100 °C 24 h
ref. MIL-68(Al)	18.5 h	130 °C	DMF	Drying
obt. MIL-68(Al/Fe)	2.25 h	90 °C	DMF	Drying 100 °C 24 h

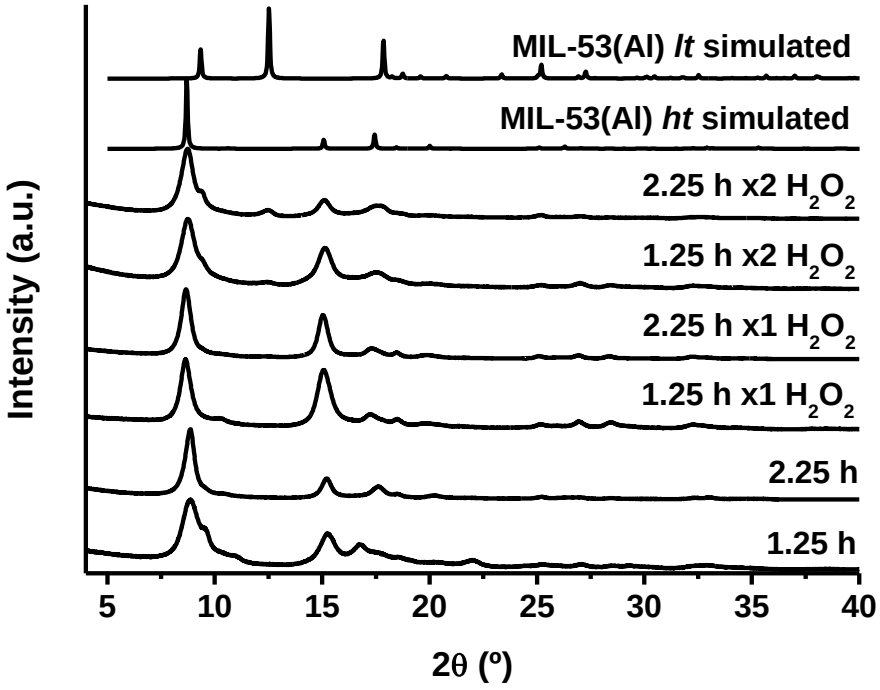

Figure S3. Diffraction patterns of the Al^{3+}-terephthalate experiments from bottom to up: **1.1**, **1.2**, **2.1**, **2.2**, **3.1**, **3.2** and simulated pattern of the pore-opened MIL-53(Al) *ht* phase and hydrated *lt* phase.[1]

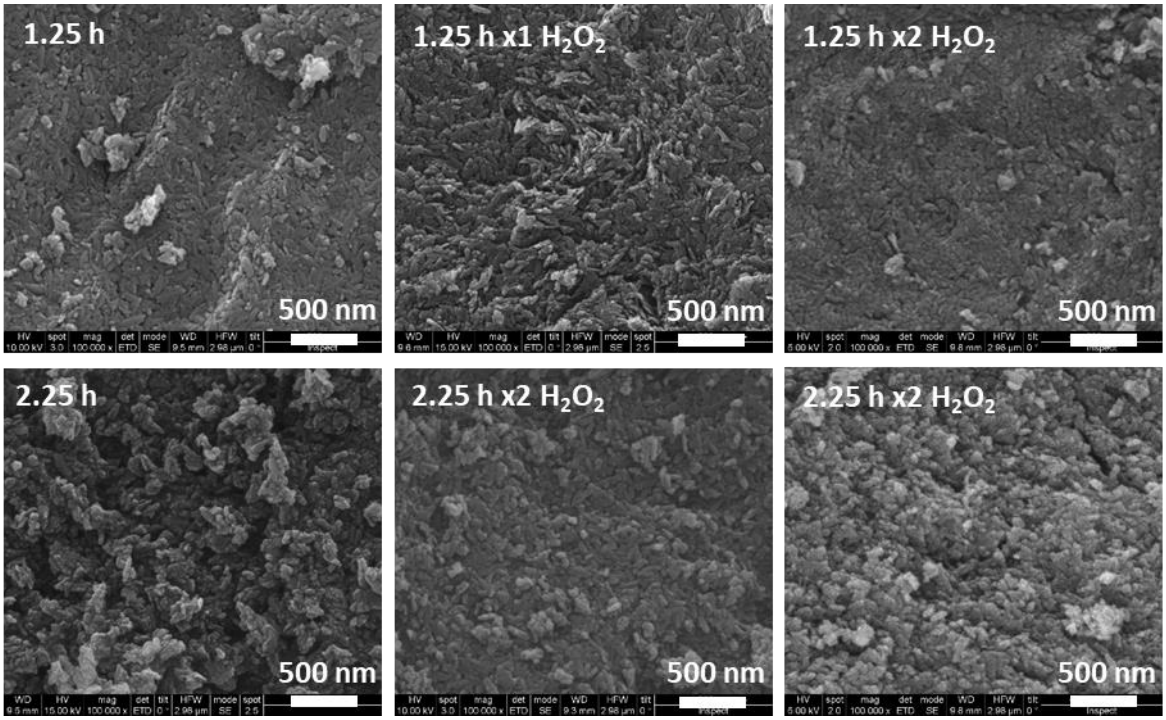

Figure S4. SEM images of Al^{3+}-terephthalate syntheses.

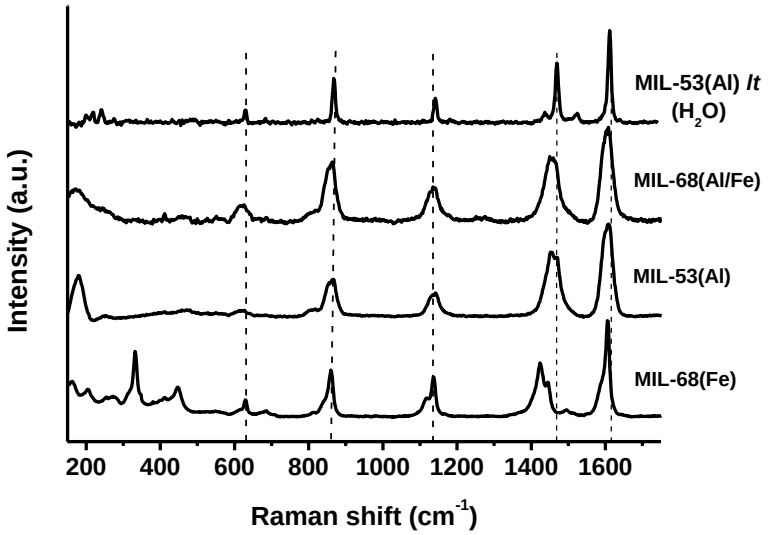

Figure S5. Raman spectra of MOF obtained with H_2O_2 from bottom to up: MIL-68(Fe) (**2.4**), MIL-53(Al) (**2.2**) and MIL-68(Al/Fe) (**2.6**). Up: reference MIL-53(Al) synthesized in water.

Table S2. MOF: terephthalate shifts of MOF obtained with H_2O_2 MIL-68(Fe) (**2.4**), MIL-53(Al) (**2.2**), MIL-68(Al/Fe) (**2.6**) and reference MIL-53(Al) synthesized in water

	MIL-68 (Fe) (cm^{-1})		**MIL-53(Al) *as* (cm^{-1})**		**MIL-68(Al/Fe) (cm^{-1})**		**MIL-53(Al) *lt* (cm^{-1})**	
ring C=C stretching	1606	vs	1608	vs	1608	vs	1612	vs
asymmetric stretching CO_2^-	1496	vw	-	-	.	-	1524	w
symmetric stretching CO_2^-	1445	m	1469	s	1460	**s**	1469	**s**
	1424	s	1452	s	1450	s	1437	w
Ar =C-H in-plane deformation	1137	m	1142	w	1135	m	1142	m
Ar =C-H out-of-plane deformation	860	m	866	m	864	s	867	m
aromatic ring deformation	629	w	620	vw	623	w	630	w
(Fe-O deformations)	447	w	-	-	-	-	-	-
	332	s	-	-	-	-	-	-
Lattice vibration	(Several bands)	w	179	m	183	m		

vs: very strong, s: strong, m: medium, w: weak, vw: very weak

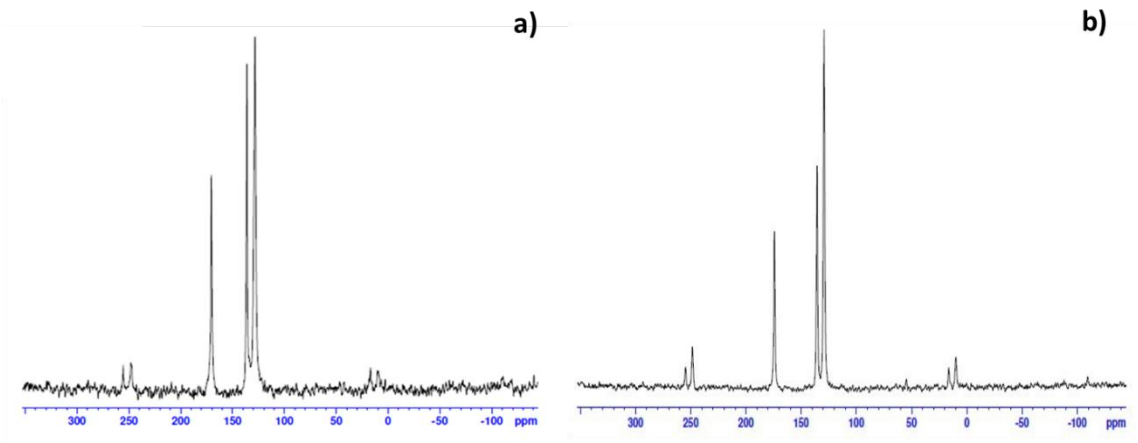

Figure S6. NMR Solid ^{13}C-NMR spectra of samples treated with x1 H_2O_2 and 2.25 h of MIL-53(Al) (a) and MIL-53(Al) synthesized accordingly to the reference.[1]

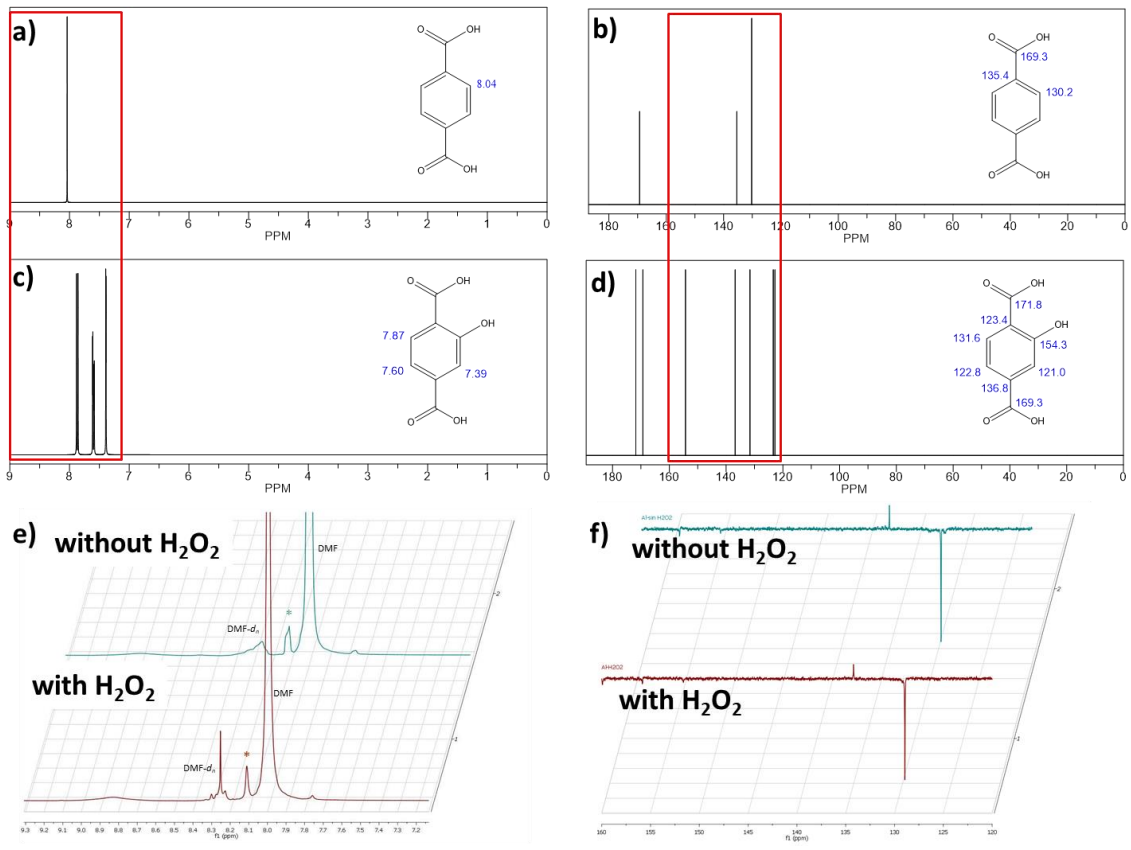

Figure S7. ^{1}H-NMR and ^{13}C-NMR of simulated spectrum of terephthalic acid (a and c, respectively) and 2-hydroxiterephthalic acid (b and d, respectively), and experimental spectra of an aliquot at 45 min of the MIL-53(Al) synthesis without and with H_2O_2 (e and f, respectively)

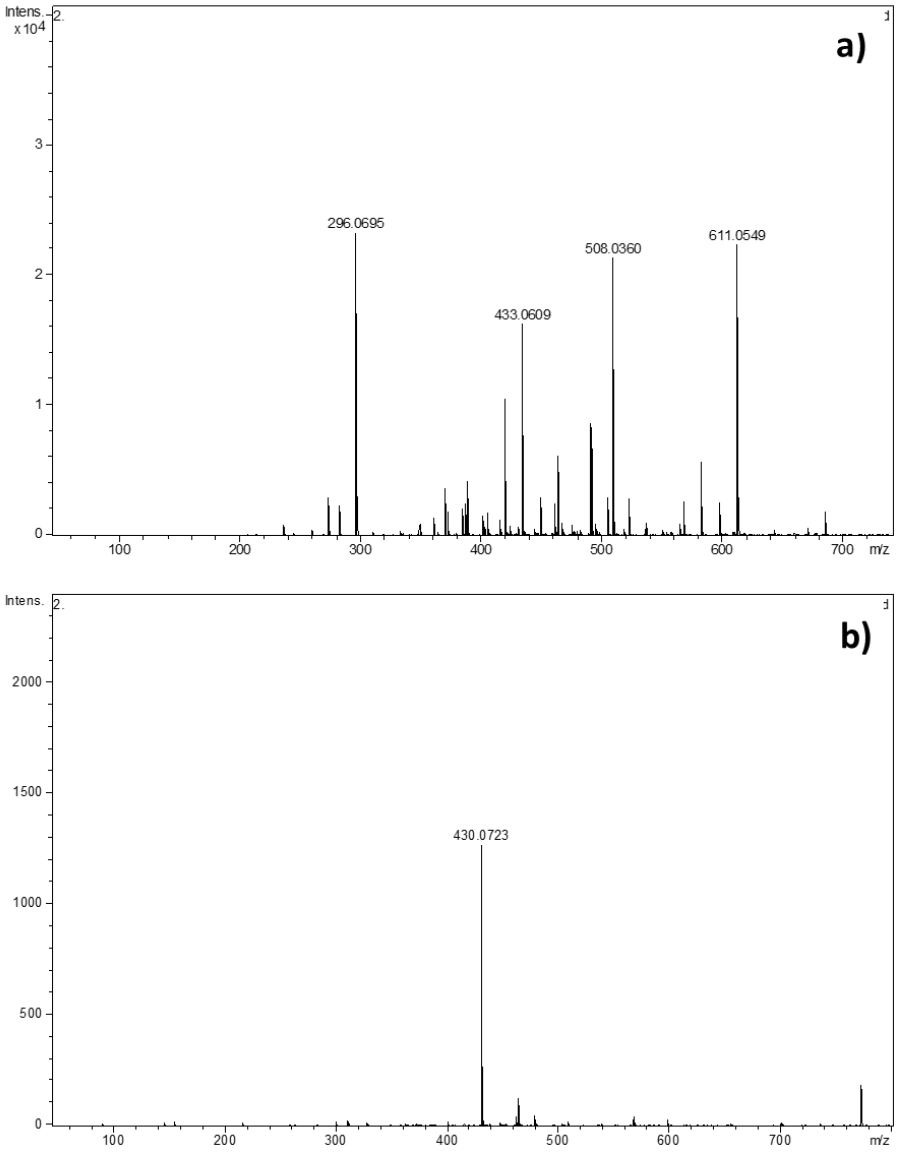

Figure S8. MS spectra of the intermediate reaction of Al^{3+}-terephthalate with H_2O_2 (a) and with H_2O_2 (b).

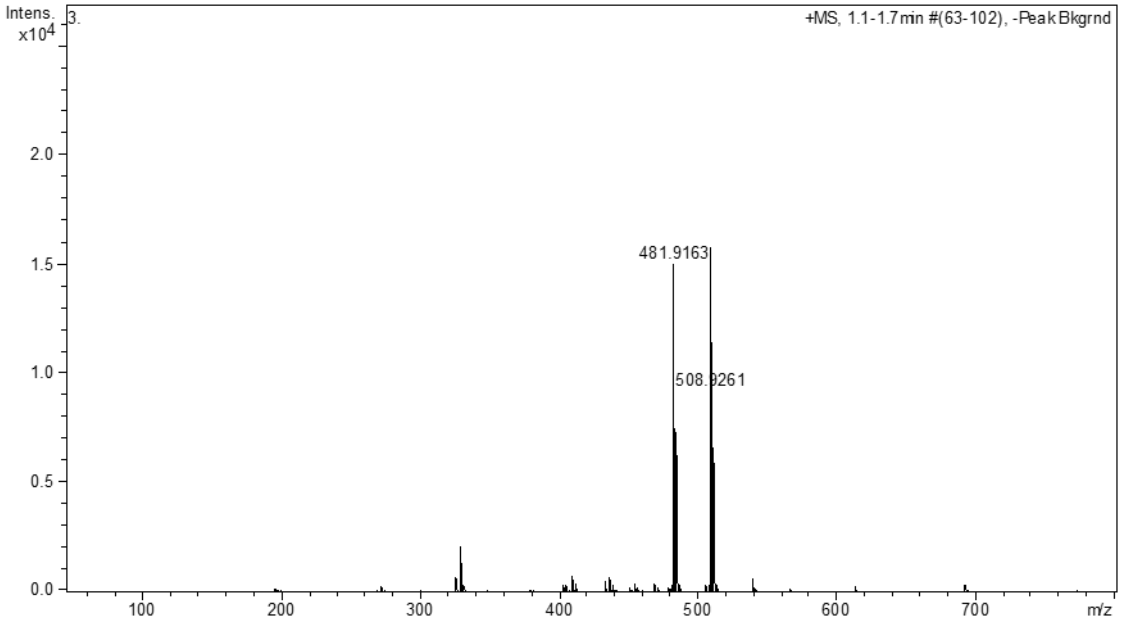

Figure S9. MS spectra of the intermediate reaction of Fe^{3+}-terephthalate with H_2O_2

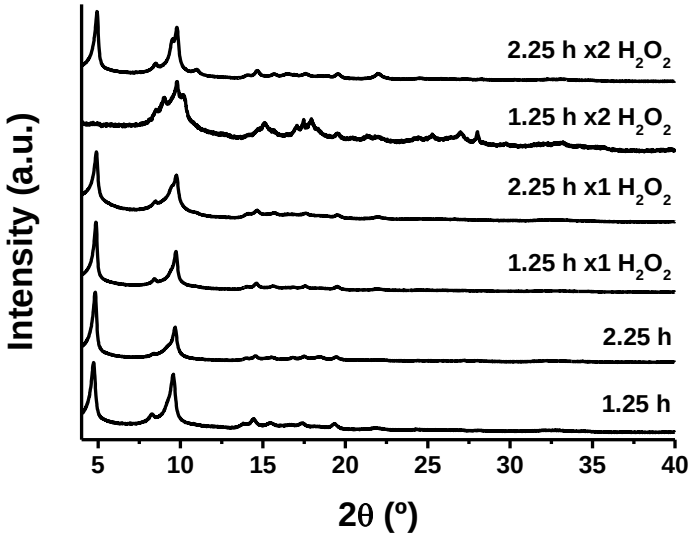

Figure S10. Diffraction patterns of the obtained solids in the Al^{3+}/Fe^{3+}-terephthalate experiments from bottom to up: **1.5**, **1.6**, **2.5**, **2.6**, **3.5** and **3.6**.

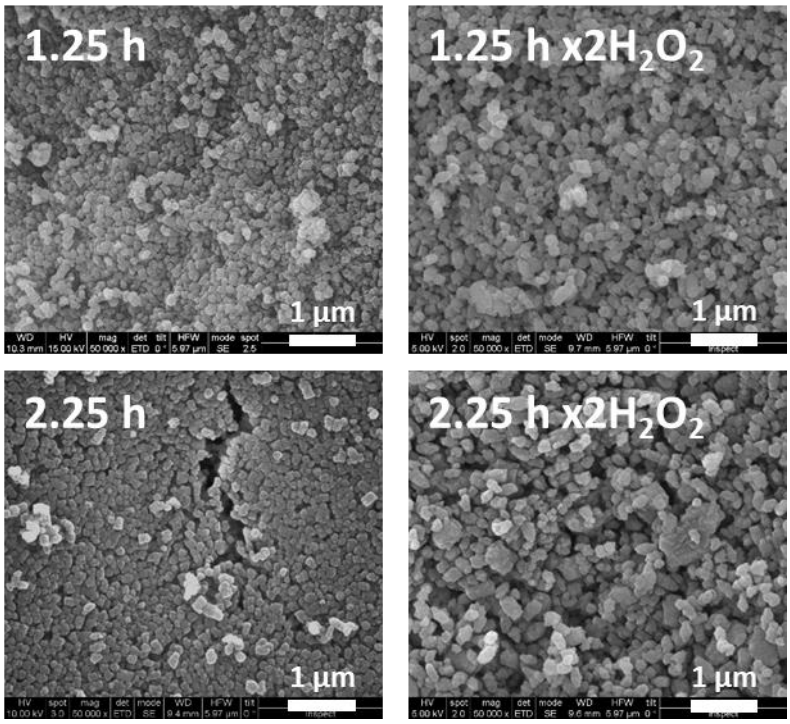

Figure S11. SEM images of Al^{3+}/Fe^{3+}-terephthalate syntheses.

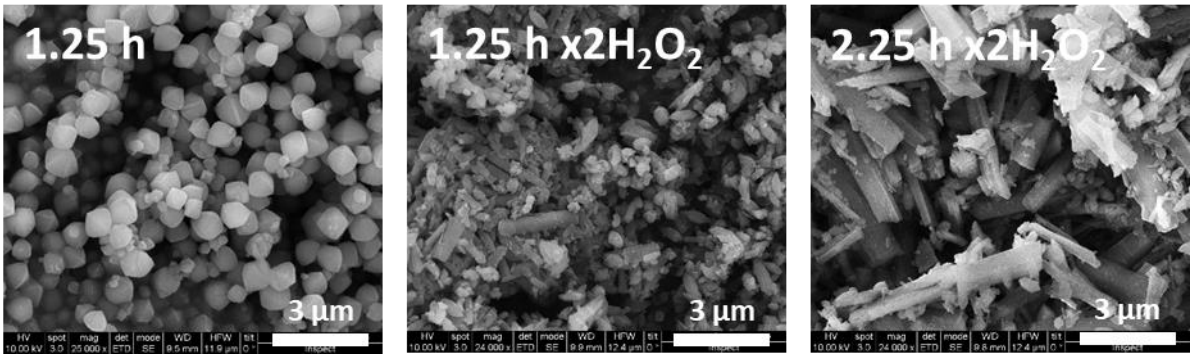

Figure S12. SEM images of Fe^{3+}-terephthalate syntheses.

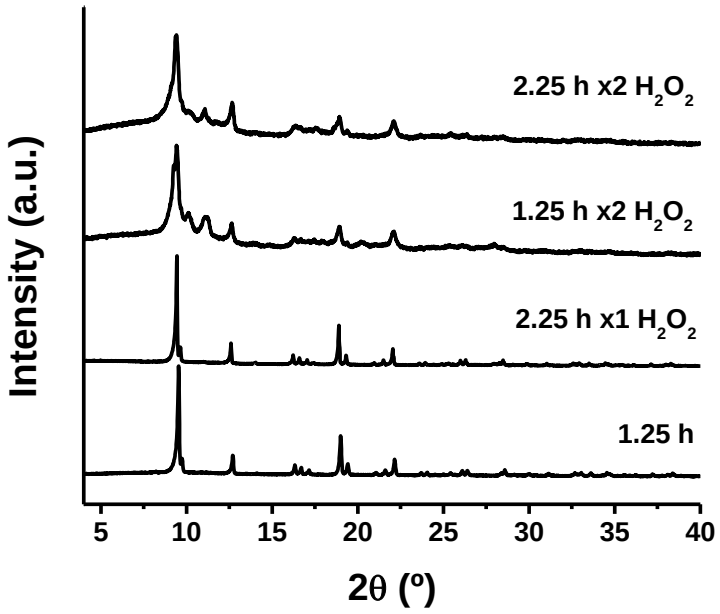

Figure S13. Diffraction patterns of the Fe^{3+}-terephthalate experiments from bottom to up: **1.3**, **2.4**, **3.3** and **3.4**

References:

1. Loiseau, T., Serre, C., Huguenard, C., Fink, G., Taulelle, F., Henry, M., Bataille, T. & Férey, G. A rationale for the large breathing of the porous aluminum terephthalate (MIL-53) upon hydration. *Chemistry* **10,** 1373–1382 (2004).

2. Fateeva, A., Horcajada, P., Devic, T., Serre, C., Marrot, J., Grenèche, J.-M., Morcrette, M., Tarascon, J.-M., Maurin, G. & Férey, G. Synthesis, Structure, Characterization, and Redox Properties of the Porous MIL-68(Fe) Solid. *Eur. J. Inorg. Chem.* **2010,** 3789–3794 (2010).

3. Yang, Q., Vaesen, S., Vishnuvarthan, M., Ragon, F., Serre, C., Vimont, A., Daturi, M., De Weireld, G. & Maurin, G. Probing the adsorption performance of the hybrid porous MIL-68(Al): a synergic combination of experimental and modelling tools. *J. Mater. Chem.* **22,** 10210 (2012).

4. Schubert, M., Mueller, U. & Marx, S. WO Pat., 2008/12905, Aktiengesellschaft, BASF. (2008).

Chapter 4:

Solvent-free encapsulation at high pressure in carboxylate-based MOFs

State of the article:

Published in European Journal of Inorganic Chemistry, 2019, 29-36 and reproduced by permission of John Wiley and Sons

DOI: 10.1002/ejic.201800985

Rebeca Monteagudo-Olivan,[a] Lorena Paseta,[a] Grégory Potier,[b] Pilar López-Ram-de-Viu,[c] Joaquín Coronas* [a]

[a]Chemical and Environmental Engineering Department and Instituto de Nanociencia de Aragón (INA), Universidad de Zaragoza, 50018 Zaragoza, Spain

[b]Département Sciences des Matériaux, Polytech Nantes, 44306 Nantes, France

[c]Organic Chemistry Department, Universidad de Zaragoza, and Instituto Universitario de Catálisis Homogénea (Universidad de Zaragoza-CSIC), 50009 Zaragoza, Spain

Journal metrics:

Impact factor: 2.501 (2019) and Q1 (Inorganic chemistry)

4.1. Summary and graphical abstract

The solvent-free encapsulation of caffeine and kojic acid is carried out in different carboxylate-based MOFs (MIL-53(Al), UiO-66 and Mg-MOF-74) by high pressure (0.32 GPa) contact. This methodology enables fast and ecofriendly encapsulation and gives rise to additive@MOFs with equivalent physical and features to materials obtained by common liquid phase encapsulation processes. It could be applied to other guest-host systems simplifying the procedures, reducing the use and waste of harmful chemicals and approaching the conditions of interest in the industry. The characterization carried out by thermogravimetry, X-ray diffraction, N_2 adsorption and ^{13}C NMR provided information about the presence and conformation of the additives in the MOFs. The highest encapsulation values for caffeine (37%) and kojic acid (32%) are obtained with MIL-53(Al).

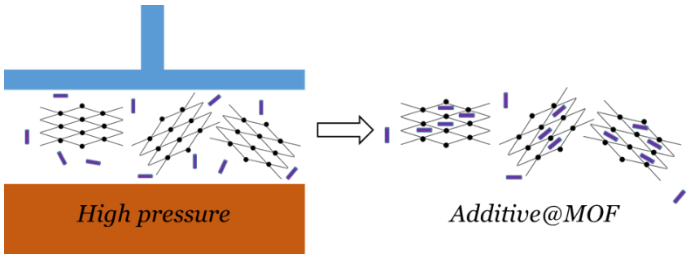

4.2. Solvent-free encapsulation at high pressure in carboxylate-based MOFs

INTRODUCTION

Metal-organic frameworks (MOFs) are porous crystalline hybrid materials made of metal ions or clusters coordinated with organic linkers to form single or multidimensional structures.[1] Due to the high surface area of these materials,[2] their relatively high chemical and thermal stability[3,4] and the possibility of modifying the pore size and the functionality by changing the metal ion or the organic ligand,[5] MOFs are useful in a wide range of fields such as catalysis,[6] adsorption and storage of gases,[7] selective membranes,[8] encapsulation,[9] and medicine.[10–13]

One of the most important families of MOFs corresponds to those based on carboxylate-type ligands. Specifically, MIL-53(Al), UiO-66 and Mg-MOF-74 are very suitable from the encapsulation point of view because of the potential biocompatibility of their corresponding organic linkers and metal centers.[14,15] MIL-53(Al) is composed of trivalent metal cations Al^{3+} interconnected through terephthalate linkers to form a three dimensional framework with rhombus-shape one-dimensional channels.[16] This MOF has attracted considerable attention due to its high thermal and chemical stability and its "breathing" behavior. This allows it to adapt its porosity, which can vary in the range of 8.5 x 8.5 Å (*ht* form) and 2.6 x 13.6 Å (*lt* form), to the size and shape of the guest molecule.[16–18] This feature makes MIL-53(Al) very interesting in the encapsulation field[19] and for the delivery of molecules of pharmacological interest.[17] The second carboxylate-based MOF UiO-66 also shows high stability compared with other MOFs due to the special structure of the corresponding Zr^{4+}-terephthalate, which displays octahedral and tetrahedral cages with triangular pore windows of 6 Å.[20] The third material studied, Mg-MOF-74, is composed of Mg^{2+} and 2,5-dihydroxyterephthalate and presents hexagonal channels of 12 Å.[21,22] This MOF is highly hydrated showing the behavior of a typical high aluminum content zeolite; due to the fact that some water molecules play a structural role, it has low stability in water.[23] Finally, MIL-101(Cr) is made of terephthalate ligands coordinated to Cr^{3+} and is well-known as an adsorbent with a high specific surface area; it has cages of 29 Å and 34 Å featuring 12 Å pentagonal and 16 Å hexagonal apertures.[24] Due to its chromium content, this material is not as biocompatible as the other three materials but has a high adsorption capability.[10] It is studied here for the purposes of comparison. Regarding traditional liquid phase encapsulation, there are two different methodologies to encapsulate a drug into a MOF denominated as "multi-step" and "one-step" encapsulations[9,27–30] The former involves three steps: the synthesis of the MOF, its subsequent activation, and the encapsulation of the drug by liquid phase adsorption.[10,31–

[34] In the latter, the drug is placed together with the reactants in the synthesis media and the MOF grows around the drug.[35–39] Moreover, after encapsulation, it has been reported the functionalization of MOF particles with different biomolecules[40,41] and magnetic nanoparticles.[42]

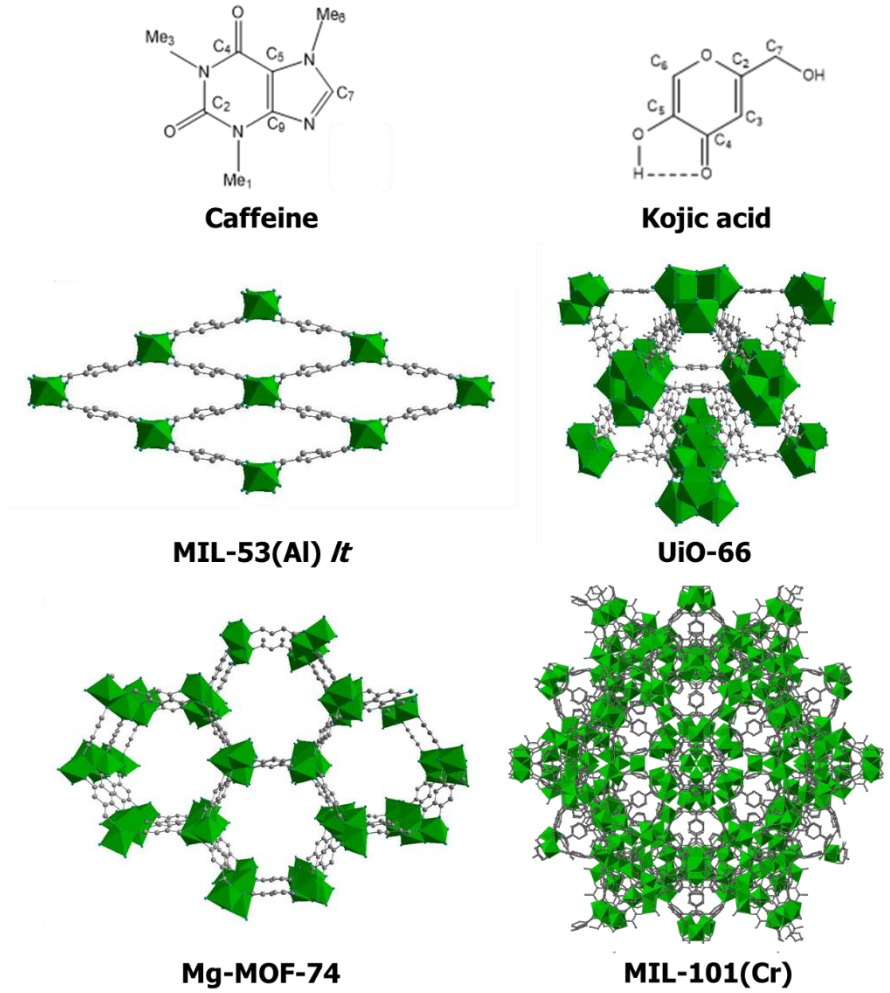

Figure 1. Guest and host systems addressed in this work. Atomic color code: carbon (grey), oxygen (blue) and metal coordination (green). These structures were made with Diamond 3.2. and Crystal Maker 9.2.7 using the corresponding CIF files.[16,21,25,26]

Herein we propose a different and new methodology: the solvent-free encapsulation by high pressure (0.32 GPa) contact of additives or drugs (caffeine and kojic acid) with several carboxylate-based MOFs (see Fig. 1). Caffeine can be considered as a model molecule[31,35] suitable for demonstrating a new encapsulation process. In addition, caffeine is widely known because of its stimulant effect in the central nervous system[43] but also as a fat reducer in the fields of cosmetics and pharmacology.[44] To broaden the scope of applicability, a second probe additive, kojic acid, has been used in the present study. This natural compound produced by several fungi is used in low doses for skin

lightening[45,46] in cosmetic products and as an antimelanogenesis agent.[47] It also has applications as a biocide.[48] The smaller molecular size of kojic acid (as compared to caffeine) will provide additional insight into the host-guest interaction.

The solvent-free encapsulation process carried out for the first time in this work can be considered as environmentally friendly, in line with others related to the synthesis of MOFs working in continuous mode,[49] using water as a solvent[50] or avoiding the use of solvents entirely.[49,50] We postulate that high pressure favors the diffusion of the additive into the material and therefore the use of any solvent is avoided. The bibliography on the effect of high pressure on MOFs is very scarce. We have previously reported the solvent-less synthesis of ZIF-8 at high pressure[49] and the behavior of this MOF at high pressure has also been described with regard to its stability[51,52] and water intrusion.[53] Moreover, the contact of MOF Cu-btc with several liquids (alcohols and perfluorotri-N-pentylamine) has been studied up to 8 GPa.[54] Interestingly, these authors concluded that "the fundamental understanding of high-pressure phenomena in MOFs will play a pivotal role in the advancement of their diverse applied functionalities." Finally, it is worth mentioning that the MOFs studied here, MIL-53(Al),[19] UiO-66,[31,57] Mg-MOF-74[55] and MIL-101(Cr),[56] have previously been applied to the conventional encapsulation of different guests. Finally, it has been recently commercialized MOF based products TruPick and ION-X as systems for food packaging and electronic gas delivery.[57] In particular, TruPick releases 1-methylcyclepropene (encapsulated in a MOF synthesized by mechanochemistry) that reduces fruit ripening during its storage. This demonstrates that MOF encapsulation is a field with great potential of industrial development.

RESULTS AND DISCUSSION

Fig. 2 depicts the typical crystal morphologies of MIL-53(Al), UiO-66, Mg-MOF-74 and MIL-101(Cr) as observed by SEM. These images are consistent with high crystalline materials (as demonstrated below by XRD characterization) which may be considered appropriate for the purpose of studying the solvent free encapsulation of caffeine and kojic acid at high pressure.

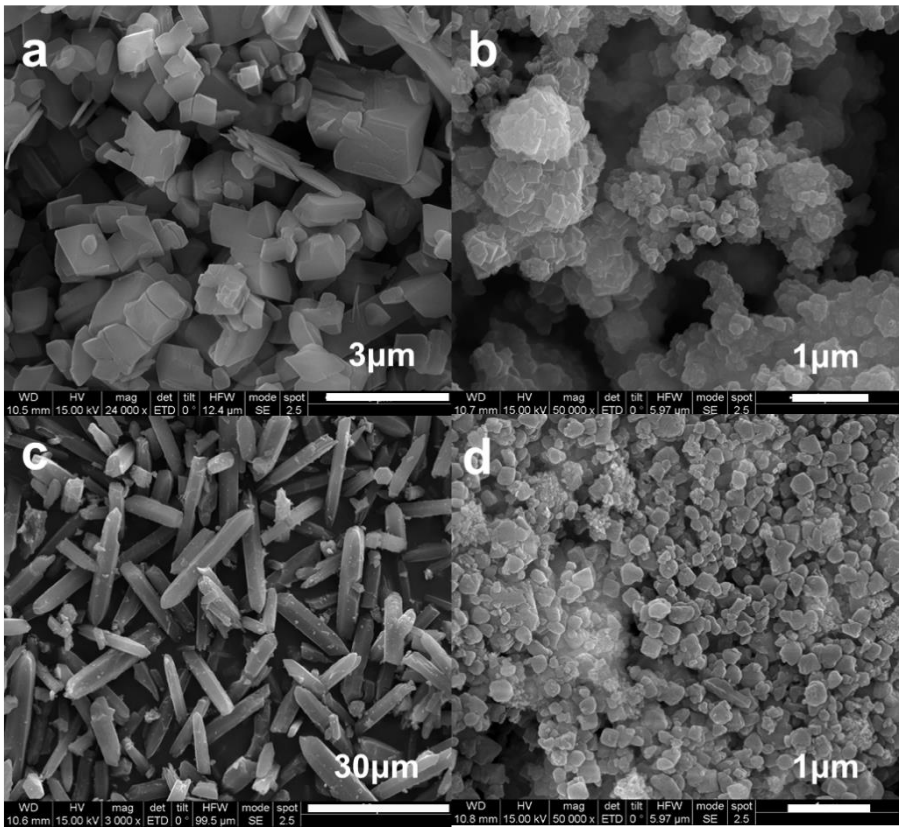

Figure 2. SEM images of the materials MIL-53(Al) (a), UiO-66 (b), Mg-MOF-74 (c) and MIL-101(Cr) (d).

High pressure stability and encapsulation

In agreement with previous publications dealing with the liquid phase encapsulation of drugs in MOFs,[19,31,32,35,37,57,61] XRD, N_2 adsorption, NMR and TGA techniques were employed to evidence the encapsulation carried out here by the new solvent-free methodology proposed. XRD is qualitative proof of encapsulation, since the guest molecule intensity in its contact with the MOF decreases due the adsorption in the MOF structure. N_2 adsorption (to calculate the BET specific surface area) is in line with XRD; if the encapsulation is produced in the MOF porosity, less porosity is available for N_2 molecules. NMR demonstrates host-guest interactions and the preservation of the guest chemical nature. Finally, TGA allows a calculation of the encapsulation yield, since encapsulated molecules show a thermal stabilization as compared with external molecules (that have not penetrated in the MOF structure). We did not carry out liquid phase characterizations of our samples to avoid alteration of the solid state encapsulation method.

Fig. 3 shows the diffraction patterns of the different materials before and after 30 min at 0.32 GPa. As an index of the effect of pressure on the decrease of the MOF crystallinity,

the FWHM (full width at half maximum height) was calculated for the main peaks of the MOFs (MIL-53(Al): 12.5° - (110) plane, UiO-66: 7.2° - (111) plane, and Mg-MOF-74: 11.7° - (300) plane) before and after pressure exposure. Table S1 shows the obtained results highlighting that the FWHM increased for the pressure treated materials in agreement with a decrease of crystallinity. In particular, MIL-53(Al) and Mg-MOF-74 seem to be less affected, maintaining their crystalline structures after the high pressure treatment, even though the relative intensities of some peaks varied in the case of MIL-53(Al) probably due to its flexible structure.[59] Regarding our results with UiO-66, low intensity peaks were still visible in the diffraction pattern after the high pressure treatment but with some noise and evident broadening (Table S1). Finally, strong amorphization was revealed for MIL-101(Cr) after the high pressure treatment treatment, and the FWMH was not calculated. Conspicuously characteristic peaks below 10° disappeared while most of the others tended to merge into broad peaks. These findings are in agreement with previous works on computational characterization of the mechanical stability of flexible MIL-53(Al) and rigid UiO-66.[60,61] These works predicted the loss of crystallinity of rigid UiO-66 at 1.83 GPa. In turn, this coincides with the experimental work carried out on UiO-66 that concluded that this MOF was not amorphized below 2 GPa, even though a gradual loss of crystallinity was detected at moderated pressures (0.3-1.7 GPa) in terms of broadening of the XRD peaks.[62]

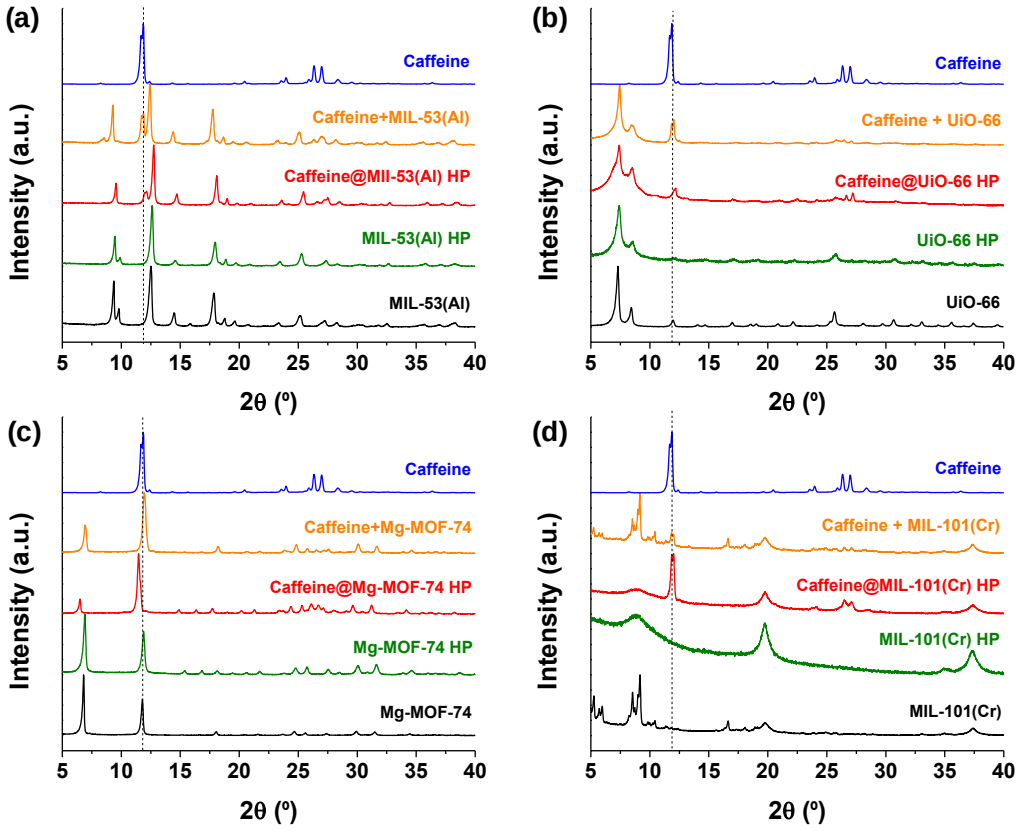

Figure 3. XRD patterns of the different samples (from bottom to top, MOF, MOF after high pressure exposure, caffeine@MOF after high pressure encapsulation, simple mixture of caffeine and MOF, and caffeine) corresponding to: MIL-53(Al) (a), UiO-66 (b), Mg-MOF-74 (c), and MIL-101(Cr) (d). Encapsulation at room temperature, 0.32 GPa and 4:1 MOF:caffeine weight ratio.

XRD is a useful tool for monitoring the effective encapsulation of the additives since the additive intensities would decrease or almost disappear upon guest adsorption in the MOF porosity, i.e. the isolated additives in the MOF porosity would not be able to form detectable crystals. Fig. 3. shows the XRD patterns corresponding to the high pressure encapsulation of caffeine into the different MOFs (MOF:caffeine weight ratio of 4:1) together with those of the simple blending of caffeine with the MOF (at the same weight ratio) for a proper comparison. Encapsulation of caffeine in MIL-53(Al) and UiO-66 produced a clear decrease in the main peak of caffeine at 11.9°, as inferred from the comparison of the XRD patterns corresponding to the simple additive-MOF mixtures and samples caffeine@MIL-53(Al) and caffeine@UiO-66. In consequence, this caffeine peak was considered to follow the encapsulation of caffeine in both MOFs. In this context, Table S2 shows the area ratios corresponding to maximum XRD peaks of additives (caffeine (CAF): 11.9° and kojic acid (KA): 19.3°) and MOFs (MIL-53(Al): 12.5° - (110) plane, UiO-66: 7.2° - (111) plane, and Mg-MOF-74: 11.7° - (300) plane) for simple additive-MOF blending (0 GPa) and encapsulation at 0.32 GPa. In all the cases, these area ratios decreased from the simple blending to 0.32 GPa encapsulation. We assume that this ratio decrease is due to the adsorption of caffeine into the MOF pores and therefore the disappearance of external caffeine impregnating the MOFs. Caffeine@MOF products would show the additive pattern if caffeine was present in the form of crystal outside the MOF. The reduction or absence of the characteristic caffeine peaks is consistent with its encapsulation, and the caffeine peaks are more evident when excess caffeine was used (2:1 MOF:caffeine weight ratio instead of 4:1, see Fig. S1).

TGA analysis was used to observe the possible thermal stabilization of additives after encapsulation usually related to their adsorption on the MOF porosity and not to their mere external impregnation. The TGA curve of sample 4:1 in MIL-53(Al) (Fig. S2a) shows only one intermediate step corresponding to thermally stabilized caffeine. In the caffeine@UiO-66 TGA curve (Fig. S2b), two removal steps can be observed due to the external caffeine at ca. 180 °C and the encapsulated caffeine at ca. 230 °C. The external caffeine step appeared when caffeine was used in high excess, as seen in Fig. S3 for caffeine@MIL-53(Al). The XRD patterns for Mg-MOF-74 are not clear enough to conclude the completion of encapsulation because the most intense peak of caffeine overlaps with one of the peaks of the MOF. In addition, Fig. S2c does not reveal any

stabilization for caffeine@MOF-74, in agreement with a mere external impregnation of caffeine on the MOF. In the pressurized sample with MIL-101(Cr), only caffeine peaks are observed, consistent with the great damage that the high pressure produced in this material, suggesting its structural collapse at 0.32 GPa.

Fig. 4 shows similar results for the encapsulation of kojic acid in MIL-53(Al) (Fig. 4a) and UiO-66 (Fig. 4b). Nevertheless, the decrease corresponding to the kojic acid peak area is greater than in the experiments with caffeine as compared to the simple blending, especially in the case of MIL-53(Al) (Table S2). This can be attributed to the more reduced size of kojic acid (MW 142.11 g/mol) as compared to caffeine (MW 194.19 g/mol), considering that it is easier to encapsulate a smaller molecule. However, the chemical interaction estimated in terms of Hansen solubility parameters[9,63] would favor caffeine-terephthalate interactions (Ra parameter 3.1 $MPa^{0.5}$) over those between kojic acid and terephthalate (9.6 $MPa^{0.5}$). TGA curves in Fig. S4 show some thermal stabilization of kojic acid with both MOFs. In the case of Mg-MOF-74, the most intense peak of kojic acid remains in the kojic acid@Mg-MOF-74 (Fig. 4c). The area ratio between the most intense peaks of the additive at 19.3° and the MOF at 11.7° is 4.5 for the simple blending and 0.55 for kojic acid@MOF-74 (Table S2), i.e. an important part of the additive disappeared from the external surface during the encapsulation process. Therefore, in this case the change in the relative intensities supports the idea that encapsulation had taken place, in agreement with the corresponding TGA curve in Fig. S4c. MIL-101(Cr) was not used to encapsulate kojic acid due to its lack of high pressure stability, as shown above.

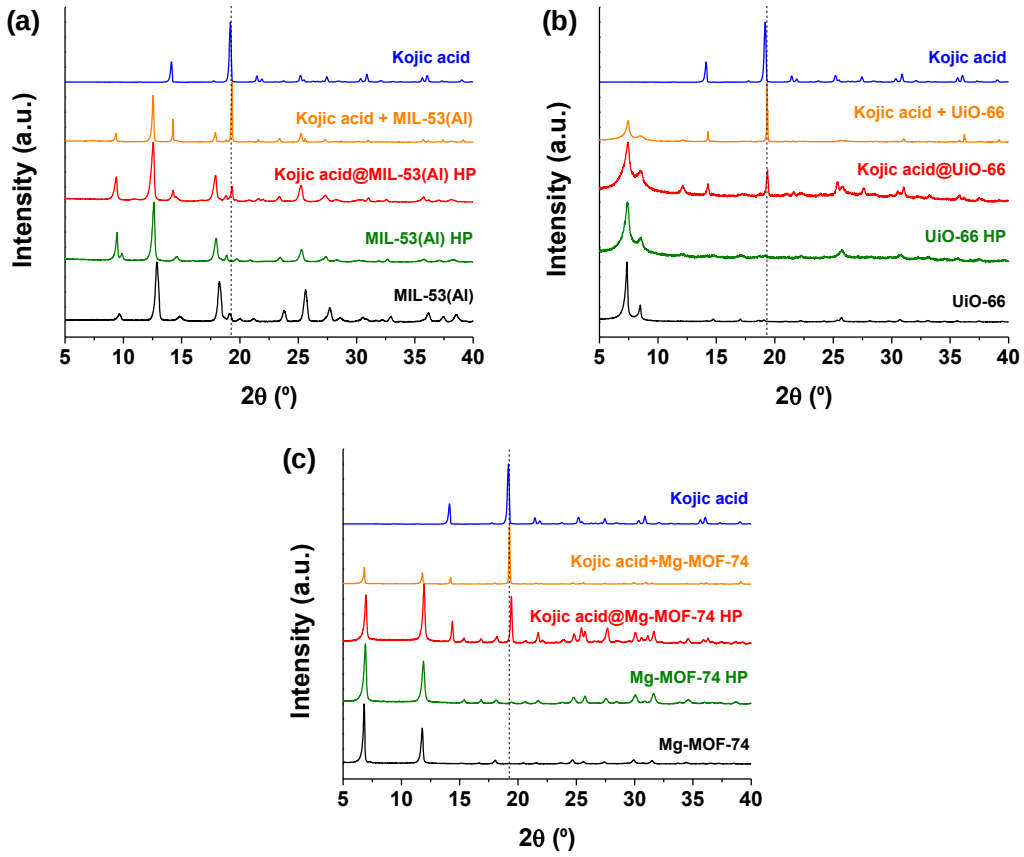

Figure 4. XRD patterns of the different samples (from bottom to top, MOF, MOF after high pressure exposure, kojic acid@MOF after high pressure encapsulation, simple mixture of kojic acid and MOF, and kojic acid) corresponding to: MIL-53(Al) (a), UiO-66 (b), and Mg-MOF-74 (c). Encapsulation at room temperature, 0.32 GPa and 4:1 kojic acid:MOF weight ratio

Table 1 shows the BET specific surface area values of some selected samples. First, the effect of high pressure reduced the surface area values for both MIL-53(Al) and UiO-66 from 1140 and 951 m^2/g to 1016 and 253 m^2/g, respectively. This suggests that the microporosity of MIL-53(Al) was not significantly affected by high pressure, in agreement with the above shown XRD pattern, while that of UiO-66 presents an important reduction, according to the somewhat noisy UiO-66 XRD pattern (suggesting some loss of crystallinity after the high pressure contact). In addition, the decrease of the BET specific surface area due to guest pore filling supports the encapsulation of caffeine and kojic acid in MIL-53(Al) and UiO-66, even though on this last case the effect of guess pore filing may overlap on the structure damage. The decrease of surface area of MIL-53(Al) (1016 m^2/g) after the encapsulation of caffeine (336 m^2/g) and kojic acid (9 m^2/g) was consistent with its pores filled with the additives. These values were 52 and 83 m^2/g for caffeine@UiO-66 and kojic acid@UiO-66, respectively.

Table 1. BET surface area of MIL-53(Al) and UiO-66 after high pressure treatment and high pressure encapsulation of caffeine and kojic acid in both MOFs.

Sample	S_{BET} (m^2/g)	Sample	S_{BET} (m^2/g)
MIL-53(Al)	1140	UiO-66	951
MIL-53(Al) HP	1016	UiO-66 HP	253
Caffeine@MIL-53(Al)	336	Caffeine@UiO-66	52
Kojic acid@MIL-53(Al)	9	Kojic acid@UiO-66	83

Solid-state ^{13}C NMR was employed to study the MOF-guest interactions upon encapsulation by high pressure contact. Figures 5 and 6 compare the ^{13}C MAS NMR spectra of caffeine and kojic acid with those of MIL-53(Al) and UiO-66 before and after encapsulation. Some trends were observed analyzing the changes in chemical shifts of additives and terephtalate ligand in additive@MOF materials (Tables S3-S5). In the case of caffeine@MIL-53(Al), the peaks corresponding to the terephthalate MOF linker remained as in the bare MIL-53(Al) (Table S3a). However, the peaks of caffeine were modified once it was encapsulated (see Fig. 5a and Table S4). Interestingly, C_2, C_4, C_5, Me_1 and Me_6 signals shifted upfield, while those for C_7, C_9 and Me_3 shifted downfield. This can be explained by the anisotropic magnetic behavior of the ligand. There are typical shielding areas due to the aromatic ring effect (affecting to upper and lower parallel planes) and also deshielding zones (anisotropic cone) generated by the carbonyl group. Therefore, the size and shape of the guest molecule and host cages determine a specific and symmetric position of caffeine inside the porosity of MIL-53(Al). An arrangement of caffeine-terephthalate planes with C_2-axis of terephthalate parallel to an imaginary line bonding N_8 and N_1 in caffeine ring (Fig. 5c) is proposed for caffeine@MIL-53(Al). However, the symmetry of the MOF linker is not affected and the ^{13}C NMR peaks are similar to those of the bare MIL-53(Al).

Caffeine@UiO-66 exhibits ^{13}C NMR peaks corresponding to the MOF ligand wider as compared to the bare UiO-66 (Figure 5b). This agrees with the loss of crystallinity after the encapsulation process and with the XRD results and BET specific surface area values above discussed. Nevertheless, taking into account the observed changes in the chemical shifts of caffeine and ligand signals, a complementary explanation is proposed. A similar trend of caffeine signals in both MIL-53 and UiO-66 (Table S4) shows a parallel arrangement between additive and terephthalate ligand in both MOFs. Simultaneously,

the slight tendency to downfield of broadened carboxylate signal of ligand (a shoulder can even be observed at 172.3 ppm, Table S3b) next to a deshielding of C_{orto} suggests the formation of hydrogen bonds that involve the carboxylic group of terephthalate. Simultaneously, the amorphization of caffeine@UiO-66 and the different kind of host-guest interactions may increase the anisotropy of the host giving rise to the observed broad peaks.

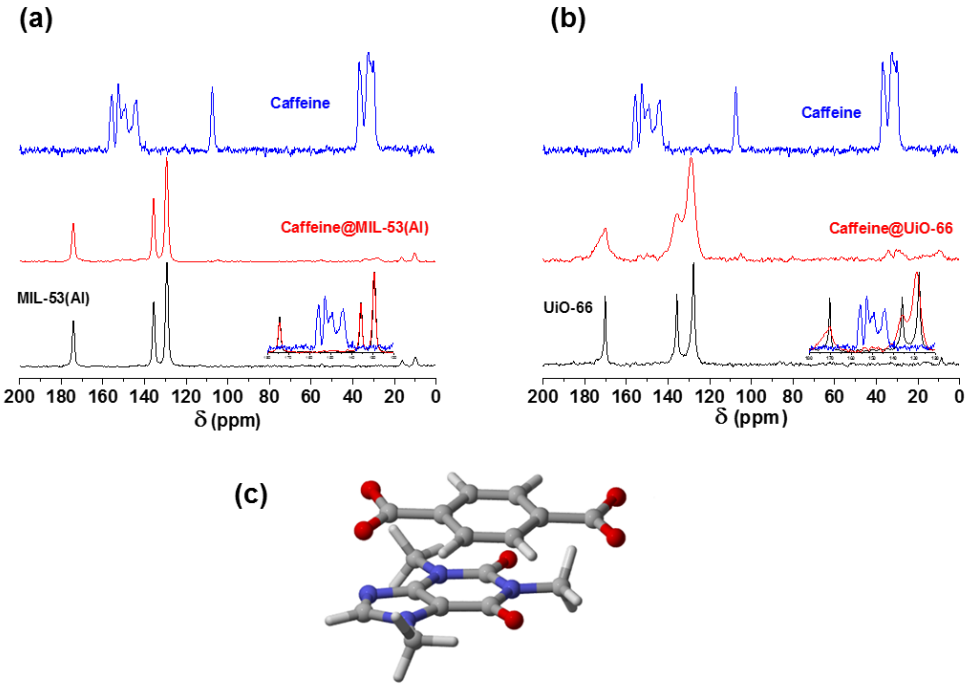

Figure 5. ^{13}C MAS NMR spectra of the different samples (from bottom to top, MOF, caffeine@MOF after high pressure encapsulation and caffeine) corresponding to: MIL-53(Al) (a), and UiO-66 (b). Encapsulation at room temperature, 0.32 GPa and 4:1 caffeine:MOF weight ratio. Proposed arrangement of caffeine-terephthalate planes with C_2-axis of terephthalate parallel to an imaginary line bonding N_8 and N_1 in caffeine ring. Color code: upfield atoms (blue) and downfield atoms (red) (c).

For kojic acid@MIL-53(Al) the terephthalate ^{13}C NMR signals were also widened (see Fig. 6a and Table S5) as compared to those of kojic acid and MIL53(Al). This is attributable to the host-guest interactions because the MIL-53(Al) structure was preserved after the high pressure treatment, in agreement with both XRD and N_2 adsorption characterizations. The chemical ^{13}C NMR signals of terephthalate in kojic acid@MIL-53(Al) followed a different pattern from those of caffeine@MIL-53(Al) and kojic acid@UiO-66 (Table S5), and carboxylate and C_{orto} signals of ligand shifted upfield. This behavior suggests that the presence of the additive modifies the metal-terephthalate interactions. It has been described that changes in binding modes of the acetate group in metallic clusters can be determined using the solid-state ^{13}C NMR: carboxylate peak

shifts upfield when it changes from chelating mode to bidentate or monodentate bridge.[64] This change in metal-terephthalate binding must be due to the effect of kojic acid. It is known that kojic acid forms stable chelates with metal acetate salts.[65] Nevertheless, the suggested interactions are reversible, as the thermodiffractometry experiments suggests (see below).

Finally, the chemical ^{13}C NMR peaks of terephthalate in kojic acid@UiO-66 did not broaden suggesting ordered host-guest interactions (Fig. 6b and Table S5). Carboxylate and C_{orto} signals of ligand were deshielded evidencing the formation of hydrogen bonds between carboxylic groups of terephthalate and hydroxyl groups of kojic acid. A slightly shielding of carbon atoms of kojic acid suggests an additional stacking of the aromatic rings of both structures in parallel planes. The behavior of carbonyl C_4 in kojic acid is different because it is the most electronically affected by the intermolecular hydrogen bond with terephthalate, since it must loss its intramolecular hydrogen bond. These kojic acid-UiO-66 interactions could preserve the symmetry of the linker and the ordered structure of MOF, in agreement with ^{13}C NMR spectra.

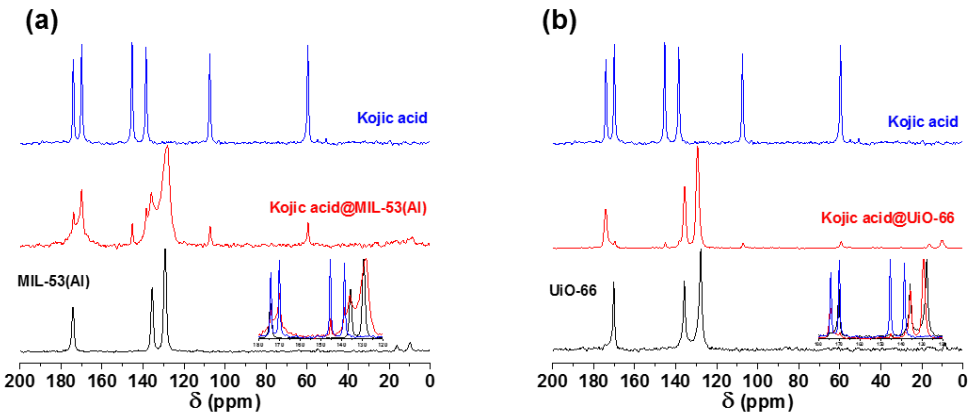

Figure 6. ^{13}C MAS NMR spectra of the different samples (from bottm to top, MOF, kojic acid@MOF after high pressure encapsulation and kojic acid) corresponding to MIL-53(Al)(a), and UiO-66 (b). Encapsulation at room temperature, 0.32 GPa and 4:1 kojic acid:MOF weight ratio.

Table 2 shows the encapsulation values achieved with the different MOFs. The calculation was made per g dry MOF, i.e. excluding from the curves in Figs. S1 and S3 solvent (in principle water from moisture) and external (non-encapsulated) additive weight losses below ca. 100 °C and above the removal temperature of the pure additive, respectively. The material that produced the best results was MIL-53(Al), with 37% and 32% loadings for caffeine and kojic acid, respectively. This can be related to its exceptional stability against mechanical treatment and the flexibility of its structure,[16]

which facilitates the successful encapsulation of the two different additives, caffeine and kojic acid. Additionally, UiO-66 showed 15% and 22% loadings for caffeine and kojic acid, respectively, but the loadings (probably due to its small porosity and lack of flexibility) and the mechanical stability (see the above XRD discussion) were lower than in the case of MIL-53(Al). Mg-MOF-74 has been demonstrated to be stable at high pressure and the encapsulation seems to be achieved only for kojic acid (24%) under the experimental conditions tested. The encapsulation in Mg-MOF-74 involves the exchange of water (present in the as-made MOF, as shown in Fig. S2c with the first step around 100 °C) by the desired guest, and only kojic acid was able to produce such an exchange. Table 2 also shows the number of molecules of additive per unit cell (u.c.): 1.6 and 1.3 molecules/u.c. for caffeine@MIL-53(Al) and caffeine@UiO-66, respectively, and 1.9, 2.5 and 2.1 molecules/u.c. for kojic acic@MIL-53(Al), kojic acid@UiO-66 and kojic acid@Mg-MOF-74, respectively. For the corresponding calculations, the unit cell formulae of $C_{32}Al_4O_{20}H_{20}$ (MIL-53(Al)),[16] $C_{192}Zr_{24}O_{120}H_{96}$ (UiO-66)[20] and $C_{16}Mg_{16}O_{40}H_8$ (Mg-MOF-74).[25] This means that the wt% loading corresponding to one molecule per u.c. is 23, 12 and 16 wt% in case of caffeine and 17, 8.7 and 12 wt% in case of kojic acid for for MIL-53(Al), UiO-66 and Mg-MOF-74, respectively.

Table 2. Caffeine and kojic acid encapsulation in different MOFs at 0.32 GPa with 4:1 MOF:guest weight ratio and room temperature in (g guest/g dry MOF)·100 and number of additive molecules per unit cell (molec./u.c.). The unit cell formulae of $C_{32}Al_4O_{20}H_{20}$, $C_{192}Zr_{24}O_{120}H_{96}$ and $C_{16}Mg_{16}O_{40}H_8$ have been considered for MIL-53(Al),[16] UiO-66[20] and Mg-MOF-74,[25] respectively, for the calculations.

Guest	**MIL-53(Al)**		**UiO-66**		**Mg-MOF-74**	
Caffeine	37%	1.6 molec./u.c.	15%	1.3 molec./u.c.	0%	0 molec./u.c.
Kojic acid	32%	1.9 molec./u.c.	22%	2.5 molec./u.c.	24%	2.1 molec./u.c.

Effect of temperature and pressure on the encapsulation in MIL-53(Al)

MIL-53(Al) is sensitive to temperature[16,66] and a sufficiently high temperature may help the desorption of the guest. We have therefore observed the effect of different temperatures on high pressure encapsulation samples in thermodiffractometry experiments. Fig.7 shows the diffraction patterns measured in the 25-300 °C range. When increasing the temperature from 50 to 100 °C, the caffeine@MIL-53 sample changed its structure from the hydrated, low temperature form (MIL-53(Al) *lt*) to the high temperature form (MIL-53(Al) *ht*,[16] maintained upon heating up to 300 °C), while caffeine peaks are scarcely apparent. However, the TGA analyses carried out on pure

caffeine and caffeine@MIL-53 are consistent with the removal of caffeine at a temperature higher than 100 °C (Fig. S2a). This suggests that the action of the high temperature favors the encapsulation of caffeine guest molecules placed in the surroundings of caffeine@MIL-53. This can be considered as a process in series. First, the high temperature increases the mobility of caffeine molecules already encapsulated, but occupying mostly external crystal pores and eventually reaching empty internal crystal pores. Second, caffeine molecules impregnating the external surfaces of MIL-53 crystals penetrate inside the porous structure.

In the case of the kojic acid@MIL-53 sample, the phase transition is also observed (Fig. 7). Additionally, the complexity of the peaks is considerably increased at 150 °C. We assume that the molecule of kojic acid interacts with the functional groups in the pores and, as occurs with water molecules, the structure changes according to this stimulus. The recovery of the structure of MIL-53(Al) *ht* upon heating at 300 °C is consistent with a reversible encapsulation process in both caffeine@MIL-53 and kojic acid@MIL-53 samples. These results are completed with the thermodiffractometries corresponding to the encapsulations of caffeine and kojic acid on UiO-66 and Mg-MOF-74 (Fig. S5).

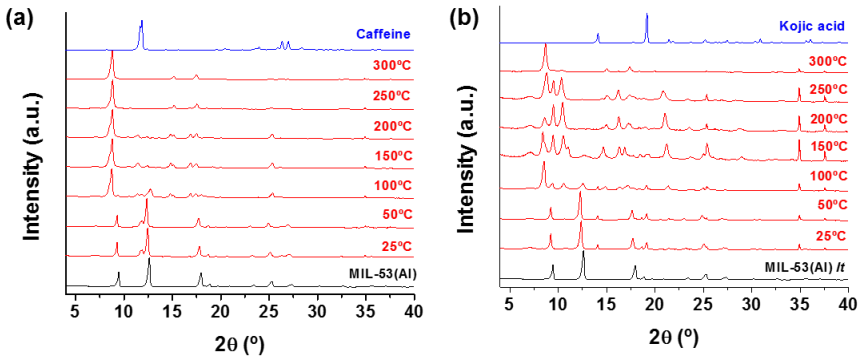

Figure 7. Thermodiffractometry in air with a heating ramp of 10°C/min of caffeine@MIL-53(Al) (a) and kojic acid@MIL-53 (b). Encapsulation at 0.32 GPa and with a 4:1 MOF:guest weight ratio.

Once demonstrated the new solventless application, to gain insight into the encapsulation at high pressure and the impact of temperature, the influence of a small amount of ethanol in the encapsulation of caffeine in MIL-53(Al) was investigated. After the addition, the mixture was still a solid considering the small amount of ethanol used in the experiment. This would improve the additive-MOF contact and hence the diffusion and dispersion of the additive into the pores of the MOF. Fig. S6 shows a more complex XRD pattern compared to those of the as-made material and those encapsulated without ethanol (Fig. 3a). As mentioned above, MIL-53(Al) "breathes" depending on the presence

of guest molecules in the pores of the MOF, and as a consequence the diffraction pattern was modified. In this experiment, caffeine and ethanol were simultaneously adsorbed on the material evidencing changes in the XRD intensities, consistent with an opening (as compared with the *lt* as-made material) of the porosity as observed for MIL-53(Cr) when adsorbing methanol and ethanol.[67]

The sample caffeine@MIL-53(Al), obtained in the presence of ethanol, was used in a thermodiffractometry experiment carried out under vacuum. Together with this sample, Fig. S6 shows for the purposes of comparison the XRD patterns of caffeine and MIL-53(Al) at the initial conditions previous to the encapsulation, i.e. in the form known as *lt*.[16] Upon heating at 200 °C, the ethanol was desorbed from the MOF and the XRD adapted the *ht* form for MIL-53(Al).[68] After subsequent heating at 300 °C, caffeine should have been removed (in agreement with the TGA shown in Fig. S7); however, no further changes were observed in the XRD pattern.

Finally, even though most of the encapsulation experiments were carried out at 0.32 GPa, Tables S6 and S7 and Fig. S8 show the encapsulation of caffeine and kojic acid on MIL-53(Al) at three different pressures from 0.32 to 0.64 GPa. The decrease of the percentage of encapsulation (MIL-53(Al)) and the similar values of BET specific surface area observed with increasing pressure suggest that 0.32 GPa was the optimum working pressure. This pressure relates to a good balance between the loss of MOF crystallinity and the encapsulation efficiency.

CONCLUSIONS

We have demonstrated the simple and ecofriendly encapsulation of caffeine in two different MOFs by means of a high pressure application (0.32 GPa). This simple procedure may be of considerable industrial interest considering its speed and the fact that it does not need further purification (i.e. separation from the encapsulation dispersion as in the case of conventional liquid phase encapsulation). This minimizes the use of solvents and the potential generation of waste. Moreover, the solvent free, high pressure approach has been carried out with three MOFs (MIL-53(Al), UiO-66 and Mg-MOF-74, since MIL-101(Cr) was strongly amorphized upon high pressure exposure) and two guests (caffeine and kojic acid), the best results being obtained with MIL-53(Al) due probably to its high structural flexibility that helps the diffusion of caffeine under the pressure effect. The XRD characterization demonstrated the encapsulation qualitatively, while TGA allowed to estimate of the amount of drug encapsulated in every case. In addition, the decrease of the BET specific surface area of MOFs after the encapsulation

of caffeine and kojic acid was consistent with its pores filled with the additives. The ^{13}C MAS NMR spectra of the additive@MOF materials support the preservation of the chemical nature of caffeine and kojic acid upon high pressure encapsulation, suggesting in some cases (caffeine@MIL-53(Al) and kojic acid@UiO-66) relatively ordered host-guest interactions. The combination of the four characterization techniques demonstrated both the qualitative and quantitative caffeine and kojic acid encapsulation in the studied MOFs using the at high pressure conditions in solvent-free conditions. Finally, the results achieved thought this research, obtained through a green process, allows one to say that MOF encapsulation is a field with great potential of industrial development where the costs and environmental impacts can be minimized.

EXPERIMENTAL SECTION

Synthesis of materials

Synthesis of MIL-53(Al). In a typical synthesis,[16] 5.20 g of aluminum nitrate nonahydrate (13.9 mmol, $Al(NO_3)_3 \cdot 9H_2O$, Sigma Aldrich, ≥98%) together with 1.12 g of terephthalic acid (6.7 mmol, H_2BDC, Sigma Aldrich, 98%) were dispersed in 100 mL of distilled water and placed in a Teflon-lined stainless steel autoclave for 3 days at 220 °C. The resulting product was recovered by centrifugation at 10,000 rpm for 10 min, washed once with ethanol followed by centrifugation under the same conditions and dried overnight at 65 °C. The solid was activated by calcination at 380 °C for 24 h.

Synthesis of UiO-66. Following a previous report,[20] 0.508 g of $ZrCl_4$ (2 mmol, Sigma Aldrich, ≥99,5 %) and 0.667 g of terephthalic acid (4 mmol, H_2BDC, Sigma Aldrich, 98%) were mixed with 100 mL of dimethylformamide (DMF) and the resulting solution placed in a Teflon-lined stainless steel autoclave for 24 h at 120 °C. The white product was recovered by centrifugation at 10,000 rpm for 10 min and washed once with ethanol followed by centrifugation under the same conditions. The solid was activated by calcination at 300 °C for 4 h.

Synthesis of Mg-MOF-74. As reported elsewhere,[21] 0.149 g of 2,5-dihydroxyterephthalic acid (0.75 mmol, DOBDC, TCI, >98%) was dissolved in 10 mL of THF after which 3 mL of a 1 M NaOH aqueous solution was added. A solution of 0.384 g of magnesium nitrate hexahydrate (1.5 mmol, $Mg(NO_3)_2 \cdot 6H_2O$, Sigma Aldrich, 98%) in 3 mL of distilled water was added and the resulting mixture placed in a Teflon-lined stainless steel autoclave for 3 days at 110 °C. The yellow product was recovered by centrifugation at 10,000 rpm for 10 min and washed several times with methanol

followed by centrifugation under the same conditions. The product was dried overnight at room temperature.

Synthesis of MIL-101(Cr). Following a previous report,[69] 0.83 g of terephthalic acid (5 mmol, H_2BDC, Sigma Aldrich, 98%) and 2.00 g of chromium nitrate nonahydrate (5 mmol, $Cr(NO_3)_3 \cdot 9H_2O$, Sigma Aldrich, 98%) were mixed in 25 mL of distilled water and placed in a Teflon-lined stainless steel autoclave for 8 h at 220 °C. The green product was recovered by centrifugation at 10,000 rpm for 10 min and washed with methanol followed by centrifugation under the same conditions. The solid was activated by treatment in DMF for 24 h at 150 °C and then boiled in a reflux in methanol overnight. The product was dried at room temperature for 8 h.

High pressure encapsulation

The procedure for the high pressure encapsulation was as follows: 100 mg of the MOF material and 25 mg of additive (weight ratio 4:1) were mixed together by 1 min hand shaking in a vial. The mixture was then placed at room temperature inside the metal cylinder of a hydraulic press (Specac 25.011). After insertion of the metal piston, pills were compacted under a pressure of 0.32-0.64 GPa for 30 min. The compacted material pill was gently milled into powder and is referred to here as additive@MOF. Blanks corresponding to the MOFs and additives separately exposed to high pressure were produced under the same conditions. Additionally, in the case of MIL-53(Al), 2:1 and 1:1 MOF:additive weight ratios were contacted at high pressure. Finally, a 2:1 weight ratio experiment was carried out at 0.32 GPa for 30 min with the addition of 20 mg (ca. 0.025 mL) of ethanol, i.e. using a 2:1:0.4 MOF:additive:ethanol weight ratio.

Characterization

Scanning electron microscopy (SEM, FEI Inspect F50) observation of the powder samples was carried out with a voltage 2-15 kV and after Pt coating. Powder X-ray diffraction (XRD) was carried out at room temperature in a Siemens diffractometer with a copper anode and a graphite monochromator so as to select Cu-$K\alpha_1$ radiation (λ=1.540 Å). Data were collected in the 4-40° 2θ range, and the scanning rate was 0.03°/s. This technique was used to check the crystallinity after the process and to observe the decrease of additive peaks in high pressure contact encapsulation due to the reduction of the external additive. Nitrogen adsorption isotherm and BET specific surface area were measured with a Micrometrics TriStar 3000 with a previous degasification at 150 °C for

5 h. The ^{13}C NMR spectra were achieved with cross-polarized magic angle spinning solid nuclear magnetic resonance (CP MAS-NMR) in a Bruker Avance III WB 400. Thermogravimetric analyses (TGA) were performed using Mettler Toledo TGA/SDTA 851e instrument. The samples were put in 70 µL alumina pans and heated up to 700 °C with a heating rate of 10 °C/min in air. Thermodiffractometry was performed under air in a furnace coupled to a Siemens diffractometer with a copper anode and a graphite monochromator to select the same Cu-$K_{\alpha 1}$ radiation. Each XRD pattern was recorded for 20 min in the 3-40° 2θ range with a 0.01°/s scanning rate at 25, 50, 100, 150, 200, 250 and 300 °C with a heating rate of 10 °C/min.

REFERENCES

1 G. Férey, *Chem. Soc. Rev.*, 2008, **37**, 191–214.

2 J. L. C. Rowsell and O. M. Yaghi, *Angew. Chem., Int. Ed.*, 2005, **44**, 4670–4679 ; *Angew. Chem.*, 2005, **117**, 48

3 N. Li, J. Xu, R. Feng, T.-L. L. Hu and X.-H. H. Bu, *Chem. Commun.*, 2016, **52**, 8501–8513.

4 J. B. DeCoste, G. W. Peterson, H. Jasuja, T. G. Glover, Y. Huang and K. S. Walton, *J. Mater. Chem. A*, 2013, **1**, 5642–5650.

5 H. Li, M. Eddaoudi, M. O'Keeffe and O. M. Yaghi, *Nature*, 1999, **402**, 276–279.

6 J. Lee, O. K. Farha, J. Roberts, K. a Scheidt, S. T. Nguyen and J. T. Hupp, *Chem. Soc. Rev.*, 2009, **38**, 1450–1459.

7 J.-R. Li, R. J. Kuppler and H.-C. Zhou, *Chem. Soc. Rev.*, 2009, **38**, 1477–1504.

8 S. Sorribas, P. Gorgojo, C. Téllez, J. Coronas and A. G. Livingston, *J. Am. Chem. Soc.*, 2013, **135**, 15201–15208.

9 L. Paseta, G. Potier, S. Abbott and J. Coronas, *Org. Biomol. Chem.*, 2015, **13**, 1724–1731.

10 P. Horcajada, T. Chalati, C. Serre, B. Gillet, C. Sebrie, T. Baati, J. F. Eubank, D. Heurtaux, P. Clayette, C. Kreuz, J.-S. Chang, Y. K. Hwang, V. Marsaud, P.-N. Bories, L. Cynober, S. Gil, G. Férey, P. Couvreur and R. Gref, *Nat. Mater.*, 2010, **9**, 172–178.

11 S. Wuttke, M. Lismont, A. Escudero, B. Rungtaweevoranit and W. J. Parak, *Biomaterials*, 2017, **123**, 172–183.

12 M. Lismont, L. Dreesen and S. Wuttke, *Adv. Funct. Mater.*, 2017, **27**.

13 P. Horcajada, R. Gref, T. Baati, P. K. Allan, G. Maurin, P. Couvreur, G. Férey, R. E. Morris and C. Serre, *Chem. Rev.*, 2012, **112**, 1232–1268.

14 V. André and S. Quaresma, eds. F. Zafar and E. B. T.-M.-O. F. Sharmin, InTech, Rijeka, 2016, p. Ch. 07.

15 A. C. McKinlay, R. E. Morris, P. Horcajada, G. Férey, R. Gref, P. Couvreur and C. Serre, *Angew. Chem., Int. Ed.*, 2010, **49**, 6260–6266; *Angew.Chem.*, 2010

16 T. Loiseau, C. Serre, C. Huguenard, G. Fink, F. Taulelle, M. Henry, T. Bataille and G. Férey, *Chemistry*, 2004, **10**, 1373–1382.

17 P. Horcajada, C. Serre, G. Maurin, N. A. Ramsahye, F. Balas, M. Vallet-Regí, M. Sebban, F. Taulelle and G. Férey, *J. Am. Chem. Soc.*, 2008, **130**, 6774–6780.

18 C. Serre, C. Mellot-Draznieks, S. Surblé, N. Audebrand, Y. Filinchuk and G. Férey, *Science (80-.).*, 2007, **315**, 1828–1831.

19 L. Paseta, E. Simón-Gaudó, F. Gracia-Gorría and J. Coronas, *Chem. Eng. J.*, 2016, **292**, 28–34.

20 J. H. Cavka, S. Jakobsen, U. Olsbye, N. Guillou, C. Lamberti, S. Bordiga and K. P. Lillerud, *J. Am. Chem. Soc.*, 2008, **130**, 13850–13851.

21 P. D. C. Dietzel, R. Blom and H. Fjellvåg, *Eur. J. Inorg. Chem.*, 2008, 3624–3632.

22 S. R. Caskey, A. G. Wong-Foy and A. J. Matzger, *J. Am. Chem. Soc.*, 2008, **130**, 10870–10871.

23 Y. Jiao, C. R. Morelock, N. C. Burtch, W. P. Mounfield, J. T. Hungerford and K. S. Walton, *Ind. Eng. Chem. Res.*, 2015, **54**, 12408–12414.

24 G. Férey, C. Mellot-Draznieks, C. Serre, F. Millange, J. Dutour, S. Surblé and I. Margiolaki, *Science (80-.).*, 2005, **309**, 2040.

25 S. Øien, D. Wragg, H. Reinsch, S. Svelle, S. Bordiga, C. Lamberti and K. P. Lillerud, *Cryst. Growth Des.*, 2014, **14**, 5370–5372.

26 O. I. Lebedev, F. Millange, C. Serre, G. Van Tendeloo and G. Férey, *Chem. Mater.*, 2005, **17**, 6525–6527.

27 M. C. Bernini, D. Fairen-Jimenez, M. Pasinetti, A. J. Ramirez-Pastor and R. Q. Snurr, *J. Mater. Chem. B*, 2014, **2**, 766.

28 R. C. Huxford, J. Della Rocca and W. Lin, *Curr. Opin. Chem. Biol.*, 2010, **14**, 262–268.

29 S. Wuttke, S. Braig, T. Preiß, A. Zimpel, J. Sicklinger, C. Bellomo, J. O. Rädler, A. M. Vollmar and T. Bein, *Chem. Commun.*, 2015, **51**, 15752–15755.

30 T. Preiß, A. Zimpel, S. Wuttke and J. O. Rädler, *Materials (Basel).*, 2017, **10**, 216.

31 D. Cunha, M. Ben Yahia, S. Hall, S. R. Miller, H. Chevreau, E. Elkaïm, G. Maurin, P. Horcajada and C. Serre, *Chem. Mater.*, 2013, **25**, 2767–2776.

32 S. Devautour-Vinot, C. Martineau, S. Diaby, M. Ben-Yahia, S. Miller, C. Serre, P. Horcajada, D. Cunha, F. Taulelle and G. Maurin, *J. Phys. Chem. C*, 2013, **117**, 11694–11704.

33 R. Anand, F. Borghi, F. Manoli, I. Manet, V. Agostoni, P. Reschiglian, R. Gref and S. Monti, *J. Phys. Chem. B*, 2014, **118**, 8532–8539.

34 P. Horcajada, F. Salles, S. Wuttke, T. Devic, D. Heurtaux, G. Maurin, A. Vimont, M. Daturi, O. David, E. Magnier, N. Stock, Y. Filinchuk, D. Popov, C. Riekel, G. Férey and C. Serre, *J. Am. Chem. Soc.*, 2011, **133**, 17839–17847.

35 N. Liedana, P. Lozano, A. Galve, C. Tellez and J. Coronas, *J. Mater. Chem. B*, 2014, **2**, 1144–1151.

36 N. Liédana, E. Marín, C. Téllez and J. Coronas, *Chem. Eng. J.*, 2013, **223**, 714–721.

37 A. Chakraborty and C. Adhikari, *Chemphyschem*, 2016, **17**, 1070–7.

38 H. Zheng, Y. Zhang, L. Liu, W. Wan, P. Guo, A. M. Nyström and X. Zou, *J. Am. Chem. Soc.*, 2016, **138**, 962–968.

39 N. Motakef-Kazemi, S. A. Shojaosadati and A. Morsali, *Microporous Mesoporous Mater.*, 2014, **186**, 73–79.

40 S. Wang, C. M. McGuirk, M. B. Ross, S. Wang, P. Chen, H. Xing, Y. Liu and C. A. Mirkin, *J. Am. Chem. Soc.*, 2017, **139**, 9827–9830.

41 R. Röder, T. Preiβ, P. Hirschle, B. Steinborn, A. Zimpel, M. Höhn, J. O. Rädler, T. Bein, E. Wagner, S. Wuttke and U. Lächelt, *J. Am. Chem. Soc.*, 2017, **139**, 2359–2368.

42 J. Zhuang, C. H. Kuo, L. Y. Chou, D. Y. Liu, E. Weerapana and C. K. Tsung, *ACS Nano*, 2014, **8**, 2812–2819.

43 A. Nehlig, J. L. Daval and G. Debry, *Brain Res. Rev.*, 1992, **17**, 139–170.

44 D. Hexsel, C. Orlandi and D. Zechmeister do Prado, *Dermatol. Surg.*, 2005, **31**, 866–872; discussion 872.

45 M. Nakagawa and K. Kawai, *Contact Dermatitis*, 1995, **32**, 9–13.

46 M. Mohammadpour, M. Behjati, A. Sadeghi and A. Fassihi, *Int. Wound J.*, 2013, **10**, 260–264.

47 J. Nawarak, R. Huang-Liu, S.-H. Kao, H.-H. Liao, S. Sinchaikul, S.-T. Chen and S.-L. Cheng, *J. Proteome Res.*, 2008, **7**, 3737–46.

48 X. Liu, W. Xia, Q. Jiang, Y. Xu and P. Yu, *J. Biosci. Bioeng.*, 2015, **120**, 335–339.

49 L. Paseta, G. Potier, S. Sorribas and J. Coronas, *ACS Sustain. Chem. Eng.*, 2016, **4**, 3780–3785.

50 S. Tanaka, K. Kida, T. Nagaoka, T. Ota and Y. Miyake, *Chem. Commun.*, 2013, **49**, 7884–7886.

51 S. A. Moggach, T. D. Bennett and A. K. Cheetham, *Angew. Chem., Int. Ed.*, 2009, **48**, 7087–7089, *Angew. Chem.,* 2009, **121**, 38

52 Y. Hu, H. Kazemian, S. Rohani, Y. Huang and Y. Song, *Chem. Commun.*, 2011, **47**, 12694.

53 I. Khay, G. Chaplais, H. Nouali, C. Marichal and J. Patarin, *RSC Adv.*, 2015, **5**, 31514–31518.

54 K. W. Chapman, G. J. Halder and P. J. Chupas, *J. Am. Chem. Soc.*, 2008, **130**, 10524–10526.

55 I. Erucar and S. Keskin, *Ind. Eng. Chem. Res.*, 2016, **55**, 1929–1939.

56 M. J. Rosseinsky, A. Grigoropoulos, A. I. McKay, A. P. Katsoulidis, R. P. Davies, A. Haynes, L. Brammer, J. Xiao and A. S. Weller, *Angew. Chem., Int. Ed.*,2018, **77**, 17; *Angew. Chem.*, 2018, **130**, 17.

57 C. Petit, *Curr. Opin. Chem. Eng.*, 2018, **20**, 132-142.

58 N. Liédana, A. Galve, C. Rubio, C. Téllez and J. Coronas, *ACS Appl. Mater. Interfaces*, 2012, **4**, 5016–5021.

59 P. Serra-Crespo, A. Dikhtiarenko, E. Stavitski, J. Juan-Alcañiz, F. Kapteijn, F.-X. Coudert and J. Gascon, *CrystEngComm*, 2015, **17**, 276–280.

60 S. M. J. Rogge, J. Wieme, L. Vanduyfhuys, S. Vandenbrande, G. Maurin, T. Verstraelen, M. Waroquier and V. Van Speybroeck, *Chem. Mater.*, 2016, **28**, 5721–5732.

61 S. M. J. Rogge, M. Waroquier and V. Van Speybroeck, *Acc. Chem. Res.*, 2017, **51**, 1, 138-148.

62 P. G. Yot, K. Yang, F. Ragon, V. Dmitriev, T. Devic, P. Horcajada, C. Serre and G. Maurin, *Dalt. Trans.*, 2016, **45**, 4283–4288.

63 C. M. Hansen, *Hansen solubility parameters: a user's handbook*, CRC Press, Boca Raton, 2nd edn., 2007.

64 B. H. Ye, X. Y. Li, I. D. Williams and X. M. Chen, *Inorg. Chem.*, 2002, **41**, 6426–6431.

65 M. M. Finnegan, T. G. Lutz, W. O. Nelson, A. Smith and C. Orvig, *Inorg. Chem.*, 1987, **26**, 2171–2176.

66 B. Seoane, S. Sorribas, Á. Mayoral, C. Téllez and J. Coronas, *Microporous Mesoporous Mater.*, 2015, **203**, 17–23.

67 S. Bourrelly, B. Moulin, A. Rivera, G. Maurin, S. Devautour-Vinot, C. Serre, T. Devic, P. Horcajada, A. Vimont, G. Clet, M. Daturi, J. C. Lavalley, S. Loera-Serna, R. Denoyel, P. L. Llewellyn and G. Férey, *J. Am. Chem. Soc.*, 2010, **132**, 9488–9498.

68 S. Devautour-Vinot, G. Maurin, F. Henn, C. Serre and G. Férey, *Phys. Chem. Chem. Phys.*, 2010, **12**, 12478–12485.

69 Z. Zhao, X. Li and Z. Li, *Chem. Eng. J.*, 2011, **173**, 150–157.

4.3. Supporting Information

Table S1. FWHM (full width at the half maximum) ratios corresponding to XRD main peaks of MOFs after and before (as-made) high pressure treatment. The following XRD peaks have been used: MIL-53(Al): 12.5° - (110) plane, UiO-66: 7.2° - (111) plane, and Mg-MOF-74: 11.7° - (300) plane. XRD data for FWHM calculations from Figs. 3 and 4.

	MIL-53(Al) $FWHM_{treated}/FWHM_{as\text{-}made}$		UiO-66 $FWHM_{treated}/FWHM_{as\text{-}made}$		Mg-MOF-74 $FWHM_{treated}/FWHM_{as\text{-}made}$
	Caffeine	Kojic acid	Caffeine	Kojic acid	Kojic acid
MOF, 0.32 GPa	0.99		2.5		1.3
Encapsulation, 0.32 GPa	0.93	1.2	5.6	3.6	1.3

Table S2. Area ratios corresponding to main XRD peaks of additives and MOFs for simple additive-MOF blending (0 GPa) and encapsulation at 0.32 GPa. Caffeine (CAF): 11.9°, kojic acid (KA): 19.3°, MIL-53(Al): 12.5° ((110) plane), UiO-66: 7.2° ((111) plane), and Mg-MOF-74: 11.7° ((300) plane). Encapsulation at room temperature and 4:1 MOF:additive weight ratio.

	MIL-53(Al)		UiO-66		Mg-MOF-74
Ratio / Pressure	$A_{CAF}/A_{(110)}$	$A_{KA}/A_{(110)}$	$A_{CAF}/A_{(111)}$	$A_{KA}/A_{(111)}$	$A_{KA}/A_{(300)}$
Blending, 0 GPa	0.56	0.72	0.33	0.49	4.5
Encapsulation, 0.32 GPa	0.40	0.15	0.08	0.10	0.55

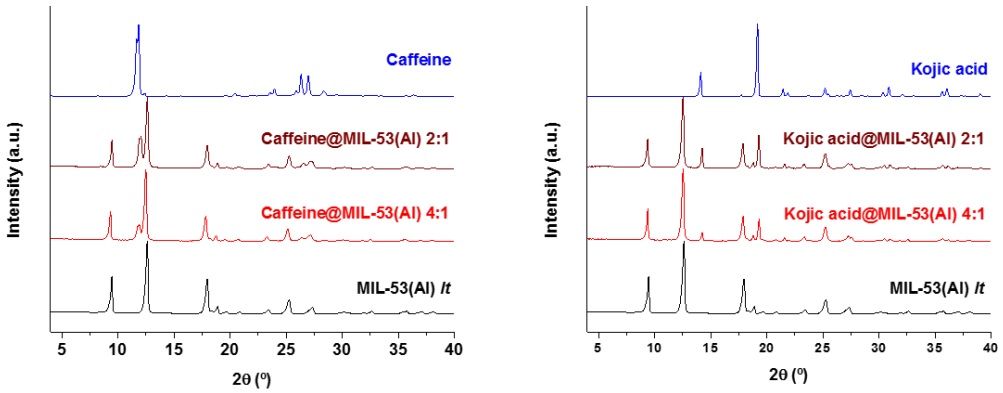

Figure S1. XRD patterns for (from bottom to up): MIL-53(Al), additive@MOF with MOF:caffeine weight ratios of 4:1 and 2:1 (100mg MOF:50mg additive), and additive.

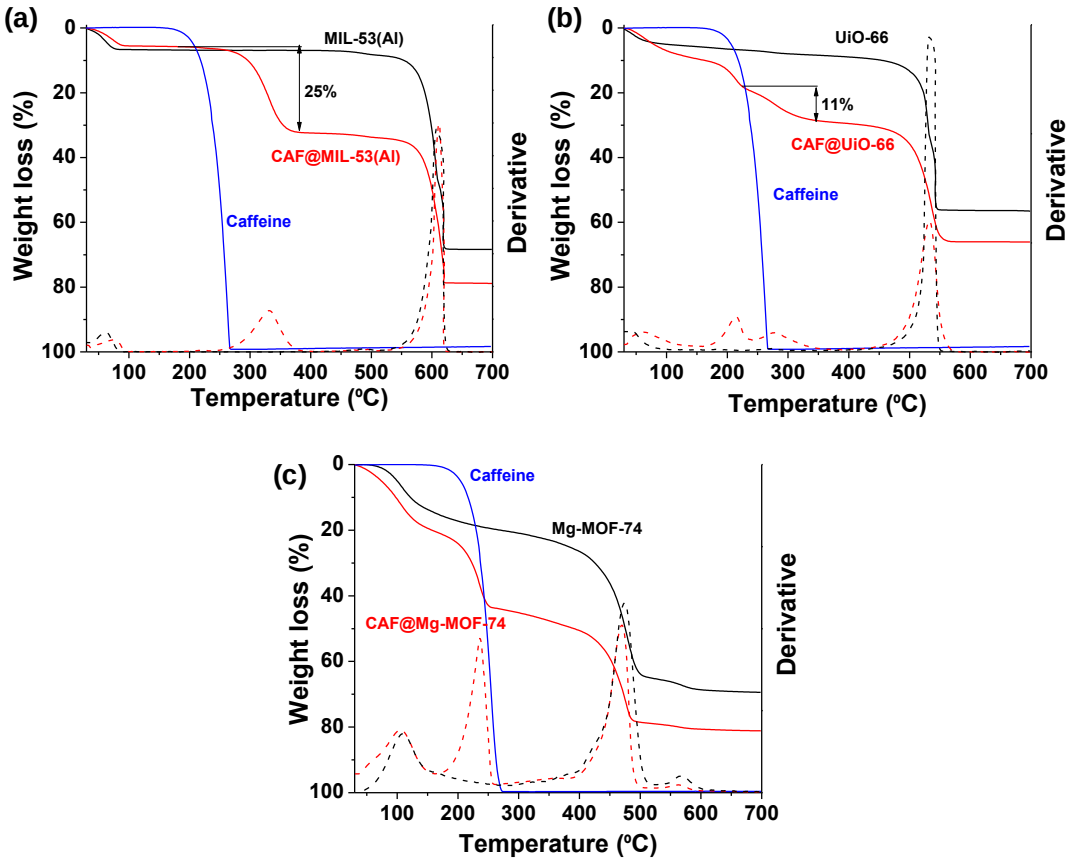

Figure S2. TGA curves of MOF (black line), caffeine (blue line) and caffeine@MOF after high pressure encapsulation (red line) with a 4:1 MOF:caffeine weight ratio.

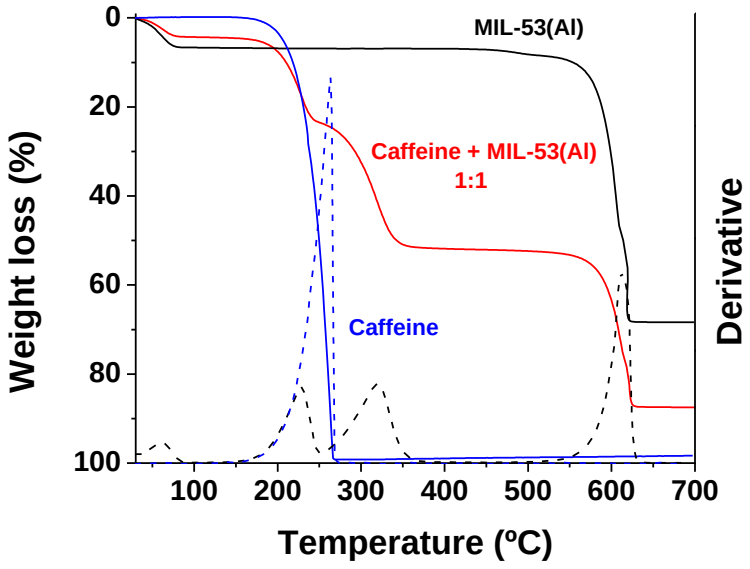

Figure S3. TGA curves of MOF (black line), caffeine (blue line) and caffeine@MOF after high pressure encapsulation (red line) with a 1:1 MOF:caffeine weight ratio.

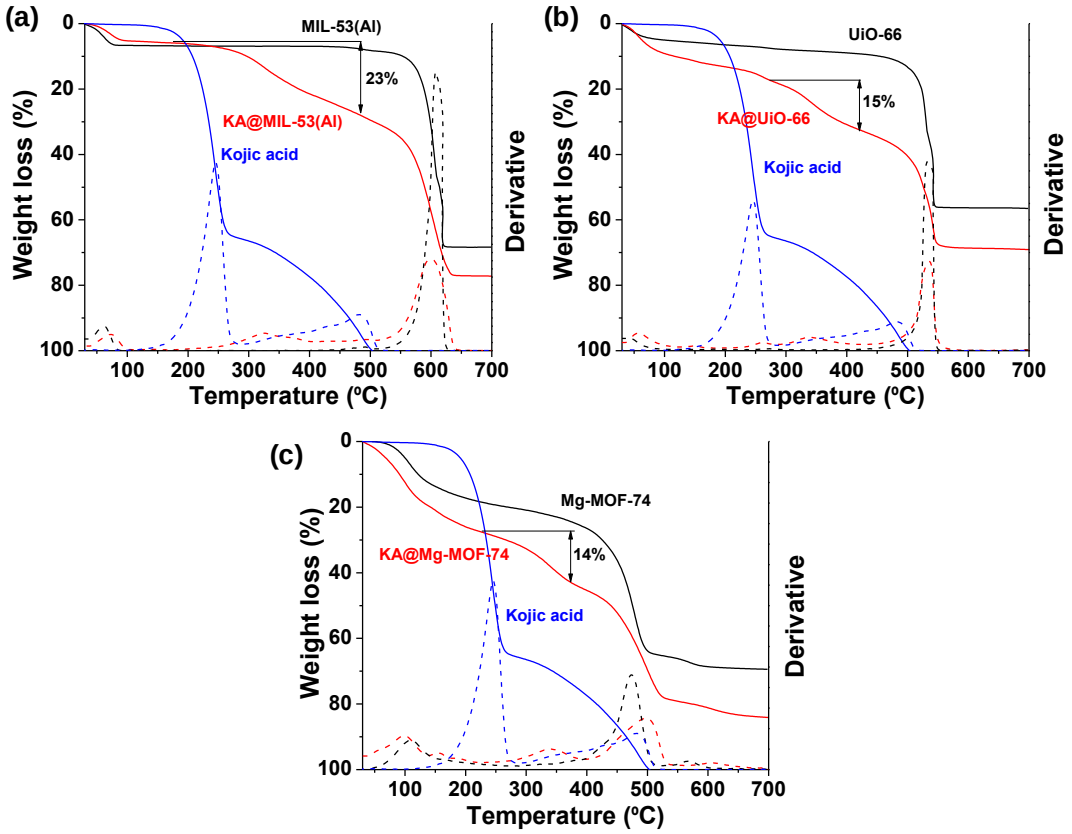

Figure S4. TGA curves of MOF (black line), kojic acid (blue line) and kojic acid@MOF after high pressure encapsulation (red line) with a 4:1 MOF:caffeine weight ratio.

Table S3. Chemical shifts (δ) in ^{13}C MAS NMR of terephthalate ligand in MIL-53(Al) and UiO-66 before and after high pressure encapsulation of caffeine (a) and kojic acid (b) (encapsulation at room temperature, 0.32 GPa and 4:1 kojic acid:MOF weight ratio). Differences in chemical shifts higher than 0.1 ppm between terephthalate signals before and after encapsulation of additives are recorded in parentheses (*d*: downfield, *u*: upfield) and they are highlighted on the figure as red and blue, respectively.

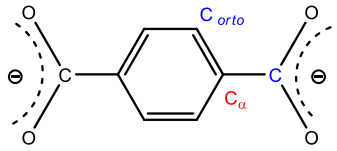

kojic acid@MIL-53

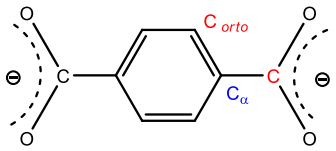

kojic acid@UiO-66

S3a)

	δ COO	δ C_α	δ C_{orto}
Terephthalate-MIL-53(Al)	174.3	135.6	129.3
Caffeine@MIL-53(Al)	174.3	135.7	129.4
Kojic acid@MIL-53(Al)	170.0 (4.3 *u*)	136.0 (0.4 *d*)	128.2 (1.1 *u*)

δ in ppm

S3b)

	δ COO	δ C_α	δ C_{orto}
Terephthalate –UiO-66	170.2	135.8	127.8
Caffeine@UiO-66	172.3 (2.1 *d*)	135.7	128.9 (1.1 *d*)
Kojic acid@UiO-66	174.2 (4.0 *d*)	135.7	129.4 (1.6 *d*)

δ in ppm

Table S4. Chemical shifts (δ) in ^{13}C MAS NMR of caffeine free and after encapsulation at high pressure into MIL-53(Al) and UiO-66 (encapsulation at room temperature, 0.32 GPa and 4:1 caffeine:MOF weight ratio). Differences in chemical shifts higher than 0.1 ppm between encapsulated and free caffeine signals are recorded in parentheses (*d*: downfield, *u*: upfield) and they are highlighted on the figure as red and blue, respectively.

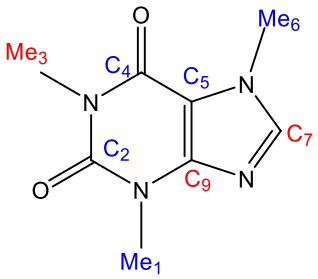

	δ C_2	δ C_4	δ C_5	δ C_7	δ C_9	Me_1	Me_3	Me_6
Caffeine	151.9	154.9	106.3	143.1	148.4	30.8	28.4	35.1
Caffeine@ MIL-538Al)	150.5 (1.4 *u*)	153.0 (1.9 *u*)	104.5 (1.8 *u*)	147.0 (3.9 *d*)	149.2 (0.8 *d*)	30.1 (0.7 *u*)	29.6 (1.2 *d*)	33.4 (1.7 *u*)
Caffeine@ UiO-66	150.2 (1.7 *u*)	153.2 (1.7 *u*)	105.0 (1.3 *u*)	147.2 (4.1 *d*)	149.3 (0.9 *d*)	30.5 (0.3 *u*)	29.2 (0.8 *u*)	34.2 (0.9 *u*)

δ in ppm

Table S5. Chemical shifts (δ) in ^{13}C MAS NMR of kojic acid free and after encapsulation at high pressure into MIL-53(Al) and UiO-66 (encapsulation at room temperature, 0.32 GPa and 4:1 kojic acid:MOF weight ratio). Differences in chemical shifts higher than 0.1 ppm between encapsulated and free kojic acid signals are recorded in parentheses (*d*: downfield, *u*: upfield) and they are highlighted on the figure as red and blue, respectively.

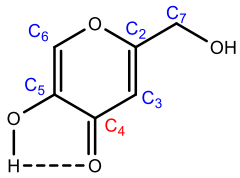

	δ C_2	δ C_3	δ C_4	δ C_5	δ C_6	δ C_7
Kojic acid	169.9	107.4	174.0	145.4	138.5	59.6
Kojic acid @ MIL-53(Al)	170	107.3	173.9	145.3	138.4	59.5
Kojic acid@ UiO-66	169.6 (0.3 *u*)	107.1 (0.3 *u*)	174.2 (0.2 *d*)	145.1 (0.3 *u*)	138.2 (0.3 *u*)	59.3 (0.3 *u*)

δ in ppm

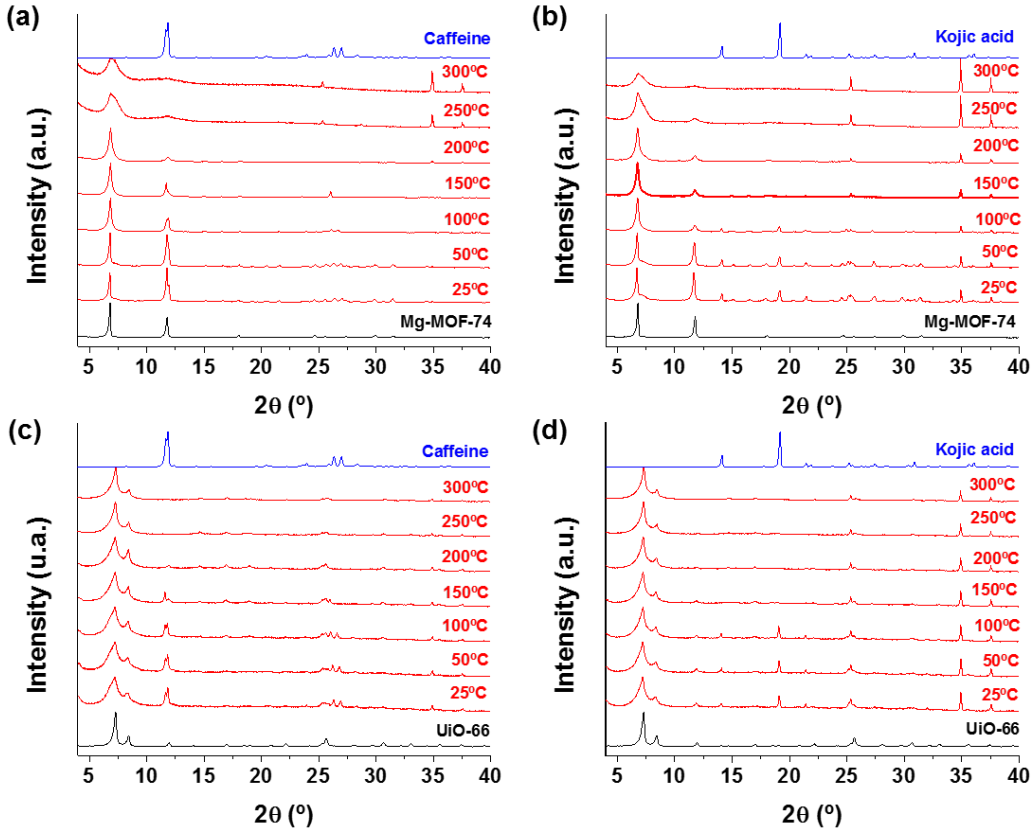

Figure S5. Thermodiffractometry in air with a heating ramp of 10°C/min of caffeine@Mg-MOF-74 (a), kojic acid@Mg-MOF-74 (b), caffeine@UiO-66 (c) and kojic acid@UiO-66 (d). Encapsulation at 0.32 GPa and with a 4:1 MOF:guest weight ratio.

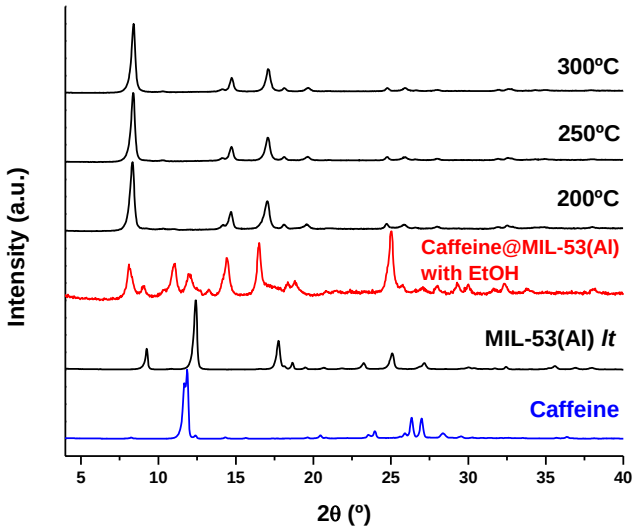

Figure S6. Thermodiffractometry of sample caffeine@MIL-53(Al). Encapsulation at 0.32 GPa and with a 2:1:0.4 MOF:caffeine:ethanol weight ratio.

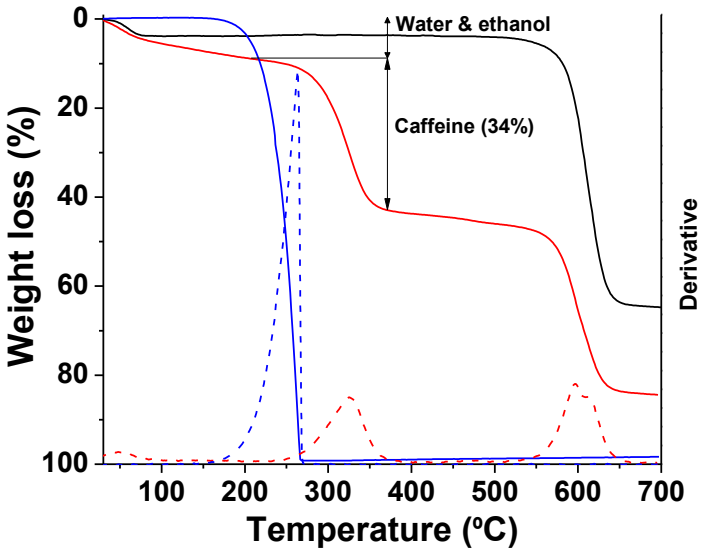

Figure S7. TGA curves of MIL-53(Al) (black line), caffeine (blue line) and caffeine@MOF (red line). Encapsulation at 0.32 GPa and with a 2:1:0.4 MOF:caffeine:ethanol weight ratio.

Table S6. Caffeine loadings and BET specific surface areas of caffeine@MIL-53(Al) samples obtained at different pressures. Encapsulation at room temperature and 4:1 MOF:additive weight ratio.

Pressure	(g caffeine/g dry MOF)·100	S_{BET} (m^2/g)
0.32 GPa	37%	336
0.48 GPa	33%	365
0.64 GPa	25%	215

Table S7. Kojic acid loadings and BET specific surface areas of caffeine@MIL-53(Al) samples obtained at different pressures. Encapsulation at room temperature and 4:1 MOF:additive weight ratio.

Pressure	(g kojic acid/g dry MOF)·100	S_{BET} (m^2/g)
0.32 GPa	32%	9
0.48 GPa	33%	8
0.64 GPa	34%	11

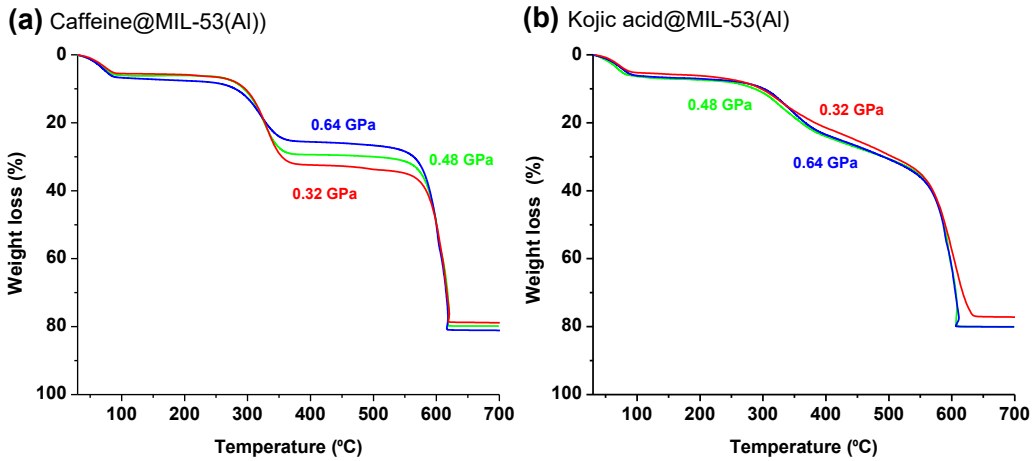

Figure S8. TGA curves corresponding to caffeine@MOF (a) and kojic acid@MOF obtained at different pressures. Encapsulation at room temperature and 4:1 MOF:additive weight ratio.

Chapter 5:

Supercritical CO2 encapsulation of bioactive molecules in carboxylate-based MOFs

State of the article:

Published in Journal of CO2 utilization, 2018, 30, 38-47 and reproduced by permission of Elsevier

DOI: 10.1016/j.jcou.2018.12.022

Rebeca Monteagudo-Olivan,[a] María José Cocero,[b] Joaquín Coronas,[a,*] Soraya Rodríguez-Rojo[b,*].

[a] Chemical and Environmental Engineering Department, Instituto de Nanociencia de Aragón (INA) and Instituto de Ciencia de Materiales de Aragón (ICMA), Universidad de Zaragoza-CSIC, 50018 Zaragoza, Spain. Email: coronas@unizar.es.

[b] Bioeconomy Institute BioEcoUVa. High Pressure Process Group, Universidad de Valladolid, 47011 Valladolid, Spain. Email: soraya.rodriguez@uva.es.

Journal metrics:

Impact factor 5.503 and Q1 (Chemical engineering, miscellaneous)

5.1. Summary and graphical abstract

Caffeine and carvacrol were encapsulated using supercritical CO_2 (sc-CO_2) technique in MOFs, MIL-53(Al) and Mg-MOF-74, to deliver the compounds into pores at different contact times. High additive loadings were achieved, 32.1 and 34.3% for caffeine, and for carvacrol 34.4 and 30.1%, respectively. The sc-CO_2 encapsulation was more effective compared to the typical liquid phase encapsulation in ethanol. In fact, the encapsulation in Mg-MOF-74 was only possible in sc-CO_2, null loading was observed in the liquid ethanol phase process. The products required no purification and the excess of additives could be reused. In all the studied cases, the materials maintained their crystalline structure and MIL-53(Al) displayed its characteristic flexibility adapting its structure to the additives. The total release of caffeine and carvacrol from Mg-MOF-74 was produced after 5 h in distilled water, while in the case of MIL-53(Al) no release was observed for 10 days.

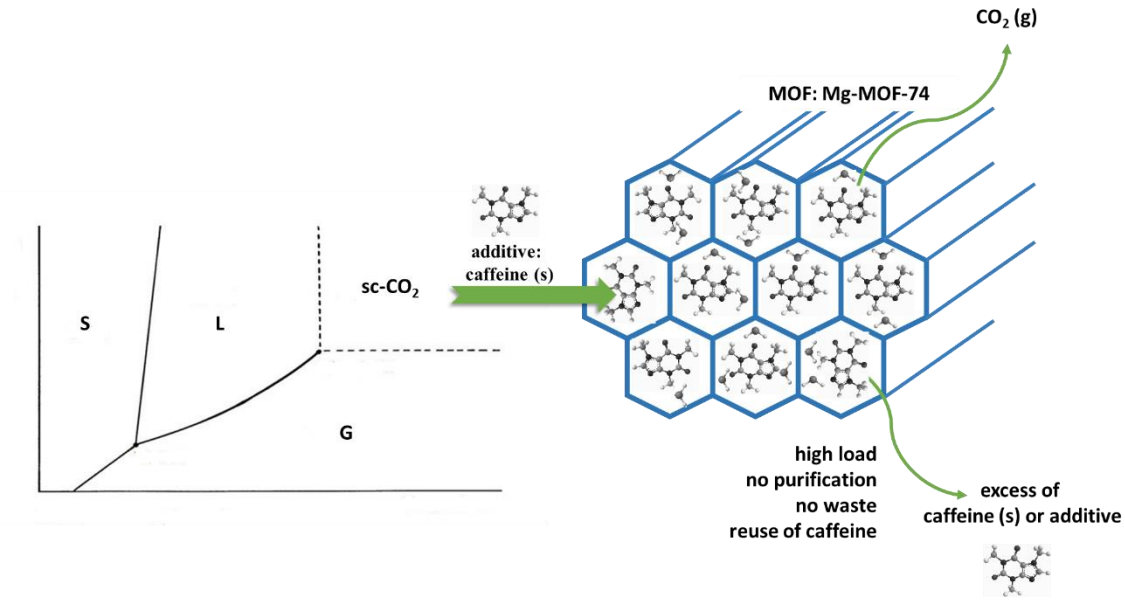

5.2. Supercritical CO_2 encapsulation of bioactive molecules in carboxylate-based MOFs

INTRODUCTION

The potential applications of metal-organic frameworks (MOFs) are extensively studied due to their demonstrated high performance in different fields such as catalysis,[1] gas adsorption,[2] selective membranes[3] and drug-delivery,[4,5] among others. MOFs are highly porous materials which are made of metal centers connected by organic linkers, commonly dicarboxylates and imidazolates. Some of the most well-known MOFs are MOF-5,[6] MILs (Materials Institute Lavoisier)[7,8] and ZIFs (zeolitic imidazolate frameworks).[9] Encapsulation in MOF has been proposed for different applications, mainly for drug delivery in medicine and controlled release in cosmetics.[10–13] However, it also finds application for luminescence based sensors in which the adsorbed molecules enhance luminescence depending on the host-guest interactions,[14] heterogenization of homogeneous catalysts,[1] and medical imaging[15]. Regarding active compounds or drugs, MOFs show different sustained release from a few hours to several days depending on the type of MOF and its stability in solution.[4] Among the MOFs studied for active molecules or drugs encapsulation, MIL-53(Fe) and MIL-53(Al) have been used in several reports,[4,16] while in vivo studies have been described for MIL-88A(Fe) and MIL-88B(Fe) modified with a polymer coating.[17] The encapsulation is normally carried out in liquid phase, after MOFs synthesis and processing, with generally good additive loadings.[18] In a previous work of the group the one-step encapsulation of caffeine in NH_2-MIL-88B(Fe) was reported, avoiding a multistep procedure, in which the synthesis and the encapsulation are carried out simultaneously.[19] Additionally, the encapsulation in MOF has been described by metal organic chemical vapor deposition (MOCVD) at high temperatures.[20]

The porosity of MOFs is not mostly accessible without an activation process, the excess of the organic linker and solvent has to be removed normally by successive washing with a specific solvent and thermal steps. In some MOFs, the thermal treatment may induce the partial collapse of their pores and the incomplete activation.[21,22] In order to overcome this handicap, several articles can be found on the use of supercritical-CO_2 (sc-CO_2) in a highly efficient activation and drying process of MOFs.[21,23] This supercritical technology has led to the largest BET specific surface areas ever reported, e.g. 7000 m^2/g for Nu-110E.[24]

The supercritical conditions of CO_2 are relatively low, with a critical point at 301 K and 74 bar (NIST Database), and therefore easily achievable if they are compared with other compounds like water (647 K and 220 bar) or ethanol (514 K and 63 bar). In supercritical conditions, CO_2 displays an intermediate behavior between a liquid and a gas. It shows high diffusivity, as gases, which is useful to spread better into the microporosity of a given porous material. The density, comparable to liquids, allows its use as a relatively weak nonpolar solvent [25], that might have sufficient strength for various applications. Regarding encapsulation and precipitation, the literature about the use of supercritical fluids covers different types of carriers, e.g. polymers, biopolymers and aerogels.[26,27] As the sc-CO_2 operation leaves no residue, the use in food and medical/pharmaceutical industry has great interest to avoid undesirable contaminations.[25,26,28] Nevertheless, the applicability of sc-CO_2 is scarce in the encapsulation in porous inorganic or hybrid materials in powder form. To the best of our knowledge, only Matsuyama and co-workers applied the encapsulation with sc-CO_2 in MOFs, although in this case sc-CO_2 assisted the encapsulation and hexane as solvent was needed.[29] For zeolites, López-Periago and co-workers used sc-CO_2 as solvent to simultaneously synthesize and insert an active compound.[30]

From an industrial point of view, this process is advantageous because it is not necessary to manage water or organic solvents, and the waste is merely CO_2, which is naturally present in the atmosphere and eventually could be reused.[31] Additionally, the final product does not have to be purified because it is in powder form as the starting material. Considering the case of poor soluble compounds in sc-CO_2, a co-solvent can be used to increase the solubility,[25,32] and then enhance the encapsulation process.

In this work, we have carried out the supercritical encapsulation of two additives, caffeine and carvacrol, into MOFs, MIL-53(Al) and Mg-MOF-74 (see Fig. 1). The former is a flexible hybrid net of 1D channels of terephthalate bidentate ligands connected by octahedral-coordinated Al^{3+}, interconnected by OH groups. The structure “breathes” or modifies the pore dimensions under different stimuli such as temperature or the presence of guest molecules, e.g. water.[7] In the hydrated material, known as MIL-53(Al) *lt*, water molecules are bound by hydrogen bonds that narrow the pore. Once the material is dried, named then MIL-53(Al) *ht*, the pores are opened.[7] This MOF shows high thermal stability to the extent that it can be activated by calcination at 380 °C.[7] Mg-MOF-74 is made of deprotonated 2,5-dihydroxyterephtelate and Mg^{2+} which are coordinated to give rise a 12 Å honeycomb structure.[33] This MOF does not show flexibility, contains structural water molecules and

presents a lower thermal stability.[33] Some MOFs can be degraded in aqueous media, and Mg-MOF-74 is sensitive to humidity.[34] This fact can be a handicap for several applications like gas separation or catalysis in presence of moisture. Nevertheless, it can be advantageous for controlled release and drug delivery, as reported for biopolymers and MOFs which are degraded leaving nontoxic residue.[25,35–37] Once MIL-53(Al) and Mg-MOF-74 were degraded, the inorganic and the organic parts would be obtained separately. The inorganic part corresponds to ions of aluminum and magnesium, both present in normal diets. Furthermore, the former is present in drugs such as almagate (Almax™), which is used as anti-acid, and the latter is used as dietary supplement. The organic rests are terephthalate and 2,5-dihydroxiterephthelate which could be potentially biocompatible like for other similar ligands.[15,38]

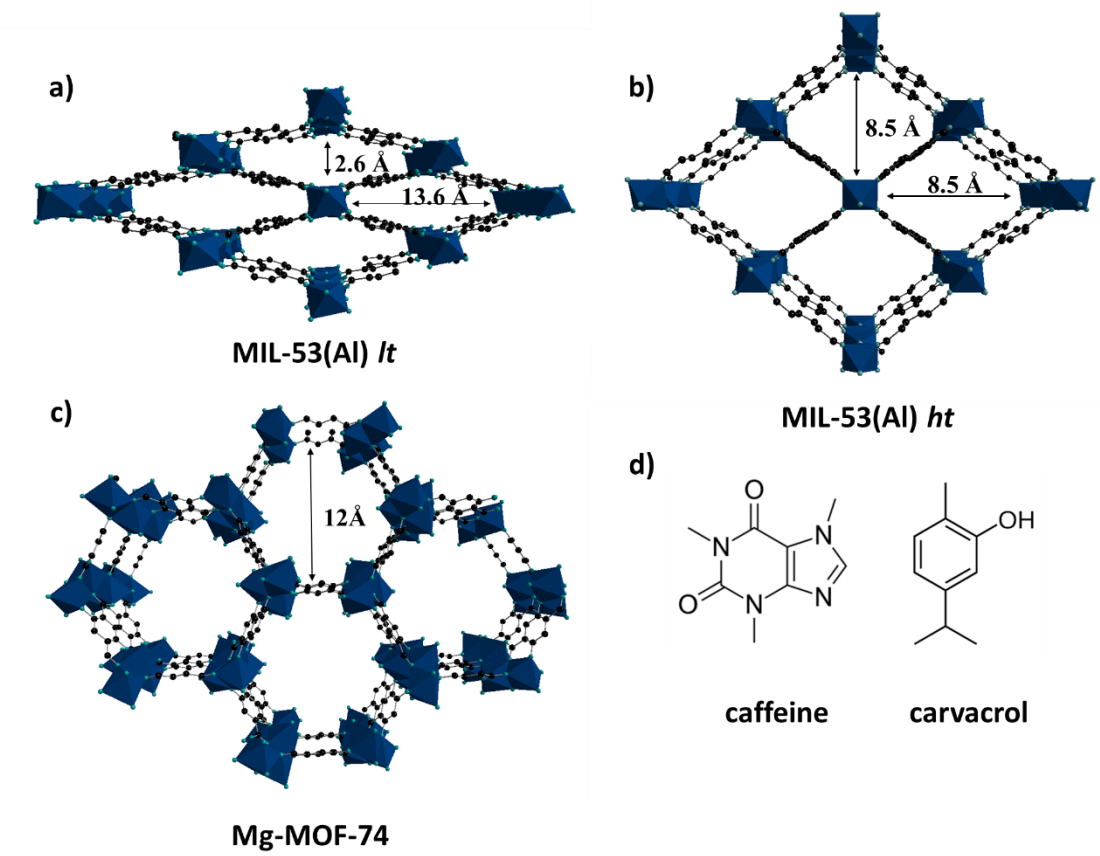

Figure 1. MOF guest structures used in this work with channels sizes, MIL-53(Al) (a and b) and Mg-MOF-74 (c). Atomic color code: carbon (black), oxygen (light blue) and metal coordination (dark blue). These structures were made with Diamond 3.2. using the corresponding CIF files.[7,33] The molecular structures of the studied guest additives (d).

The pure additive compounds tested for this work are caffeine and carvacrol (see Fig. 1d), both of them show relatively high solubility in sc-CO_2. In fact, caffeine is commonly used as additive and is broadly studied in supercritical fluids.[39,40] Decaffeination of coffee is mass produced by extraction with sc-CO_2 in substitution of toxic and pollutant dichloromethane.[41] Caffeine is commonly used as model drug or additive for demonstration of novel encapsulation procedures, e.g. in MOFs[18,19,42], silica[43], and polymers.[44] Even though encapsulation find major applications for non hidrosoluble or sensitive compounds, the encapsulation and release of hydrosoluble caffeine has been reported useful in textiles for cosmetic applications[44,45] or for oral administration with chewing gum *versus* capsules.[46] Carvacrol is also a natural occurring compound, one of the main components of oregano essential oil. It has been studied with supercritical fluids and its solubility has been reported at different conditions.[47] Carvacrol shows antimicrobial properties[48,49] and has been previously encapsulated in different matrices such as starch,[27] milk protein[50] and chitosan.[51] Carvacrol has been studied as additive for food preservation in packaging materials[52] and biofilms[53] with controlled release.

Herein we achieved the encapsulation in pure supercritical CO_2 phase of soluble additives, caffeine and carvacrol, in carboxylate based MOFs, MIL-53(Al) and Mg-MOF-74. This process required no purification and produced no waste. We compared the results of the sc-CO_2 impregnation with those achieved in liquid impregnation to highlight the benefits of the proposed process. Additionally, the effects of the encapsulation on the materials were characterized by X-ray diffraction (XRD) to check the crystalline structure stability after processing the starting materials and the potential changes in the flexible structure of MIL-53(Al).[7,8] We analyzed the samples by Raman spectroscopy to study the additive-MOF interactions; this technique has been widely used for host-guest systems[54–57] to gather information about the configuration of the guest additive in the host MOF. Finally, as a proof of concept of the potential use for controlled release, the additive release of the sc-CO_2 impregnated samples was monitored through time.

EXPERIMENTAL

Materials

For MOF synthesis the reactants were aluminum nitrate nonahydrate ($Al(NO_3)_3 \cdot 9H_2O$, Sigma Aldrich, ≥98%), magnesium hydroxide ($Mg(OH)_2$, Alfa Aesar, 95-100 %), terephthalic acid (H_2BDC, Sigma Aldrich, 98%) and 2,5-dihydroxyterephthalic acid (6 mmol, H_4DOBDC, TCI, >98%). The synthesis solvents were distilled water and tetrahydrofuran (THF, Scharlab, >98%). Methanol (MeOH, Scharlab, >99%) was used for washing. Additives were carvacrol (150 g/mol, Sigma Aldrich, 99% FG) and caffeine (194 g/mol, Sigma Aldrich, 99%). For supercritical CO_2 encapsulation (Carburos Metálicos S.A., 99.95%) and for liquid encapsulation absolute ethanol were used. Analysis solvents for CG-MS were MeOH (Scharlab, analysis grade) and acetone (PanReac, analysis grade). Analysis solvents for HPLC were Milli-Q water (Millipore), phosphoric acid (Acros Organic, aqueous solution 85%), MeOH (Scharlab, analysis grade) and acetonitrile (Scharlab, analysis grade). All the chemicals were used as received.

Synthesis of MOFs

Synthesis of MIL-53(Al), Al(OH)BDC. From a previous report,[7] 15.6 g of $Al(NO_3)_3 \cdot 9H_2O$ (41.7 mmol) and 3.36 g of H_2BDC (20.1 mmol) were added to a 400 mL Teflon-lined stainless steel autoclave (Berghof DAB-3) where 250 mL of distilled water was poured to form a white dispersion. The system was sealed and placed in an oven for 3 days at 220 °C. The product was recovered by centrifugation at 10,000 rpm for 10 min (Allegra® X-15R Centrifuge), washed with distilled water and recovered also by centrifugation at the same conditions. The white product was dried at room temperature overnight and activated by calcination for 24 h at 380 °C (see Fig S1). Yield with respect to H_2BDC: 61%

Synthesis of Mg-MOF-74, $[Mg_2(DOBDC)(H_2O)_2] \cdot 8H_2O$. From the original synthesis,[33] including some small variations, 1.188 g of H_4DOBDC (6 mmol) was dissolved in 120 mL of THF in a glass flask. Then a solution of 0.699 g of $Mg(OH)_2$ (12 mmol) in 40 mL of distilled water was added and the mixture was heated at 80 °C for 5 h under reflux. A yellow solid was recovered by centrifugation at 10,000 rpm for 10 min and washed several times with MeOH with an ultrasound treatment for 2 min between washings. The yellow

product was dried at room temperature overnight (see Fig S1). Yield with respect to H_4DOBDC: 79%.

Supercritical CO_2 and liquid impregnation

Supercritical CO_2 impregnation. The experimental set-up used to prepare encapsulated additive@MOFs (i.e. carvacrol@MOF and caffeine@MOF) is shown in Fig. 2. The stored CO_2 (1) is carried to a cooler in order to assure liquid state (2) and pumped (3) to reach a pressure of 100 bar inside the vessel (4). Liquid carvacrol or solid caffeine was placed at the bottom of the stainless steel vessel (4) and the MOF was separated above by a metallic mesh to avoid direct contact. The vessel was put in an oven (5) which was connected to a temperature sensor inside the recipient (4). The selected temperature was 40 °C, a little above the supercritical conditions, but not a very high value because it was intended to have soft conditions of temperature so that this methodology can be extended to temperature sensitive molecules like carvacrol, and additionally, in this manner, the potential large scale costs are also reduced. As mentioned above, both compounds exhibit high solubility in sc-CO_2. The temperature and pressure were selected to achieve a high value of solubility of both additives, and the amount of additive was chosen above the saturation concentration in the described conditions. The volume of the recipient was 85 cm^3 and the density of sc-CO_2 in the working conditions was 0.686 g/mL (NIST database). The solubilities of caffeine and carvacrol in CO_2 at supercritical conditions of 40 °C and 100 bar (the working pressure) are $6.3 \cdot 10^{-5}$[39,40] and 0.02[47] (in molar fraction), respectively. To have a large excess, 1.00 g caffeine was used and in case of carvacrol 5.00 mL. To ensure the solubilization of the additive in the CO_2, the cell was provided with a magnetic mixer. After the predefined contact time, the cell was depressurized through a micrometric valve with a velocity of depressurization of 20 bar/min. To avoid freezing, a heater was placed in the exit pipe (6). After the experiments, the excess of additive could be re-used as it was not damaged during the process.

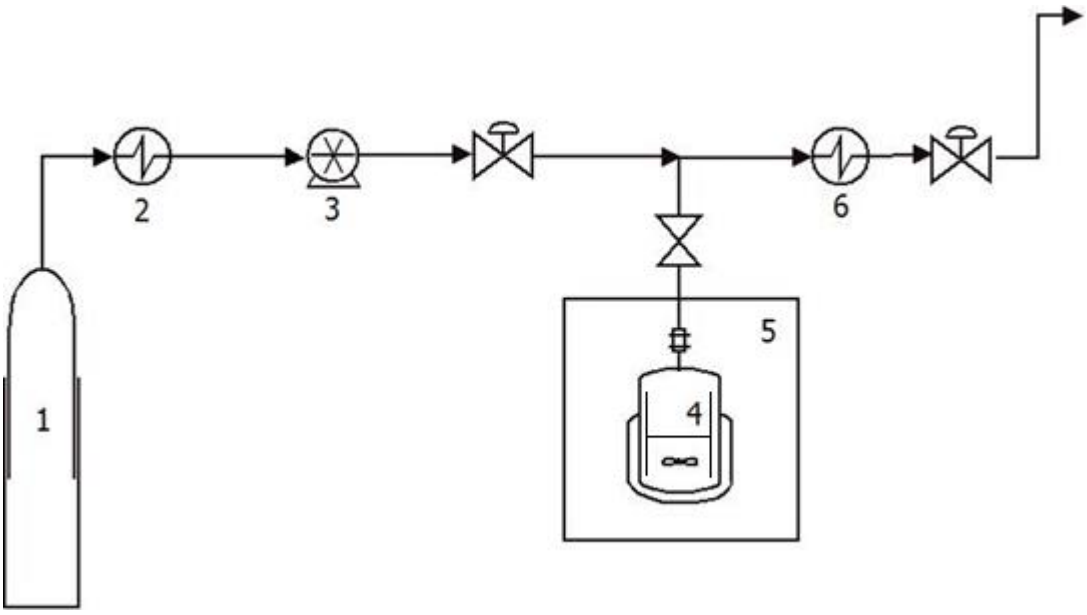

Figure 2. Schematic set-up for sc-CO_2 encapsulation: (1) CO_2 cylinder, (2) cooler, (3) pump, (4) encapsulation vessel, (5) oven, (6) Heater.

Liquid ethanol impregnation. In a vial, 100 mg of MOF, MIL-53(Al) or Mg-MOF-74, was suspended in a concentrated solution (10 mL) of caffeine (4 g/L) or carvacrol (50 g/L). The use of ethanol as medium was selected considering the low stability of Mg-MOF-74 in water and the better solubility of the additives in this alcohol. At room temperature the samples are impregnated with magnetic stirring. After 14 h, the solids were recovered by centrifugation at 10,000 rpm for 10 min and dried at room temperature overnight.

Controlled release

The releases of caffeine and carvacrol from MIL-53(Al) and Mg-MOF-74 were monitored as a function of time. The selected samples were those with the highest obtained loadings with sc-CO_2, i.e. caffeine@MIL-53(Al) and caffeine@Mg-MOF-74, both samples impregnated for 24 h, and carvacrol@MIL-53(Al) and carvacrol@Mg-MOF-74 impregnated for 14 h. The loaded material (additive@MOF, 20 mg) was suspended in a beaker with 0.5 L of distilled water with magnetic stirring bar at 25 °C. At each selected time an aliquot of 1.2 mL was collected, and the same volume was replaced with water. The sample was

centrifuged for 2 min at 5,000 rpm (Microfuge 16, Beckman Coulter) and the supernatant was filtered (PTFE, 0.22 μm) for HPLC analysis.

Characterization

Determination of caffeine and carvacrol loadings

Extraction and gas chromatography-mass spectroscopy (CG-MS). The extraction was carried out with 10.0 mg of additive@MOF in 1.5 mL of acetone for caffeine and 1.5 mL of ethanol for carvacrol containing samples. Each suspension was sonicated for 0.5 h and the liquid was separated from the solid by centrifugation at 5,000 rpm for 5 min. The solution of the extracted additive was filtered previously to the analysis with 0.22 μm filters. The concentrations were determined by CG-MS (7890C GC/5977A MSD Agilent Technologies) equipped with a HP-5MS capillary column (30 m x 0.25 mm x film thickness 0.25 μm). The carrier gas was helium at a flow rate of 0.7 mL/min with 1 μL of injection volume and a 300:1 split ratio. The injection was carried out with the column oven at 105 °C, then heated to 220 °C (4 °C/min) and to 250 °C (15 °C/min). MSD transfer line temperature was 250 °C. The electron ionization system for detection operated at an ionization voltage of 70 eV. The calibration ranges for caffeine and carvacrol were, respectively, 0.5-1.5 mg/mL and 1.0-4.0 mg/mL. Samples analyses were performed in duplicate and the corresponding standard deviations were calculated. The loading values were calculated as (g additive/g dry MOF)·100 and dry MOF was determined by thermogravimetry (see below).

Pore occupation: N_2 and CO_2 adsorption. The N_2 adsorption capacity of MIL-53(Al) and additive@MIL-53(Al) was analyzed at 77 K with a TRIStar 3000 instrument and specific surface area was calculated by BET method. The CO_2 isotherms and uptakes at 273.15 K of Mg-MOF-74 and additive@Mg-MOF-74 were obtained with a Micrometrics ASAP 2020 instrument. Previously to analysis, outgassing was carried out under vacuum for 5 h at 150 °C.

X-ray diffraction (XRD) of crystalline materials. The MOF and additive@MOF samples were characterized by XRD to check the effects in crystallinity before and after the sc-CO_2 and common liquid phase encapsulations. The measurements were recorded in a Siemens D-5000 diffractometer (45 kV, 40 mA) with a copper anode with a graphite

monochromator in $CuK_{\alpha 1}$ radiation (λ=1.540 Å) in the 4-40° 2θ range and a scanning rate of 0.03°/s.

Raman spectroscopy. The host-guest interactions between the additive and the MOF were studied by Raman spectroscopy (WITec alpha 300) with the 783 nm laser and working at 17 mW. The integration time for each measurement was 1.5 s and the data recording were taken with 25 accumulations and a resolution of 2 cm^{-1}.

Thermogravimetric analysis (TGA). Using a Mettler Toledo TGA/SDTA 851e instrument, the TGA analyses of the samples were carried out in 70 µL alumina pans and heated up under air atmosphere to 700 °C with a ramp of 10 °C/min.

Particle morphology and scanning electron microscopy (SEM). The powder materials, before and after the encapsulation processes, were studied by SEM (Inspect F50) coated previously with a thin film of platinum to ensure the conductivity of samples.

Monitoring caffeine and carvacrol release by high performance liquid chromatography (HPLC). The concentrations of additives during the release experiments were analyzed by HPLC, in a Waters 1515 system equipped with a C18 column (SunFire 4.6 x 250 mm, 5 µm) and coupled with a UV-Vis dual λ absorbance detector (Waters 2487), operating in isocratic mode at 40 °C with a mobile phase flow of 2 mL/min. The mobile phase for caffeine was composed by 75% of phosphate buffer 0.025 M in Milli-Q water at pH 3 and 25% of MeOH, meanwhile for carvacrol determination it was composed of 50% acetonitrile and 50% Milli-Q water. Calibration ranges for caffeine and carvacrol were for both 2.0-10.0 mg/L. Sample analyses were performed in duplicate and the corresponding standard deviations were calculated.

RESULTS AND DISCUSSION

Effect of contact time

Fig. 3 shows the effect of contact time in the sc-CO_2 encapsulation of caffeine and carvacrol in MIL-53(Al) and Mg-MOF-74 in the conditions described above. For caffeine@MIL-53(Al) (see Fig. 3a) a gradual increase was observed until 24 h when the loading reached a value of 32.1%. In opposition, the sc-CO_2 encapsulation of caffeine in Mg-MOF-74 showed a remarkable difference between 4 and 14 h, from 3.2% to 17.7%. This

difference was not observed in MIL-53(Al), which shows a more gradual loading increase. It could be explained by the high content of water present in Mg-MOF-74 (see the ca. 35% weight loss below 150 °C in Fig. S2c) and by the structural role of part of it as described by Dietzel *et al.* 2008[33]. This water cannot be thermally evacuated during pore activation (removing molecules inside the pores) without inducing the structure collapse.[33] It might create some transport resistance against the diffusion of sc-CO_2 and caffeine into the pores; therefore, the encapsulation kinetics was slower in this case. The low solubility of water in CO_2[58,59] can contribute to the resistance of the withdrawal of water from the MOF (to release its porosity for the guest) and consequently the loading is hindered. After the removal of water, high caffeine loadings were achieved after 24 h (34.3%) in Mg-MOF-74.

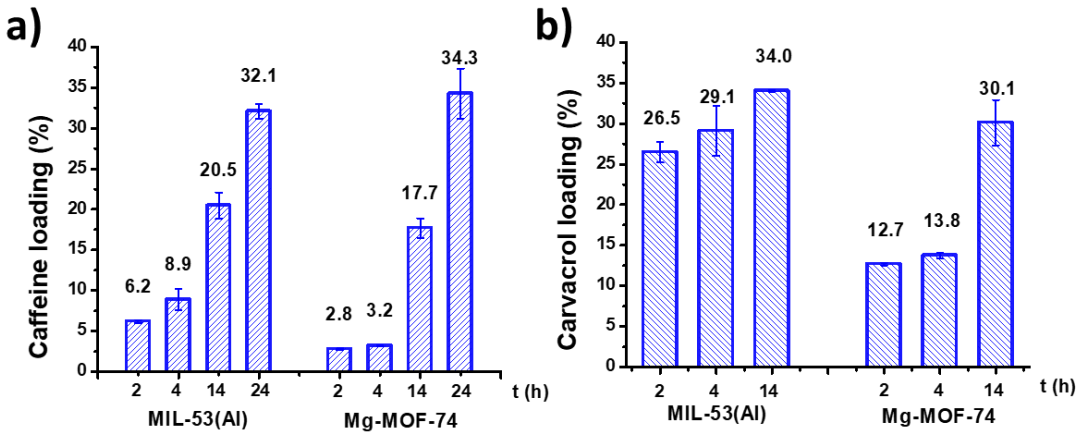

Figure 3. Effect of contact time in sc-CO_2 encapsulation at 40 °C and 100 bar in MIL-53(Al) and Mg-MOF-74 for caffeine (a) and carvacrol (b).

A fast encapsulation of carvacrol in MIL-53(Al) was observed after 2 h of contact time with a loading value of 26.5% (Fig. 3b). If the contact time was increased to 14 h the loading achieved was 34.0%. The relatively high solubility of carvacrol in the working conditions (40 °C and 100 bar, see section 2.3) and its size, smaller than that of caffeine, favored a more efficient and faster loading. Carvacrol was considered a smaller molecule than caffeine in agreement with their respective molar masses of 150 g/mol and 194 g/mol and the bulkier molecular structure of the latter (see Fig. 1). In the case of the encapsulation of carvacrol in Mg-MOF-74, the same kinetic effect was observed, the loading increase was more remarkable between 4 and 14 h than in the 2-4 h interval.

Fig. 4c shows the thermal step removal of caffeine in Mg-MOF-74 corresponding to the sc-CO_2 encapsulation at 14 h and the reduced amount of water with respect to the starting

material. Therefore, it seems that the encapsulation is concomitant with a partial substitution of the water by the additive. On the contrary, the loading of caffeine in MIL-53(Al) was directly produced, considering that the presence of water in the starting material was significantly lower (3%, see Fig. 4). Noticeably, in the curve for carvacrol@Mg-MOF-74 impregnated with sc-CO_2, the removal steps of water and carvacrol are consecutives and a single step is observed in the corresponding TGA curve.

After the encapsulation the pore occupation was verified by the decrease in the capacities of MIL-53(Al) to adsorb N_2 and of Mg-MOF-74 to adsorb CO_2 (Table 1 and Fig. S2). The previous outgassing was carried out at 150 °C in all cases, thus the additives were not removed during this step. Consequently, the BET specific surface area for MIL-53(Al) was low (761 m^2/g), while if degasification was carried out at 200 °C it increased to 1100 m^2/g, in agreement with the reported value of 1140 m^2/g.[7] The impregnated MIL-53(Al) samples show almost null BET area, which is in agreement with high encapsulations of caffeine and carvacrol in the MOF pores. Analogous results were found in terms of CO_2 adsorption capacities (see Table 1) of caffeine@Mg-MOF-74 (1.4 mmol/g) and carvacrol@Mg-MOF-74 (0.4 mmol/g), compared to that of Mg-MOF-74 (12.0 mmol/g), similar to the reported value ca. 10.7 mmol/g.[60] These lower CO_2 adsorption capacities agree with the Mg-MOF-74 porosity occupied by the additive molecules. Nevertheless, the retained CO_2 adsorption capacity suggests that not all the porosity was occupied by the additives because of the rigid structure of this MOF and the water structural molecules, which do not allow a facilitated diffusion through the pores.

Table 1. Adsorption before and after the sc-CO_2 encapsulation with a contact time of 14 h at 100 bar and 40 °C. BET specific surface areas of MIL-53(Al) and impregnated samples (left) and CO_2 adsorption capacities at 0 °C and 1 atm of Mg-MOF-74 and impregnated samples (right).

	S_{BET} (m^2/g)		CO_2 uptake (mmol/g)
MIL-53(Al)	761	Mg-MOF-74	12.0
caffeine@ MIL-53(Al)	7	caffeine@ Mg-MOf-74	1.4
carvacrol@ MIL-53(Al)	5	carvacrol@ Mg-MOF-74	0.4

Comparison of sc-CO_2 versus liquid ethanol phase encapsulations

Fig. 5 compares the sc-CO_2 encapsulation with the traditional liquid phase (using ethanol which shows good solubility for caffeine and carvacrol) after 14 h of contact time in both cases. In general, the loading values were higher for supercritical encapsulation, even if in case of MIL-53(Al), the difference was not very substantial for caffeine. However, only a 6% of carvacrol loading was achieved in liquid phase *vs* a 34.0% in sc-CO_2. The loading of caffeine in MIL-53(Al) in liquid phase of ethanol (16.4%) was significantly higher than that of carvacrol (6.3%), meanwhile the behavior was reversed in supercritical conditions and less caffeine (20.5%) was loaded than carvacrol (34.0%).

For Mg-MOF-74 the differences were more noticeable between sc-CO_2 and ethanol. In fact, the encapsulation in liquid phase was not achieved in Mg-MOF-74 with none of the additives. In agreement with this, the corresponding TGA curves also show the differences among these samples (see Fig. 4). In the liquid phase encapsulation, the resulting materials have almost identical curves to the starting Mg-MOF-74. Meanwhile, the samples with sc-CO_2 show the removal step of caffeine and an increased amount of the organic part for carvacrol at a temperature similar to that corresponding to the removal of structural water. For MIL-53(Al) the TGA curves suggest that some non-desired ethanol solvent would remain in the pores of the material after the liquid encapsulation of caffeine (Fig 4a) and the subsequent drying at room temperature.

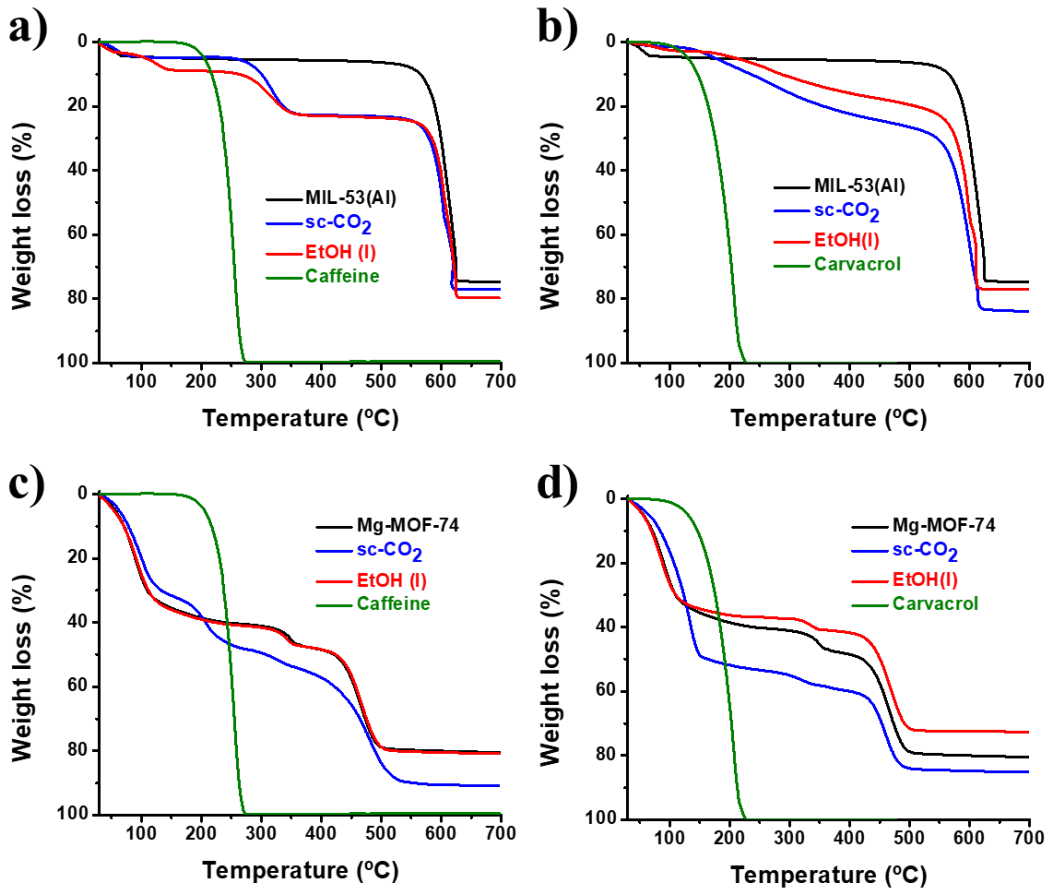

Figure 4. TGA curves of sc-CO_2 encapsulations at 40 °C and 100 bar and ethanol liquid encapsulations at 25ºC in MIL-53 of caffeine (a) and carvacrol (b), and in Mg-MOF-74 of caffeine (c) and carvacrol (d). The encapsulation contact time was 14 h in all the experiments.

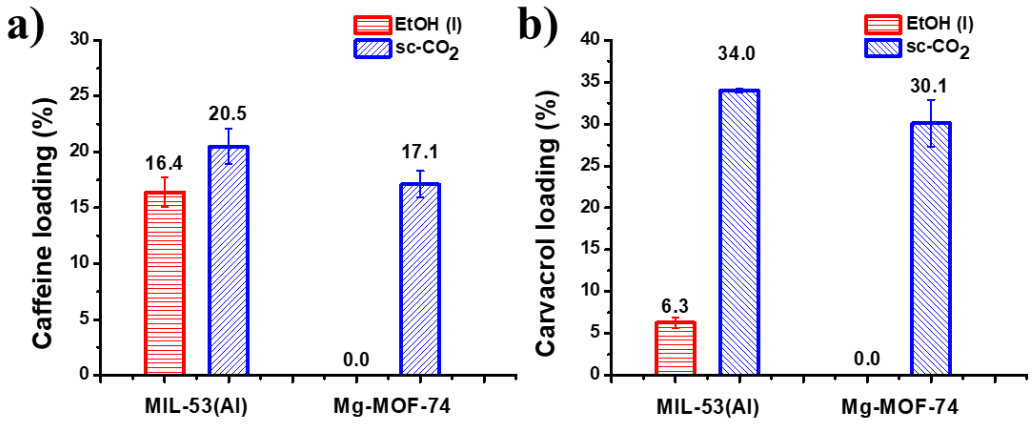

Figure 5. Compared encapsulation values of caffeine (a) and carvacrol (b) in MIL-53(Al) and Mg-MOF-74 with sc-CO_2 encapsulation versus ethanol liquid phase encapsulation at 25 °C for a contact time of 14 h.

Finally, Figs. S3 and S4 depict SEM images of MIL-53(Al) and Mg-MOF-74, respectively, before and after encapsulations. As reported elsewhere,[7,33] the former displays a polyhedral morphology, while in the later the particles are needle-like. These shapes were maintained after both types of encapsulations in the described conditions.

Structural Characterization: XRD and Raman spectroscopy studies

The MOF crystalline structure was studied by XRD before and after sc-CO_2 and liquid ethanol phase encapsulations. The interpretations were correlated with the flexible structure for MIL-53(Al)[7] and the rigidity of Mg-MOF-74.[33] The water molecules of the MIL-53(Al) pores create hydrogen bonds between the carboxylates of the terephthalate ligands that narrow the pores, giving rise to the so-called *lt* form, after calcination the pores open producing the *ht* form.[7] The caffeine@MIL-53(Al) pattern obtained by sc-CO_2 treatment seems to arise from a combination of *ht* and *lt* configurations (Fig. 6Ab). The *lt* peaks (Fig. 6Aa) are kept with lower intensity although the main peak in the *ht* form (Fig. 6Ae) appears clearly. The size of caffeine is considerable, therefore its diffusion through the MOF pores may be hindered and with different potential configurations. Other additional peaks present in the XRD pattern suggest a mixture of the two MIL-53(Al) pore structures adapted to the guest caffeine molecule. The peaks of caffeine are not observed, consistent with the absence of external caffeine.[61] The XRD pattern corresponding to the liquid encapsulation in Fig. 6Ac seems undefined, suggesting the presence of retained solvent. Fig. 6B shows the different patterns corresponding to carvacrol@MIL-53(Al). The liquid and supercritical encapsulations arose with similar patterns between them (Figs. 6Bb and 6Bc) and with some common peaks of the pattern of MIL-53(Al) *ht*, implying the pore opening in both and the removal of the hydrogen bonding water, in agreement with the absence of water in the TGA curves (Fig. 4b).

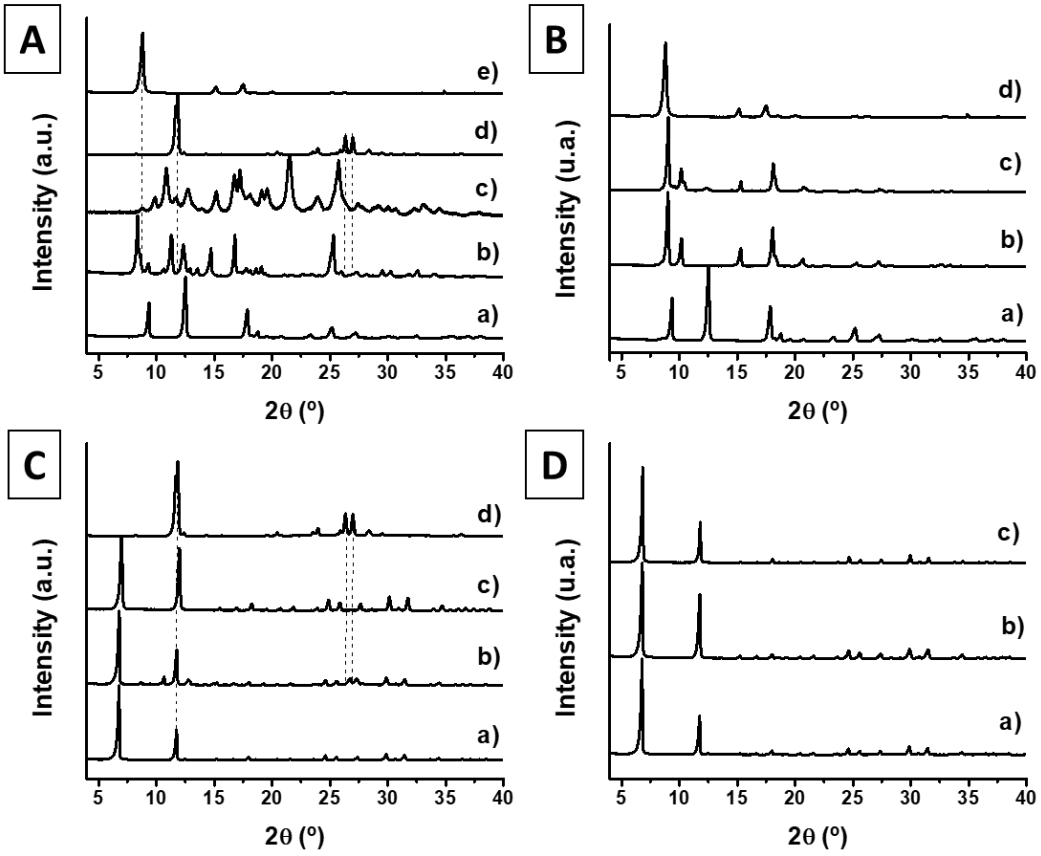

Figure 6. XRD patterns of (A) MIL-53(Al) *lt* (a), caffeine sc-CO_2 encapsulation (b), caffeine liquid phase encapsulation (c), caffeine (d) and MIL-53(Al) *ht* (e); (B) MIL-53(Al) *lt* (a), carvacrol sc-CO_2 encapsulation (b), carvacrol liquid phase encapsulation (c), and MIL-53(Al) *ht*; (C) Mg-MOF-74 (a), caffeine sc-CO_2 encapsulation (b), caffeine liquid phase encapsulation (c) and caffeine (d); and (D) Mg-MOF-74 (a), carvacrol sc-CO_2 encapsulation (b) and carvacrol liquid phase encapsulation (c). The encapsulation contact time was 14 h in all the experiments.

For the encapsulations in Mg-MOF-74, the XRD patterns are similar to that of the starting Mg-MOF-74 (see Figs. 6C and 6D). These data imply that none of the encapsulation processes affected the bulk crystallinity of the rigid structure.

The host-guest interactions were studied by Raman spectroscopy which provides information about the structure of the samples and the molecular interactions. The nature of the material structure has influence on the interpretation of the Raman results shown in Fig. 7 and Tables S1-S4. The encapsulations of caffeine in MIL-53(Al) show similar Raman shifts corresponding to the terephthalate bands of the MOF, although the relative intensity is remarkably changed for sc-CO_2 encapsulation (see Fig. 7A and Table S1) with respect to

the starting material or to that achieved by liquid phase encapsulation for bands at 867, 1469 and 1612 cm^{-1} which corresponds to the deformation of aromatic C-H, symmetric stretching of CO_2^- and ring C=C stretching. The modification of the intensities in case of supercritical encapsulation may be attributed to the modification of the polarization of terephthalate intramolecular bonds in the MIL-53(Al) structure and to the more effective pore occupation by caffeine (See Fig. 4). The molecule of caffeine can be placed in parallel with the ligand terephthalate and hence the heteroatoms of caffeine induce the polarizability of C-H bonds of the ligand increasing the Raman intensity (in Raman spectroscopy the intensity is related with the polarizability of the vibrational mode). Interestingly, this fact induces the contrary effect on the stretching of C=C of the aromatic ring. The opening of the MIL-53(Al) pore (observed by XRD, see Fig. 6A) had to remove the hydrogen bonding in the *lt* form between two adjacent carboxylates and can be the cause of the reduced intensity of one of the modes of the carboxylate. The hydrogen bonding may be partially present considering that there is some water after the supercritical encapsulation (see TGA curves in Fig 4a) and that the XRD is altered (with respect to the pristine MOF) which arises from different pore fillings or configurations (see Fig 6A). As opposed, the Raman spectrum of the sample caffeine@MIL-53(Al) obtained in liquid phase encapsulation shows almost no changes with respect to the starting material which indicates the weaker interactions with pore walls.

Fig. 7B shows the Raman spectra for carvacrol@MIL-53(Al) encapsulations (see also Table S2). The most important differences are in the stretching modes of the MOF carboxylates for both processes. In agreement with TGA and XRD, in which the open structure of the *ht* form is observed, no water, displaced by carvacrol, is present in the MOF porosity. The shifts of the CO_2^- stretching (*st*) bands can be caused by the breaking of the water-MOF hydrogen bond and its potential substitution by hydrogen bonds between the aromatic alcohol of carvacrol and the MOF. The more acidic character of the phenol in carvacrol favors its actuation as hydrogen donor which it is not present with the saturated molecule of ethanol (media for liquid encapsulation). Therefore, in both liquid and sc-CO_2 phases, the Raman spectroscopy suggests that hydrogen bond interactions carvacrol-MIL-53(Al) influenced the encapsulation. Another noticeable difference is the single new band at 187 cm^{-1} for both encapsulations which is assigned to lattice vibrations of the expansion and contraction of MIL-53(Al) *ht* flexible network (this fact reminds to the radial breathing mode of carbon nanotubes).[62] In this region of the spectrum, there are several very weak bands

in the *lt* form and in the caffeine encapsulation a band appears with higher intensity than others but the pore is not totally open, as it is observed in the diffraction pattern.

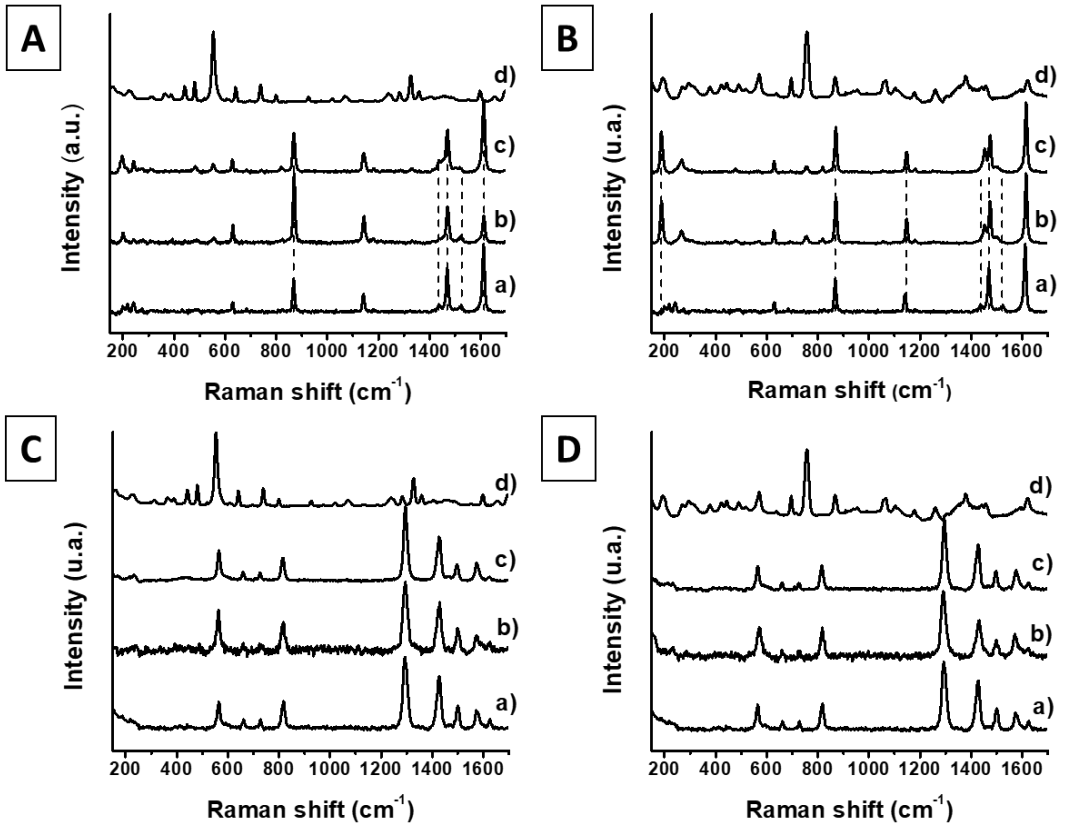

Figure 7. Raman spectra of (A) MIL-53(Al) *lt* (a), caffeine sc-CO_2 encapsulation (b), caffeine liquid phase encapsulation (c) and caffeine (d), (B) MIL-53(Al) *lt* (a), carvacrol sc-CO_2 encapsulation (b), carvacrol liquid phase encapsulation (c) and carvacrol (d), (C) Mg-MOF-74 (a), caffeine sc-CO_2 encapsulation (b), caffeine liquid phase encapsulation (c) and caffeine (d), (D) Mg-MOF-74 (a), carvacrol sc-CO_2 encapsulation (b), carvacrol liquid phase encapsulation (c) and carvacrol (d). The encapsulation contact time was 14 h in all the experiments.

In opposition, the Raman spectra of the encapsulations in Mg-MOF-74 show no remarkable shifting neither for caffeine nor carvacrol (see Fig. 7C-D and Tables S3-S4). This fact was expected for the liquid phase encapsulation considering that the loading of additives was null (or, in any case, perhaps some water could have been replaced by ethanol). Alternatively, the spectra of the encapsulation in sc-CO_2 show more background noise for both additives, caffeine and carvacrol, which could be due to the increase of unspecific interactions. In the pure MOF the pores are filled with water (around 35% in weight, see the TGA in Fig. 4) which was not totally removed after the encapsulation (around 25%) for caffeine@Mg-MOF-74, neither for carvacrol@Mg-MOF-74, in which the remaining water

cannot be estimated from the TGA curve because the removal step of water is consecutive to that of carvacrol. This presence of water could lead to reduced additive-MOF interactions. Additionally, the structure of Mg-MOF-74 is rigid and less changes can be expected in comparison with MIL-53(Al). The increased noise can also be assigned to punctual crystal damage although the bulk crystallinity of Mg-MOF-74 seems unaltered (see Figs. 6C-D).

Controlled release

The release of caffeine and carvacrol in aqueous media was studied at room temperature for the highest loaded samples in sc-CO_2 (24 h for caffeine@MOF and 14 h for carvacrol@MOF). Two different behaviors were observed for additive@Mg-MOF-74 and additive@MIL-53(Al). In distilled water the former releases most of the impregnated caffeine and carvacrol in 5 h (see Fig. 8a) due to the simultaneous hydrolysis of Mg-MOF-74.[63] However, the two additive@MIL-53(Al) materials showed no release for 10 days. The suspended material in the release media was recovered by centrifugation after that time and analyzed by thermogravimetry to evidence the presence of caffeine and carvacrol remained in the corresponding two additive@MIL-53(Al) materials (see Fig. 8b). The compared curves with the starting materials shows a small decrease of both additives in MIL-53(Al) that was not evidenced during the release experiments or the amount was below the limit of quantification.

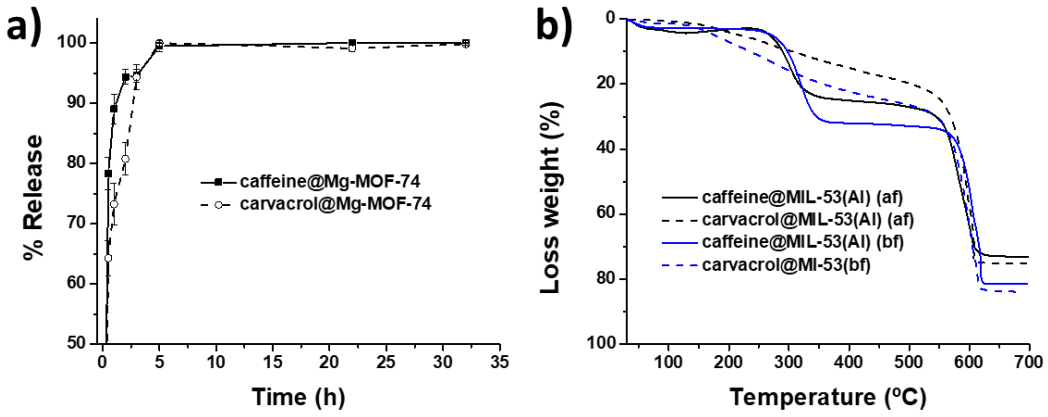

Figure 8. Release profiles at 25 ºC for caffeine@Mg-MOF-74 and carvacrol@Mg-MOF-74 in distilled water (a) and TGA curves of the solids before (bf) and after (af) the release experiment, i.e. the remaining solids recovered by centrifugation from aqueous solution after 10 days in the release system, for caffeine@MIL-53(Al) and carvacrol@MIL-53(Al) (b).

CONCLUSIONS

The encapsulation of bioactive molecules caffeine and carvacrol in two different MOFs, the flexible MIL-53(Al) and the rigid Mg-MOF-74, has been demonstrated. In all cases, the loadings were higher under supercritical CO_2 conditions than applying the conventional liquid phase procedure in ethanol. In fact, the encapsulation in Mg-MOF-74 was only possible in the supercritical phase. The encapsulation was demonstrated using the measurements of XRD diffraction, TGA analysis and gas adsorption, while the Raman spectroscopy was useful to study the host-guest interactions. The encapsulation with sc-CO_2 showed clear advantages compared with the conventional technique: it required no later purification avoiding in this manner the steps of separation and drying in liquid phase, no ethanol contaminated the product and the excess of additive remained in the system as pure solid or liquid, therefore it could be reused easily. This methodology could be potentially applied to any soluble additive in sc-CO_2 and particularly to those sensitive to temperature or unstable in solution. Consequently, and after the displayed results, this is a promising applicable procedure for encapsulation in MOFs.

REFERENCES

[1] J. Lee, O.K. Farha, J. Roberts, K. a Scheidt, S.T. Nguyen, J.T. Hupp, Metal-organic framework materials as catalysts., Chem. Soc. Rev. 38 (2009) 1450–1459. doi:10.1039/b807080f.

[2] J.-R. Li, R.J. Kuppler, H.-C. Zhou, Selective gas adsorption and separation in metal-organic frameworks., Chem. Soc. Rev. 38 (2009) 1477–1504. doi:10.1039/b802426j.

[3] S. Sorribas, P. Gorgojo, C. Téllez, J. Coronas, A.G. Livingston, High flux thin film nanocomposite membranes based on metal-organic frameworks for organic solvent nanofiltration, J. Am. Chem. Soc. 135 (2013) 15201–15208. doi:10.1021/ja407665w.

[4] P. Horcajada, C. Serre, G. Maurin, N.A. Ramsahye, F. Balas, M. Vallet-Regí, M. Sebban, F. Taulelle, G. Férey, Flexible Porous Metal-Organic Frameworks for a Controlled Drug Delivery, J. Am. Chem. Soc. 130 (2008) 6774–6780. doi:10.1021/ja710973k.

[5] L. Paseta, G. Potier, S. Abbott, J. Coronas, Using Hansen solubility parameters to study the encapsulation of caffeine in MOFs, Org. Biomol. Chem. 13 (2015) 1724–1731. doi:10.1039/C4OB01898B.

[6] O.M. Yaghi, H. Li, M. Eddaoudi, M. O'Keeffe, Design and synthesis of an exceptionally stable and highly porous metal-organic framework, Nature. 402 (1999) 276–279. doi:10.1038/46248.

[7] T. Loiseau, C. Serre, C. Huguenard, G. Fink, F. Taulelle, M. Henry, T. Bataille, G. Férey, A rationale for the large breathing of the porous aluminum terephthalate (MIL-53) upon hydration., Chemistry. 10 (2004) 1373–1382. doi:10.1002/chem.200305413.

[8] C. Serre, C. Mellot-Draznieks, S. Surblé, N. Audebrand, Y. Filinchuk, G. Férey, Role of Solvent-Host Interactions That Lead to Very Large Swelling of Hybrid Frameworks, Science (80-.). 315 (2007) 1828–

1831. doi:10.1126/science.1137975.

[9] K.S. Park, Z. Ni, A.P. Cote, J.Y. Choi, R. Huang, F.J. Uribe-Romo, H.K. Chae, M. O'Keeffe, O.M. Yaghi, A.P. Côté, J.Y. Choi, R. Huang, F.J. Uribe-Romo, H.K. Chae, M. O'Keeffe, O.M. Yaghi, Exceptional chemical and thermal stability of zeolitic imidazolate frameworks., Proc. Natl. Acad. Sci. U. S. A. 103 (2006) 10186–91. doi:10.1073/pnas.0602439103.

[10] R.C. Huxford, J. Della Rocca, W. Lin, Metal-organic frameworks as potential drug carriers, Curr. Opin. Chem. Biol. (2010). doi:10.1016/j.cbpa.2009.12.012.

[11] D. Cunha, C. Gaudin, I. Colinet, P. Horcajada, G. Maurin, C. Serre, Rationalization of the entrapping of bioactive molecules into a series of functionalized porous zirconium terephthalate MOFs, J. Mater. Chem. B. (2013). doi:10.1039/c2tb00366j.

[12] H. Zheng, Y. Zhang, L. Liu, W. Wan, P. Guo, A.M. Nyström, X. Zou, One-pot Synthesis of Metal-Organic Frameworks with Encapsulated Target Molecules and Their Applications for Controlled Drug Delivery, J. Am. Chem. Soc. (2016). doi:10.1021/jacs.5b11720.

[13] S.R. Miller, D. Heurtaux, T. Baati, P. Horcajada, J.M. Grenèche, C. Serre, Biodegradable therapeutic MOFs for the delivery of bioactive molecules, Chem. Commun. (2010). doi:10.1039/c001181a.

[14] L.E. Kreno, K. Leong, O.K. Farha, M. Allendorf, R.P. Van Duyne, J.T. Hupp, Metal-organic framework materials as chemical sensors, Chem. Rev. (2012). doi:10.1021/cr200324t.

[15] J. Della Rocca, D. Liu, W. Lin, Nanoscale Metal-Organic Frameworks for Biomedical Imaging and Drug Delivery, Acc. Chem. Res. (2011). doi:10.1021/ar200028a.

[16] L. Paseta, E. Simón-Gaudó, F. Gracia-Gorría, J. Coronas, Encapsulation of essential oils in porous silica and MOFs for trichloroisocyanuric acid tablets used for water treatment in swimming pools, Chem. Eng. J. 292 (2016) 28–34. doi:10.1016/j.cej.2016.02.001.

[17] P. Horcajada, T. Chalati, C. Serre, B. Gillet, C. Sebrie, T. Baati, J.F. Eubank, D. Heurtaux, P. Clayette, C. Kreuz, J.-S. Chang, Y.K. Hwang, V. Marsaud, P.-N. Bories, L. Cynober, S. Gil, G. Férey, P. Couvreur, R. Gref, Porous metal-organic-framework nanoscale carriers as a potential platform for drug delivery and imaging., Nat. Mater. 9 (2010) 172–178. doi:10.1038/nmat2608.

[18] D. Cunha, M. Ben Yahia, S. Hall, S.R. Miller, H. Chevreau, E. Elkaïm, G. Maurin, P. Horcajada, C. Serre, Rationale of drug encapsulation and release from biocompatible porous metal-organic frameworks, Chem. Mater. 25 (2013) 2767–2776. doi:10.1021/cm400798p.

[19] N. Liédana, P. Lozano, A. Galve, C. Tellez, J. Coronas, The template role of caffeine in its one-step encapsulation in MOF NH2-MIL-88B(Fe), J. Mater. Chem. B. 2 (2014) 1144–1151. doi:10.1039/C3TB21707H.

[20] S. Hermes, M.-K. Schröter, R. Schmid, L. Khodeir, M. Muhler, A. Tissler, R.W. Fischer, R. a Fischer, Metal@MOF: loading of highly porous coordination polymers host lattices by metal organic chemical vapor deposition., Angew. Chem. Int. Ed. Engl. 44 (2005) 6237–41. doi:10.1002/anie.200462515.

[21] O.K. Farha, J.T. Hupp, Rational design, synthesis, purification, and activation of metal-organic framework materials, Acc. Chem. Res. 43 (2010) 1166–1175. doi:10.1021/ar1000617.

[22] J.E. Mondloch, O. Karagiaridi, O.K. Farha, J.T. Hupp, Activation of metal–organic framework materials, CrystEngComm. 15 (2013) 9258. doi:10.1039/c3ce41232f.

[23] A.P. Nelson, O.K. Farha, K.L. Mulfort, J.T. Hupp, Supercritical Processing as a Route to High Internal Surface Areas and Permanent Microporosity in Metal Organic Framework Materials, J. Am. Chem. Soc.

131 (2009) 458–460. doi:doi:10.1021/ja808853q.

[24] O.K. Farha, I. Eryazici, N.C. Jeong, B.G. Hauser, C.E. Wilmer, A.A. Sarjeant, R.Q. Snurr, S.T. Nguyen, A.Ö. Yazaydin, J.T. Hupp, Metal-organic framework materials with ultrahigh surface areas: Is the sky the limit?, J. Am. Chem. Soc. 134 (2012) 15016–15021. doi:10.1021/ja3055639.

[25] M.J. Cocero, Á. Martín, F. Mattea, S. Varona, Encapsulation and co-precipitation processes with supercritical fluids: Fundamentals and applications, J. Supercrit. Fluids. 47 (2009) 546–555. doi:10.1016/j.supflu.2008.08.015.

[26] M.P. Fernández-Ronco, J. Kluge, J. Krieg, S. Rodríguez-Rojo, B. Andreatta, R. Luginbuehl, M. Mazzotti, J. Sague, Improving the wear resistance of UHMWPE implants by in situ precipitation of hyaluronic acid using supercritical fluid technology, J. Supercrit. Fluids. 95 (2014) 204–213. doi:10.1016/j.supflu.2014.08.031.

[27] A.P. Almeida, S. Rodríguez-Rojo, A.T. Serra, H. Vila-Real, A.L. Simplicio, I. Delgadilho, S. Beirão Da Costa, L. Beirão Da Costa, I.D. Nogueira, C.M.M. Duarte, Microencapsulation of oregano essential oil in starch-based materials using supercritical fluid technology, Innov. Food Sci. Emerg. Technol. 20 (2013) 140–145. doi:10.1016/j.ifset.2013.07.009.

[28] M. Salgado, F. Santos, S. Rodríguez-Rojo, R.L. Reis, A.R.C. Duarte, M.J. Cocero, Development of barley and yeast β-glucan aerogels for drug delivery by supercritical fluids, J. CO2 Util. 22 (2017) 262–269. doi:10.1016/j.jcou.2017.10.006.

[29] K. Matsuyama, N. Hayashi, M. Yokomizo, T. Kato, K. Ohara, T. Okuyama, Supercritical carbon dioxide-assisted drug loading and release from biocompatible porous metal–organic frameworks, J. Mater. Chem. B. 2 (2014) 7551–7558. doi:10.1039/C4TB00725E.

[30] A.M. López-Periago, J. Fraile, C.A. García-González, C. Domingo, Impregnation of a triphenylpyrylium cation into zeolite cavities using supercritical CO2, J. Supercrit. Fluids. 50 (2009) 305–312. doi:10.1016/j.supflu.2009.06.016.

[31] K. Leicht, G. Hartigan, R. D´Orazio, CO2 recovery process for supercritical extraction US6960242B2, 2003.

[32] K.P. Johnston, J.M. Dobbs, J.M. Wong, Nonpolar Co-Solvents for Solubility Enhancement in Supercritical Fluid Carbon Dioxide, J. Chem. Eng. Data. 31 (1986) 303–308. doi:10.1021/je00045a014.

[33] P.D.C. Dietzel, R. Blom, H. Fjellvåg, Base-induced formation of two magnesium metal-organic framework compounds with a bifunctional tetratopic ligand, Eur. J. Inorg. Chem. (2008) 3624–3632. doi:10.1002/ejic.200701284.

[34] J.B. DeCoste, G.W. Peterson, B.J. Schindler, K.L. Killops, M. a. Browe, J.J. Mahle, The effect of water adsorption on the structure of the carboxylate containing metal–organic frameworks Cu-BTC, Mg-MOF-74, and UiO-66, J. Mater. Chem. A. 1 (2013) 11922. doi:10.1039/c3ta12497e.

[35] J. Heller, Biodegradable polymers in controlled drug delivery., Crit. Rev. Ther. Drug Carrier Syst. 1 (1984) 39–90.

[36] A. Kumari, S.K. Yadav, S.C. Yadav, Biodegradable polymeric nanoparticles based drug delivery systems, Colloids Surfaces B Biointerfaces. 75 (2010) 1–18. doi:10.1016/j.colsurfb.2009.09.001.

[37] S.R. Miller, D. Heurtaux, T. Baati, P. Horcajada, J.-M. Grenèche, C. Serre, Biodegradable therapeutic MOFs for the delivery of bioactive molecules, Chem. Commun. 46 (2010) 4526. doi:10.1039/c001181a.

[38] W. Cai, C.C. Chu, G. Liu, Y.X.J. Wáng, Metal-Organic Framework-Based Nanomedicine Platforms for

Drug Delivery and Molecular Imaging, Small. 11 (2015) 4806–4822. doi:10.1002/smll.201500802.

[39] U. Kopcak, R.S. Mohamed, Caffeine solubility in supercritical carbon dioxide/co-solvent mixtures, J. Supercrit. Fluids. 34 (2005) 209–214. doi:10.1016/j.supflu.2004.11.016.

[40] G.I. Burgos-Solórzano, J.F. Brennecke, M.A. Stadtherr, Solubility measurements and modeling of molecules of biological and pharmaceutical interest with supercritical CO2, Fluid Phase Equilib. 220 (2004) 57–69. doi:10.1016/j.fluid.2004.01.036.

[41] E. Lack, H. Seidlitz, Commercial scale decaffeination of coffee and tea using supercritical CO2 BT - Extraction of Natural Products Using Near-Critical Solvents, in: M.B. King, T.R. Bott (Eds.), Springer Netherlands, Dordrecht, 1993: pp. 101–139. doi:10.1007/978-94-011-2138-5_5.

[42] S. Devautour-Vinot, C. Martineau, S. Diaby, M. Ben-Yahia, S. Miller, C. Serre, P. Horcajada, D. Cunha, F. Taulelle, G. Maurin, Caffeine confinement into a series of functionalized porous zirconium MOFs: A joint experimental/modeling exploration, J. Phys. Chem. C. 117 (2013) 11694–11704. doi:10.1021/jp402916y.

[43] N. Liédana, E. Marín, C. Téllez, J. Coronas, One-step encapsulation of caffeine in SBA-15 type and non-ordered silicas, Chem. Eng. J. 223 (2013) 714–721. doi:10.1016/j.cej.2013.03.041.

[44] C. Labay, J.M. Canal, A. Navarro, C. Canal, Corona plasma modification of polyamide 66 for the design of textile delivery systems for Cosmetic therapy, Appl. Surf. Sci. (2014). doi:10.1016/j.apsusc.2014.07.191.

[45] L. Rubio, C. Alonso, L. Coderch, J.L. Parra, M. Martí, J. Cebrián, J.A. Navarro, M. Lis, J. Valldeperas, Skin Delivery of Caffeine Contained in Biofunctional Textiles, Text. Res. J. (2010). doi:10.1177/0040517509358798.

[46] G.H. Kamimori, C.S. Karyekar, R. Otterstetter, D.S. Cox, T.J. Balkin, G.L. Belenky, N.D. Eddington, The rate of absorption and relative bioavailability of caffeine administered in chewing gum versus capsules to normal healthy volunteers, Int. J. Pharm. (2002). doi:10.1016/S0378-5173(01)00958-9.

[47] G.A. Leeke, R. Santos, M.B. King, Vapor-liquid equilibria for the carbon dioxide + carvacrol system at elevated pressures, J. Chem. Eng. Data. 46 (2001) 541–545. doi:10.1021/je000342k.

[48] R.J.W. Lambert, P.N. Skandamis, P.J. Coote, G.J.E. Nychas, A study of the minimum inhibitory concentration and mode of action of oregano essential oil, thymol and carvacrol, J. Appl. Microbiol. 91 (2001) 453–462. doi:10.1046/j.1365-2672.2001.01428.x.

[49] A. Nostro, T. Papalia, Antimicrobial Activity of Carvacrol: Current Progress and Future Prospectives, Recent Pat. Antiinfect. Drug Discov. 7 (2012) 28–35. doi:10.2174/157489112799829684.

[50] R. Baranauskiene, P.R. Venskutonis, K. Dewettinck, R. Verhé, Properties of oregano (Origanum vulgare L.), citronella (Cymbopogon nardus G.) and marjoram (Majorana hortensis L.) flavors encapsulated into milk protein-based matrices, Food Res. Int. 39 (2006) 413–425. doi:10.1016/j.foodres.2005.09.005.

[51] L. Keawchaoon, R. Yoksan, Preparation, characterization and in vitro release study of carvacrol-loaded chitosan nanoparticles, Colloids Surfaces B Biointerfaces. 84 (2011) 163–171. doi:10.1016/j.colsurfb.2010.12.031.

[52] M. Ramos, A. Beltrán, M. Peltzer, A.J.M. Valente, M. del C. Garrigós, Release and antioxidant activity of carvacrol and thymol from polypropylene active packaging films, LWT - Food Sci. Technol. 58 (2014) 470–477. doi:10.1016/j.lwt.2014.04.019.

[53] A. Iannitelli, R. Grande, A. di Stefano, M. di Giulio, P. Sozio, L.J. Bessa, S. Laserra, C. Paolini, F. Protasi,

L. Cellini, Potential antibacterial activity of carvacrol-loaded poly(DL-lactide-co-glycolide) (PLGA) nanoparticles against microbial biofilm, Int. J. Mol. Sci. 12 (2011) 5039–5051. doi:10.3390/ijms12085039.

[54] J.E.D. Davies, Vibrational spectroscopic studies of host-guest compounds, ARI - An Int. J. Phys. Eng. Sci. 51 (1998) 120–125. doi:10.1007/s007770050043.

[55] Y. Huang, J.H. Leech, E.A. Havenga, R.R. Poissant, Investigations of host-guest interactions in zeolitic systems by FT-Raman spectroscopy, Microporous Mesoporous Mater. 48 (2001) 95–102. doi:10.1016/S1387-1811(01)00363-8.

[56] S.G. Kazarian, G.G. Martirosyan, Spectroscopy of polymer/drug formulations processed with supercritical fluids: in situ ATR–IR and Raman study of impregnation of ibuprofen into PVP, Int. J. Pharm. 232 (2002) 81–90. doi:https://doi.org/10.1016/S0378-5173(01)00905-X.

[57] D.Y. Siberio-Pérez, A.G. Wong-Foy, O.M. Yaghi, A.J. Matzger, Raman Spectroscopic Investigation of CH4 and N2 Adsorption in Metal-Organic Frameworks, Chem. Mater. 19 (2007) 3681–3685. doi:10.1021/cm070542g.

[58] A. Bamberger, G. Sieder, G. Maurer, High-pressure (vapor+liquid) equilibrium in binary mixtures of (carbon dioxide+water or acetic acid) at temperatures from 313 to 353 K, J. Supercrit. Fluids. 17 (2000) 97–110. doi:https://doi.org/10.1016/S0896-8446(99)00054-6.

[59] A.N. Sabirzyanov, A.P. Il'in, A.R. Akhunov, F.M. Gumerov, Solubility of Water in Supercritical Carbon Dioxide, High Temp. 40 (2002) 203–206. doi:10.1023/A:1015294905132.

[60] D. Britt, H. Furukawa, B. Wang, T.G. Glover, O.M. Yaghi, Highly efficient separation of carbon dioxide by a metal-organic framework replete with open metal sites., Proc. Natl. Acad. Sci. U. S. A. 106 (2009) 20637–20640. doi:10.1073/pnas.0909718106.

[61] N. Liédana, A. Galve, C. Rubio, C. Téllez, J. Coronas, CAF@ZIF-8: One-step encapsulation of caffeine in MOF, ACS Appl. Mater. Interfaces. 4 (2012) 5016–5021. doi:10.1021/am301365h.

[62] J. Maultzsch, H. Telg, S. Reich, C. Thomsen, Radial breathing mode of single-walled carbon nanotubes: Optical transition energies and chiral-index assignment, Phys. Rev. B - Condens. Matter Mater. Phys. 72 (2005) 205438. doi:10.1103/PhysRevB.72.205438.

[63] S. Zuluaga, E.M.A. Fuentes-Fernandez, K. Tan, F. Xu, J. Li, Y.J. Chabal, T. Thonhauser, Understanding and controlling water stability of MOF-74, J. Mater. Chem. A. 4 (2016) 5176–5183. doi:10.1039/c5ta10416e.

5.3. Supporting information

1.- MOFs characterization

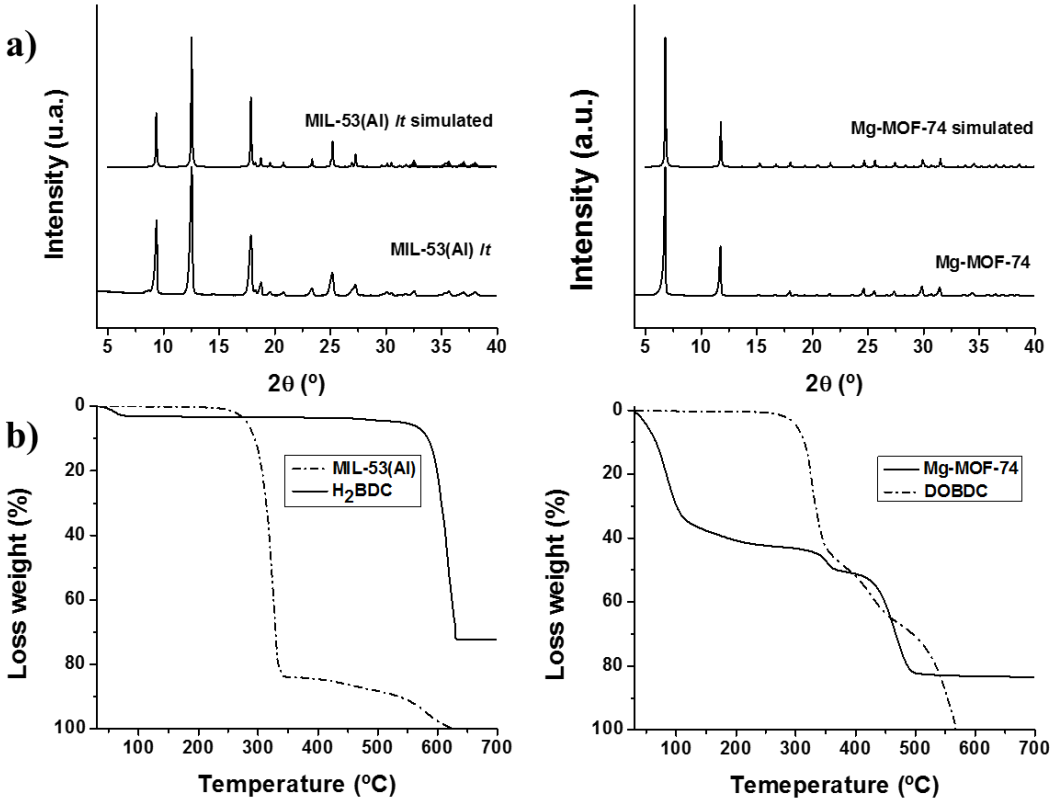

Figure S1. MIL-53(Al) *lt* and Mg-MOF-74 XRD patterns compared to the simulated (ref) (a) and TGA curves to the starting ligand (b).

2.-N_2 and CO_2 adsorption

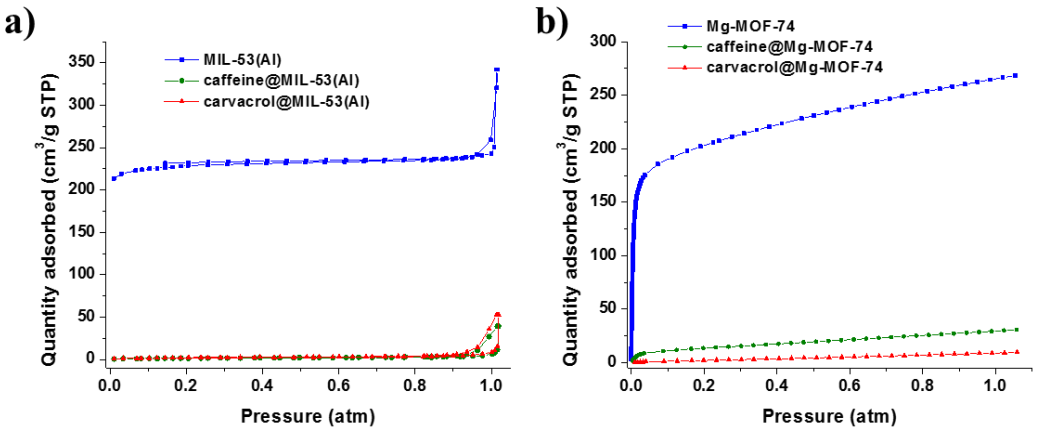

Figure S2. Adsorption capacity of MOFs and the corresponding sc-CO_2 impregnated MOFs for 14 h at 40 ºC and 100 bar (a) N_2 adsorption isotherms of MIL-53(Al) samples and (b) CO_2 adsorption isotherm of Mg-MOF-74 samples. The outgassing in all cases was carried out at 150 ºC.

3.- SEM characterization

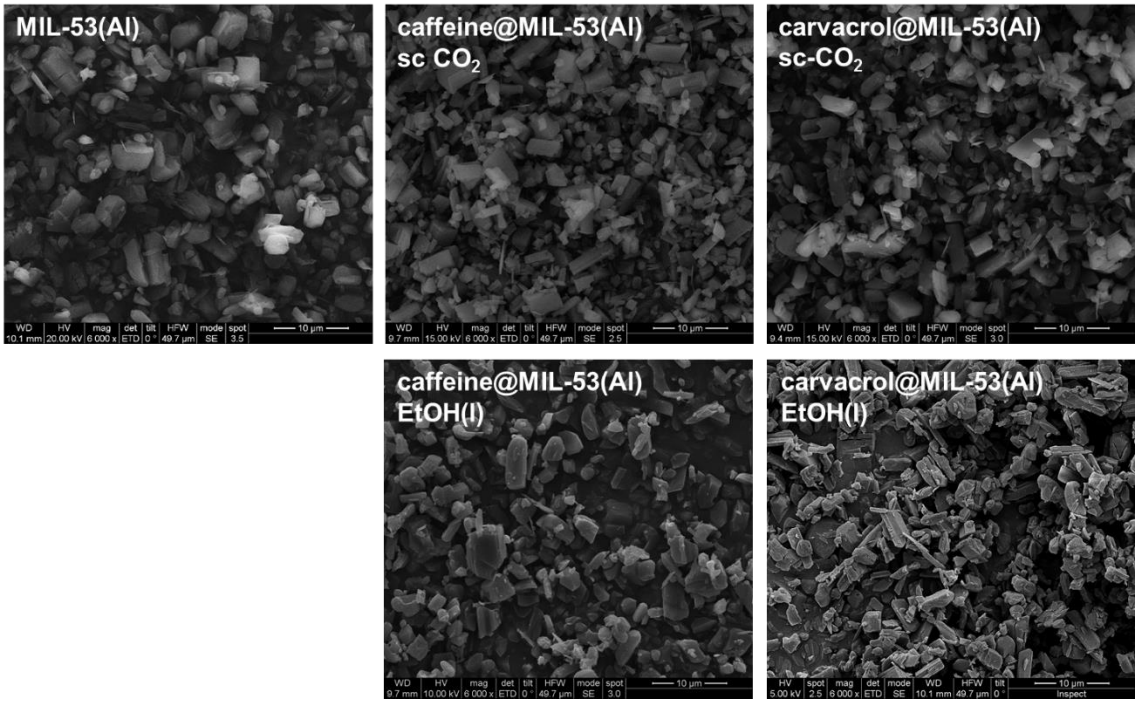

Figure S3. SEM images of MIL-53(Al) before and after the impregnation in sc-CO_2 at 40ºC and 100 bar and in ethanol solution for 14 h of caffeine and carvacrol.

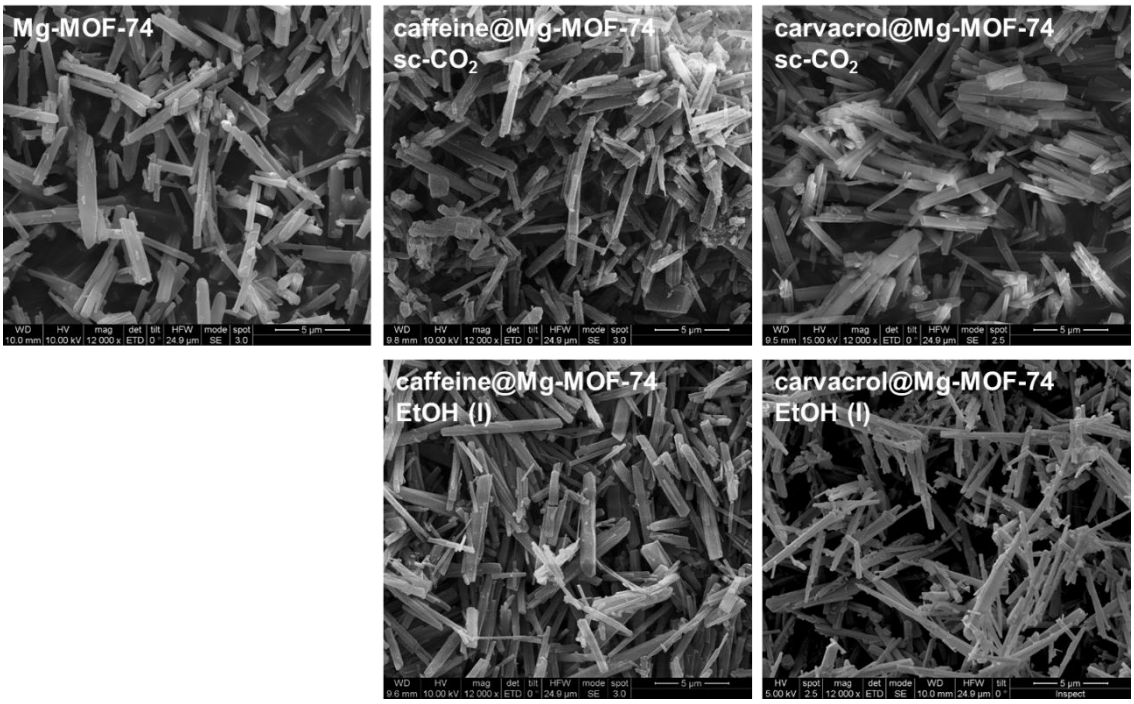

Figure S4. SEM images of Mg-MOF-74 before and after the impregnation in sc-CO_2 at 40ºC and 100 bar and in ethanol solution for 14 h of caffeine and carvacrol

4.- Raman spectroscopy

Table S1. Caffeine@MIL-53(Al): terephthalate shifts

MIL-53(Al) *lt*			**sc-CO_2 (cm^{-1})**		**EtOH (l) (cm^{-1})**	
1612	**vs**	ring C=C stretching	1613 (1)	m	1612 (0)	vs
1524	w	asymmetric stretching CO_2^-	1522 (-2)	w	1518 (-6)	vw
1469	**s**	symmetric stretching CO_2^-	1470 (1)	m	1470 (1)	**s**
1437	w		1439 (2)	w	1437 (0)	w
1142	m	Ar =C-H in-plane deformation	1144 (2)	m	1141 (0)	m
867	m	Ar =C-H out-of-plane deformation	870 (3)	vs	869 (2)	m
630	w	aromatic ring deformation	630 (0)	w	628 (-2)	w

vs: very strong, s: strong, m: medium, w: weak, vw: very weak

Table S2. Carvacrol@MIL-53(Al): terephthalate shifts

MIL-53(Al) *lt*		**Vibration**	**sc-CO_2 (cm^{-1})**		**EtOH (l) (cm^{-1})**	
1612	vs	ring C=C stretching	1615 (3)	vs	1615 (3)	vs
1524	w	asymmetric stretching CO_2^-	1503 (-21)	w	1503 (-21)	w
1469	s	symmetric stretching CO_2^-	1475 (7)	s	1475 (7)	s
1437	w		1453 (16)	m	1453 (16)	m
1142	m	Ar =C-H in-plane deformation	1148 (6)	m	1148 (6)	m
867	m	Ar =C-H out-of-plane deformation	871 (4)	s	871 (4)	s
630	w	Aromatic ring deformation	629 (-1)	w	629 (-1)	w
		Lattice vibration	187	vs	186	vs

Table S3. Caffeine@Mg-MOF-74: 2,5-dihydroxyterephthalate shifts

Mg-MOF-74		**Vibration**	**sc-CO_2 (cm^{-1})**		**EtOH (l) (cm^{-1})**	
1626	w	ring C=C stretching	1626 (0)	w	1626 (0)	w
1576	m	asymmetric stretching CO_2^-	1574 (-2)	m	1573 (-3)	m
1500	m	symmetric stretching CO_2^-	1499 (-1)	m	1497 (-3)	m
1429	s		1429 (0)	s	1428 (-1)	s
1293	vs	Ar-O^-	1295 (2)	vs	1295 (2)	vs
818	m	Ar =C-H in-plane deformation	817 (-1)	m	816 (-2)	m
728	w	Ar =C-H out-of-plane deformation	730//725 (2)	w	725 (-3)	w
661	w	aromatic ring deformation	660 (-1)	w	660 (-1)	w
564	m		563 (-1)	m	565 (1)	m

Table S4. Carvacrol@Mg-MOF-74: 2,5-dihydroxyterephthalate shifts

Mg-MOF-74		**Vibration**	**sc-CO_2 (cm^{-1})**		**EtOH (l) (cm^{-1})**	
1626	w	ring C=C stretching	1626 (0)	w	1626 (0)	w
1576	m	asymmetric stretching CO_2^-	1574 (-2)	m	1574 (-2)	m
1500	m	symmetric stretching CO_2^-	1499 (-1)	m	1497 (-3)	m
1429	s		1429 (0)	s	1428 (-1)	s
1293	vs	Ar-O^-	1295 (2)	s	1295 (2)	s
818	m	Ar =C-H in-plane deformation	817 (-1)	m	816 (-2)	m
728	w	Ar =C-H out-of-plane deformation	730//723 (2)	vw	726 (-2)	w
661	w	aromatic ring deformation	660 (-1)	w	660 (-1)	w
564	m		563 (-1)	m	565 (1)	m

Conclusiones

Durante el desarrollo de esta tesis doctoral se han alcanzado varios objetivos e innovaciones en el campo de los MOF.

En el campo de la síntesis de híbridos, dos nuevas estrategias se han propuesto y aplicado:

- Se ha descrito el uso de atmósferas reactivas (CO and O_2) por primera vez en la síntesis de MOF. La síntesis asistida de MOF se había estudiado anteriormente mediante sistemas físicos o por medio de la adición de diferentes compuestos químicos en disolución, pero no con gases reactivos a alta presión. Al emplear los dos gases de manera consecutiva, se observó un incremento significativo del rendimiento en la síntesis de fumarato de Fe(III), a la vez que se mejoró la cristalinidad y se obtuvieron partículas con morfología más definida. Además, se obtuvo una distribución asimétrica de un híbrido de fumarato de Al y Fe(III) usando también de manera consecutiva los dos gases: un núcleo rico en hierro y una corteza exterior más concentrada en aluminio. Finalmente, se llevó a cabo la calcinación parcial de una muestra de material híbrido y se obtuvo un material superparamagnético que conservaba cierta área superficial BET (244 m^2/g). Los resultados de esta investigación se publicaron en Journal of Materials Chemistry A, 2018, 6, 14352-14358.
- Se estudió el uso de H_2O_2 en la síntesis de tereftalato de M(III). Se demostró que el H_2O_2 promovía la síntesis de MOF basados en tereftalato de aluminio (MIL-53(Al)), hierro (MIL-68(Fe)) y la combinación de ambos (MIL-68(Al/Fe)). El rendimiento se incrementó sustancialmente, particularmente para MIL-53(Al). La cristalinidad y el área BET de los materiales se mantuvieron para MIL-53(Al) y MIL-68(Al/Fe). Se estudió la reacción mediante varias técnicas y se hizo la hipótesis de que el H_2O_2 promovía la formación de puentes μ-OH, los cuales son precursoras de las estructuras finales de los MOF estudiados. De esta manera se favoreció la nucleación y se mejoró el rendimiento de la síntesis. Estos resultados se han enviado a una revista científica y están en revisión.

En el campo de la encapsulación de moléculas bioactivas en MOF, se han estudiado dos nuevas estrategias en el desarrollo de esta tesis en las que se evita el uso de disolventes orgánicos, a saber:

- Se estudió el uso de una prensa hidráulica para aplicar alta presión en la mezcla en polvo de aditivos, cafeína y ácido kójico, y diferentes MOF promoviendo la difusión de los aditivos en los poros, es decir, su encapsulación. De esta manera, se encapsularon cafeína y ácido kójico en MIL-53(Al) y UiO-66, evitando para ello el uso de disolventes, mientras que en Mg-MOF-74 y MIL-101(Cr) no se consiguieron encapsulaciones tan efectivas. La estabilidad mecánica y la estructura cristalina jugaron un papel decisivo en la efectividad de la encapsulación, que no se logró en todos y cada uno de los cuatro MOF estudiados (MIL-53(Al), UiO-66, Mg-MOF-74 y

MIL-101(Cr)). Entre aquellos en los que sí se consiguió, MIL-53(Al) mantuvo su estructura cristalina, mientras que UiO-66 la perdió en parte. Por otro lado, la estructura del Mg-MOF-74 se mantuvo, pero la encapsulación de cafeína no resulto eficaz. Finalmente, la inestabilidad mecánica del MIL-101(Cr) se evidenció en su evidente amorfización al aplicar la alta presión. Los resultados de esta investigación se publicaron en European Journal of Inorganic Chemistry 2019, 29-36.

- El uso de CO_2 supercrítico (sc-CO_2) se estudió para encapsular cafeína y carvacrol en los MOF MIL-53(Al) y Mg-MOF-74 a diferentes tiempos. La carga de los aditivos se mejoró respecto a los valores obtenidos en fase líquida de etanol. De hecho, la encapsulación en Mg-MOF-74 solo se consiguió en sc-CO_2. De esta manera, se evitó el uso de disolventes y se mejoraron los resultados. Finalmente, los materiales encapsulados mediante sc-CO_2 y etanol líquido se caracterizaron y compararon para observar diferencias estructurales y en las interacciones MOF-aditivo. Los resultados de esta investigación se publicaron en Journal of CO2 Utilization, 2019, 30, 38-47.

Conclusions

During the accomplishment of this Doctoral Thesis, different goals and innovations were achieved in the MOF field.

Regarding the synthesis of MOFs, two new approaches have been developed:

- The use of gas atmospheres (CO and O_2) was reported for the first time to synthesize MOFs. The assisted synthesis had been previously studied by a physical external help and by the addition of different chemical compounds, but not with reactive gases at high pressure. When both gases were consecutively combined, Fe-fumarate synthesis increased the yield and the crystallinity was improved, simultaneously more defined morphology was obtained. Additionally, an asymmetric distribution of hybrid Fe/Al-fumarate was obtained using both gases: a core rich in iron and a shell more concentrated in aluminum. Finally, the partial calcination of a hybrid sample yielded superparamagnetic particles that kept some texture (244 m^2/g). The results of this research were published in Journal of Materials Chemistry A, 2018, 6, 14352-14358.

- The use of H_2O_2 was studied for M^{3+}-terephthalate synthesis. It was shown that H_2O_2 promoted the synthesis of terephthalate MOFs of aluminium (MIL-53(Al)), iron (MIL-68(Fe)) and the combination of both (MIL-68(Al/Fe)). The yield was substantially increased, especially for MIL-53(Al). The crystallinity and the BET specific surface area were roughly kept for MIL-53(Al) and MIL-68(Al/Fe). The reaction was studied through different techniques and it was hypothesized that H_2O_2 promoted the construction of μ-hydroxo bridges that are precursors for the final MOF structures, in the end favoring nucleation and then improving the MOF synthesis yield. The results of this research are under revision of a scientific journal.

Regarding the encapsulation of bioactive molecules in MOF, two new strategies have been studied in this PhD thesis avoiding the use of organic solvents:

- The use of a hydraulic press was studied to apply high pressure into the powder mixture of additives, caffeine and kojic acid, and different MOFs promoting the diffusion of the additives into the pores, i.e. their encapsulation. In this manner, caffeine and kojic acid were encapsulated into MIL-53(Al) and UiO-66 avoiding the use of any solvent. Mechanical stability and crystalline structure play an important role in the effective encapsulation: even if four different MOFs were tested (MIL-53(Al), UiO-66, Mg-MOF-74 and MIL-101(Cr)) not all of them yielded effective encapsulations. Regarding those for which encapsulation was achieved, MIL-53(Al) kept its crystalline structure, although that of UiO-66 decreased in some extent.

For Mg-MOF-74, the structure was maintained, although the encapsulation of caffeine was hindered. Finally, the mechanical stability limited the encapsulation in MIL-101(Cr) because the material was amorphized under the studied pressure. The results of this research were published in European Journal of Inorganic Chemistry 2019 29-36.

- The use of supercritical CO_2 (sc-CO_2) was studied to encapsulate caffeine and carvacrol in MIL-53(Al) and Mg-MOF-74 with different contact times. The additive loadings were improved from those values obtained in ethanol liquid phase. In fact, encapsulation for Mg-MOF-74 was only possible in sc-CO_2. In this way, the use of solvent was avoided, and the results were improved. Finally, the encapsulated materials with sc-CO_2 and ethanol liquid encapsulation were characterized and compared to observe the difference in the material structures and in the host-guest interactions. The results of this research were published in Journal of CO2 Utilization, 2019, 30, 38-47.